POPULATION DENSITIES OF He I AND He II EXCITED STATES IN NON-LTE HELIUM PLASMAS

A Thesis Submitted
in Partial Fulfilment of the Requirements
for the Degree of

DOCTOR OF PHILOSOPHY

by

MANJANATH SUBRAYA HEGDE

to the

DEPARTMENT OF CHEMISTRY
INDIAN INSTITUTE OF TECHNOLOGY KANPUR

JULY, 1976

DEPARTMENT OF CHEMISTRY
INDIAN INSTITUTE OF TECHNOLOGY, KANPUR, INDIA

CERTIFICATE I

This is to certify that Mr. M. S. Hegde has satisfactorily completed all the courses required for the Ph.D. degree programme. These courses include:

Chm 501	Advanced Organic Chemistry I
Chm 521	Chemical Binding
Chm 523	Chemical Thermodynamics
Chm 524	Modern Physical Methods in Chemistry
Chm 541	Advanced Inorganic Chemistry I
Chm 500	Basic Course in Mathematics I
Chm 600	Basic Course in Mathematics II
Chm 622	Chemical Kinetics
Chm 634	Symmetry and Molecular Structure
Chm 800	General Seminars
Chm 801	Graduate Seminars
Chm 900	Graduate Research

Mr. M. S. Hegde has successfully completed his Ph.D. Qualifying Examination in August 1971.

A. Chakravorty
Professor and Head
Department of Chemistry

P. S. Goel
Professor and Convener
Post-Graduate Studies Committee
Department of Chemistry

CERTIFICATE

Certified that the work "Population Densities of HeI and HeII Excited States in non-LTE Helium Plasmas" has been carried out by Sri M. S. Hegde under my supervision and the same has not been submitted elsewhere for a degree.

P. K. Ghosh

P. K. Ghosh
Thesis Supervisor

CONTENTS

ACKNOWLEDGEMENTS

It is with great pleasure that I express my deep sense of gratitude and indebtedness to Professor P. K. Ghosh who suggested the problem and guided me at all stages of the work. I am grateful to him for his keen interest and constant encouragement at every walk of my life.

I am thankful to my teachers of this Institute for their valuable contributions in my education pertaining to modern aspects of chemistry. My special thanks are due to Professor C. N. R. Rao and Professor A. Chakravorty for their encouragement.

Sincere thanks are due to Dr. A. K. Hui, my senior, and Mr. U.K. Roy Chowdhury, my colleague, for their excellent cooperation and for many useful discussions. I am thankful to my other colleagues, Mr. A.S. Arora, Miss Sunita Verma and Mr. Lakshmi Narayan for their kind cooperation. I owe my gratitude to Dr. M.G. Subramanian who introduced me to the programming techniques.

I am thankful to Mr. Nihal Ahmad for typing the thesis with great patience. I am thankful to the staff of Central Facilities of this Institute, in general, and in particular to Messrs. J.N. Sharma, S.L. Yadav, B.L. Rajani, R.K. Jha and H.N. Singh for their kind cooperation throughout this work.

I acknowledge with gratitude the grant of a fellowship for the first two years by the Department of Atomic Energy for developmental research in quadrupole mass spectrometry, and to the authorities of IIT Kanpur for granting me an assistantship for the last three years. Financial support of the research by the Petroleum Research Fund of the American Chemical Society and the Department of Atomic Energy is gratefully acknowledged.

I recall the hardship my parents have undergone in the early part of my education. My wife Malati's help and encouragement is understandable only from the true spirit of Hindu way of life.

M.S. Hegde

LIST OF ILLUSTRATIONS

LIST OF TABLES

LIST OF SYMBOLS

$A(p,q), A(i,j)$	-	Probability of spontaneous emission of HeI(p-q), HeII (i-j) states
B	-	Magnetic field
E_p, E_i	-	Energy of states p,i from ground state of HeI
E_e	-	Energy of electron in eV
E_1^H	-	Ionization potential of hydrogen
$f(p,q), f(i,j)$	-	Absorption oscillator strength of HeI, and HeII states
g_p, g_i	-	Weight factor of HeI(p), HeII(i)
i,j	-	HeII states
p,q	-	HeI states
i_{ep}	-	Probe electron current
i_p	-	Total probe current
i_e	-	Emission current
I_B	-	Emission intensity at magnetic field B
J_+	-	Probe ion saturation current
$K(p,q), K(q,p)$	-	Electron impact excitation, deexcitation coefficient of HeI
$K(i,j), K(j,i)$	-	Electron impact excitation, deexcitation coefficient of HeII
$K(p,i)$	-	Electron impact ionization-excitation coefficient of HeI(p) → HeII(i)
$K(i,c), K(c,i)$	-	Electron impact ionization and recombination coefficient for HeII
$KN(p,q)$, $KN(q,p)$	-	Neutral-neutral excitation, deexcitation coefficients for HeI
$KN(p,i)$, $KN(i,p)$	-	Neutral-neutral collisional ionization, recombination coefficient of HeI

n, i	-	Principal quantum number for HeI and HeII respectively
$n(p)$, $n^+(i)$	-	Number density of HeI(p), HeII(i) respectively
n_e	-	Number density of electrons
n^{++}	-	Number density of He^{++}
$n_E(p), n_E^+(i)$	-	Saha equilibrium population density of HeI(p), HeII(i)
$r_o(p), r_1(p)$	-	Population coefficients of HeI
$r_o^+(i)$, $r_1^+(i)$, $r_2^+(i)$	-	Population coefficients of HeII
α	-	Collisional-radiative recombination coefficient
$\beta(p)$, $\beta(i)$	-	Radiative recombination coefficients from He^+ to HeI(p), and He^{++} to $He^+(i)$
λ_{pq}	-	Wavelength for the transition $p \rightarrow q$
Λ_{pq}, Λ_{ij}	-	Optical escape factors for HeI and HeII transitions
σ_c	-	Photoionization cross-section
τ_{pq}	-	Optical depth for transition $p \rightarrow q$
σ_d	-	Momentum transfer cross-section for $He(2^3S)$-$He(1^1S$
$I_{B=700}/I_{B=0}$ and $(I_B/I_o)_{700}$	-	Both have been synonymously used to represent emission enhancement factor at 700 gauss

ABSTRACT

Emission intensity measurements of HeI and HeII lines have been made from a helium plasma in a longitudinal magnetic field (0-700 gauss) at neutral particle density $\sim 10^{14}$ cm^{-3}. The lines include HeI transitions $n^3D \rightarrow 2^3P$ (n=3,4,5), $n^3S \rightarrow 2^3P$ (n=3,4,5), $n^3P \rightarrow 2^3S$ (n=3,4), $n^1D \rightarrow 2^1P$ (n=3,4,5,6), $n^1P \rightarrow 2^1S$ (n=3,4), $n^1S \rightarrow 2^1P$ (n=4,5) and HeII transition n=4 → n=3. Diagnostic measurements are made using Langmuir probes, triplet-singlet emission intensity ratios involving the transitions $4^3S \rightarrow 2^3P$ and $4^1S \rightarrow 2^1P$, and application of population coefficient r_1 ratios. As the magnetic field is varied in the 0-700 gauss range, the axial electron density changes from $\sim 10^{10}$ cm^{-3} to $\sim 10^{12}$ cm^{-3}. The electron temperature falls from ~11 eV to ~6 eV.

A collisional-radiative model is used for explaining the observed emission intensity enhancements in the magnetic field. The model consists of completely separated singlet and triplet sublevels of HeI up to n=5 and combined levels for n=6-12. Helium ionic levels up to n=13 are also incorporated. In addition to usual electron-impact excitation-deexcitation processes, atom-atom collisions for HeI states and direct ionization to excited Helium ionic states from all the HeI states are included. HeI and HeII equations are solved simultaneously to yield populations of various states. The results show that the model explains the observed emission enhancements satisfactorily, and in this regard it is considerably better than some other models reported in the literature. Further, the model used in the present work also explains HeI and HeII excited state populations in some recent helium plasma experiments reported by other workers.

Chapter I

INTRODUCTION

In astrophysical plasmas, densities of particles in various excited states is determined by both physical and chemical processes. Since the excited states control the line emissivity of a plasma, measurement of line or continuum radiation often is a good probe for information about the plasma processes. A thorough quantitative understanding of these processes however is many times more difficult than a qualitative impression of the undergoing phenomena. Plasmas simulated under laboratory conditions often is the best recourse one finds to investigate plasmas of astrophysical interest. There is now a great deal of interest not only on the natural plasmas but also on plasmas to realize fusion conditions and laser plasmas. While processes that are of major importance in fusion plasmas are not the plasma emissivities, though the latter contribute to plasma cooling, but in

laser plasmas, afterglow plasmas, in all types of discharge plasmas, in beam-plasma and laser-plasma interactions detailed studies on population of excited states are of major interest. The present work is involved with emission of line radiation from a helium plasma and correlation of plasma conditions with excited state populations.

Although it is true that emission of radiation from plasmas is perhaps the most easily noted plasma phenomenon, the emission processes do not necessarily constitute the most important processes among the plasma rate processes. What however is important, that for plasmas which are remote, as is true for astrophysical plasmas, emissivities are means by which not only the plasma constituents can be identified but are often the sole means by which the plasma conditions can be investigated. Had it been true that only a handful of processes are involved in excitation phenomena, it would have been indeed rather simple to understand plasma conditions and processes from the emissivities. But the processes which are responsible for the atomic excited state population at a given time are numerous and their rates are dependent in a complex way on plasma conditions. The usual particles being the neutrals, positive ions, negative ions, and electrons, the excited state populations of heavy particles are determined by atom-atom, atom-ion, atom-electron collisions, ion-electron recombination processes, spontaneous emission processes, and, if the photon

flux in the plasma is significant, then by photo absorption processes as well. The population in an atomic bound state is thus controlled by a multitude of rate processes and though under particular conditions the relative importance of various processes change, even in the simplest of cases it is a formidable task to find an unambiguous answer about the sources of excitation and causes of population decay. In laboratory plasmas, the density and energy distribution of electrons in the plasma almost always play a dominant role in the excitation processes, particularly so when the photon flux is negligible. While theoretical emissivities can be calculated regardless of whether the actual energy distribution of plasma particles follows a simple Maxwellian pattern, categorization of plasmas on the basis of the degree and nature of equilibration attained is quite often used and this makes understanding of plasma excitation-deexcitation processes considerably simpler.

If a plasma is contained within isothermal walls at temperature T and all its properties can be uniquely described by this temperature, then the plasma is said to be in complete thermodynamic equilibrium[1] (CTE). In CTE the distribution of energies of all the plasma constituents are uniquely derivable from the information on temperature and detailed information on the plasma system is not essential. From information on the temperature, determination of both the state of matter and radiation is uniquely possible. Under CTE conditions the laws

of Maxwell, Boltzmann and Saha are operative, from which energy distribution of particles and population of particles in various states can be derived. The spectral distribution of plasma radiation under CTE condition is controlled by Planck's law.

A more limited case of equilibration takes place when the criteria of local thermodynamic equilibrium (LTE) is satisfied. Under these conditions the electron velocity distribution is Maxwellian and this can be designated by an electron temperature T_e. In LTE, the plasma equilibrium is entirely determined by electron collisions and hence population of heavy particle energy states are compatible with T_e satisfying Boltzmann and Saha distributions, and the radiated energy is given by Kirchoff's law. For LTE to be satisfied, a criterion in terms of electron density and temperature is[2]

$$n_e > 1.2 \times 10^{12} T_e^{\frac{1}{2}} \chi(p,q)^3 \text{ cm}^{-3} \qquad (1.1)$$

where $\chi(p,q)$ is the excitation potential from level p to level q in eV. For example, when applied to the helium system at $T_e = 5$ eV, at $n_e > 10^{17}$ LTE condition holds.

When however the population of the energy states of heavy particles cannot be described by the T_e values alone, one has non-LTE plasmas. For non-LTE plasmas, the population of excited states under a set of plasma conditions cannot be easily determined and one needs to consider all the excitation

and deexcitation processes in detail, and, depending on the physical conditions, transport processes like diffusion also need to be given due consideration. For non-LTE theoretical calculations, one therefore uses models in which collisional and radiative processes are taken into account in various degrees.

In a typical such non-LTE model the processes that need to be taken into account, for calculations on excited state populations, are (i) electron impact excitation, deexcitation and ionization, (ii) ion-electron recombination processes, i.e., continuum to bound state transitions either through three-body recombination or by radiative recombination, and (iii) photo-excitation, deexcitation, and ionization. Each of these processes has its characteristic energy dependent cross-section, which can be used to obtain a characteristic rate coefficient if the energy distribution of the colliding particles is known. As the importance of the electron impact excitation-deexcitation processes depend on the electron density n_e and electron temperature T_e values, the relative importance of photon induced transitions in a plasma depends on the ambient photon flux and energy. In this regard, one can thus further classify the plasmas as optically thick or optically thin. In optically thin plasmas, radiation does freely escape from the plasma and no reabsorption of the emitted radiation occurs. Optical escape factors[3] of all radiation can then be taken as unity. In

optically thick plasma, reabsorption of the emitted radiation takes place, and hence for such plasmas photoexcitation must be an integral part of the non-LTE model. Here the escape factors vary depending on the transition, the lowest value arises for the resonance lines of the system, and is numerically taken as zero in the case of complete absorption.

At lower electron densities ($n_e \leq 10^{13}$) a 'steady state corona model'[2] has been sometimes used to explain plasma line radiation from solar corona and also from low density laboratory plasmas. In this model, which assumes optically thin condition, the balancing processes are collisional excitation ionization from the ground state on one side, and, the radiative recombination and spontaneous decay on the other. However, this simplified model is not very satisfactory because, even at electron densities 10^{10}-10^{13}, collisional excitation-deexcitations of excited states and three-body recombinations contribute significantly to the population densities. So a theoretical model which accommodates all the collisional and radiative processes taking place between various quantum states becomes desirable. Such a 'collisional-radiative model', which is of much wider applicability than the corona model, can be expected to give more realistic population densities of excited states.

The first detailed collisional-radiative model on both optically thin and optically thick hydrogenic plasmas was

Giovanelli[60]

proposed by Bates, Kingston and McWhirter.[4] The theory involves the following processes:

$$N^{(Z-1)+} + e \underset{K(c,p)}{\overset{K(p,c)}{\rightleftharpoons}} N^{Z+} + e + e \qquad (1.2)$$

$$N^{(Z-1)+}(p) + e \underset{K(q,p)}{\overset{K(p,q)}{\rightleftharpoons}} N^{(Z-1)+}(q) + e \qquad (1.3)$$

$$N^{Z+} + e \xrightarrow{\beta(p)} N^{(Z-1)+}(p) + h\nu \qquad (1.4)$$

$$N^{(Z-1)+}(p) \xrightarrow{A(p,q)} N^{(Z-1)+}(q) + h\nu \qquad (1.5)$$

where $K(p,c)$ is the ionization rate coefficient from the pth quantum state, $K(c,p)$ is the rate coefficient for three-body recombination, $K(p,q)$ is the rate coefficient of excitation (deexcitation) from the pth to the qth quantum state, $\beta(p)$ is the rate coefficient for radiative recombination resulting in populating the pth state, $A(p,q)$ is the spontaneous transition probability from state p to state q. Neglecting transitions due to atom-atom, atom-ion or ion-ion collisions, assuming uniform distribution among degenerate levels, ignoring diffusion effects, for optically thin plasmas one can write

$$\frac{\dot{n}(p)}{n_E(p)} = -\rho(p)\left\{n_e\left[K(p,c) + \sum_{q\neq p} K(p,q)\right] + \sum_{q<p} A(p,q)\right\}$$

$$+ \sum_{q\neq p} \rho(q)\, n_e\, K(p,q) + \sum_{q>p} \rho(q)\, \frac{n_E(q)}{n_E(p)}\, A(q,p) + n_e\, K(p,c)$$

$$+ \frac{n_e^2}{X n_E(p)}\, \beta(p) \qquad (1.6)$$

where $\rho(p) = n(p)/n_E(p)$, $X = n_e/n(N^{Z+})$. $n_E(p)$ is the number density of the species $N^{(Z-1)+}$ in level p in Saha equilibrium with free electrons at density n_e such that

$$X\, n_E(p)/n_e^2 = p^2\, (h^2/2\pi\, mkT)^{3/2} \exp\, (I_p/kT) \qquad (1.7)$$

I_p being the ionization potential of the pth state. Eq. (1.6) should also contain a diffusion term if such effects are important. By substituting numerical values in eq. (1.7) Bates and others[4] have shown that for a wide range of plasmas $n_p \ll n_e,\ n(N^{Z+})$ for $p \neq 1$, violated only in dense plasmas. However, if this condition is valid and the mean thermal energy is significantly less than the first excitation energy then $n(p) \ll n(1)$ when the steady state condition is reached. In transient plasmas n(p) ($p \neq 1$) values reach quasi-equilibrium values very rapidly after which the change in n(p) is insignificant as the plasma decays. Under such condition $\dot{n}(p)$s s($p \neq 1$) can be equated to zero and a set of infinite linear equations can be obtained. For homogeneous steady state plasmas $\dot{n}(p)=0$ is directly obtained. The diffusion term goes to zero as there is no density gradient. For inhomogeneous stationary state plasmas[5] the diffusion term has to be incorporated if diffusion loss of n(p) is significant. For solution of eqn. (1.6), an infinite matrix is avoided by grouping together all the levels with high quantum numbers above p and designating them by σ such that $\rho(\sigma)$ is close to unity. The latter is true for higher states where the collisional processes are relatively

more important than the radiative ones, and n(p) almost satisfies Saha equilibrium densities. If $\rho(1)$ is considered as known, a solution of the set of equations (1.6) can be expressed as $\rho(p) = r_o(p) + r_1(p)\ \rho(1)$, $r_o(p)$ and $r_1(p)$ being the population coefficients of the pth state and are functions of only n_e and T_e. This means that from a knowledge of $r_o(p)$ and $r_1(p)$ the population of the pth quantum state can be determined if n_e and T_e are known.

Determination of $r_o(p)$ and $r_1(p)$ requires information on atomic parameters like rate coefficients, transition probabilities etc. Therefore, the accuracy to which the population coefficients can be obtained depends on the accuracy to which the atomic parameters are known or can be calculated. For hydrogenic plasmas, McWhirter and Hearn[6] worked out the formalism for calculation of $r_o(p)$, $r_1(p)$ coefficients using reduced variables $\theta = T/Z^2$, $\eta(c) = n_e/Z^7$ and $\eta(p) = Xn(p)/Z^{11}$ On hydrogen plasmas, Johnson and Hinnov[7] have recently made extensive calculations based on a new set of electron collisional cross-sections and computed the values of $r_o(p)$ and $r_1(p)$ in the electron density range 10^5-10^{18} and electron temperature range 250^o-8.2×10^6 ^oK for the states p=2,3,4,5,6.

Whereas the collisional-radiative model is simplest to apply in the case of atomic hydrogen plasmas, the need for quantitative understanding is far more general, which means application to non-hydrogenic plasmas. Clearly the complexities

are enormous when the energy levels multiply many times and various sublevels are to be considered, which implies that drastic simplifications in the model are essential in order to make the problem tractable. Before discussing the work hitherto done on the problem of helium plasmas, a brief mention about some of the recent applications of the collisional radiative model to non-hydrogenic plasmas will be informative.

Park[8] has calculated spectral line intensities in a non-equilibrium nitrogen plasma using the method of Bates, Kingston and McWhirter.[4] The objective of his work has been to derive populations of atomic nitrogen states as a function of electron density, electron temperature, and then use intensities of any two atomic nitrogen lines to determine the electron temperature of any nitrogen plasma. In his model, he grouped some of the bound states of nitrogen atom, and a total of 41 groups were involved. He showed that if the equilibrium relation is used for temperature determination, non-equilibrium effects cause the apparent T_e to be higher than the true T_e in an expanding plasma. Above 8000°K, in an expanding non-equilibrium plasma, the departure from the equilibrium line intensity ratio becomes negligibly small.

Recently Giannaris and Incropera[9] have studied a cylindrically confined argon arc plasma and applied the collisional-radiative model to obtain the excited state populations. Here

also, the precise energy level structure of Argon was not retained and levels were grouped, according to common electron configuration, and levels of principal quantum number higher than 15 were assumed to be in equilibrium with free electrons in the plasma. Assuming that the net absorption and emission rates equal for resonant transitions, and using known n_e, n_o and T_e from thermochemical properties of Argon arc, local values of the rate coefficients and radial distribution of the level populations were determined. They found that for the most severe condition of the study, at the wall of 35 A arc, excitation non-equilibrium effects extend to the 6f level. For all arc regions other than the near-wall region, non-equilibrium effects extend only to the 4p level. Further, the non-equilibrium effect is always an overpopulation of the levels relative to the Boltzmann-Saha equilibrium value.

Helium plasmas are interesting for several reasons. Relative to hydrogen, helium is the first atom where the atomic sublevels play an important part in plasma excited state population distribution, yet helium being the simplest of the multi-electronic atoms, the system is relatively most convenient to handle. At the same time, the upper quantum states in helium resemble the atomic hydrogen states more closely than any other atomic system. It is also the simplest atomic system with metastable states (2^1S and 2^3S) which do not have optical transitions to the ground state and hence requires a collisional

mechanism for depopulation to the lowest state. Helium is also known[5] to show the widest deviation from LTE under a set of electron density and electron temperature conditions. Experimentally, helium being monoatomic, it is a relatively simple matter to ascertain its neutral concentration in plasmas, whereas hydrogen being a diatomic gas, it is often difficult to determine the percent atomic concentration in hydrogen plasmas where the gas is only partially dissociated. Further, collisional-radiative model already worked out for hydrogenic ions can be easily applied to He^+ ions in a helium plasma.

A mention of some of the helium plasma experiments will be appropriate here though all of them are not directly related to the present work. Most of the experiments in which helium excited state population have been the subject of study used afterglows. In Princeton plasma physics laboratories Motley and Kuckes[10] studied He afterglow discharges in the B-1 stellarator and showed, using microwave phase shift measurements for determination of n_e and conductivity measurements for T_e, that the principal mechanism of charge removal in low temperature highly ionized helium plasma is the three-body recombination reaction. Hinnov and Hirschberg[11,12] measured absolute intensities from the spectrum of afterglow obtained from B-1 stellarator and their conclusions are compatible with those of Motley and Kuckes. Further, Hinnov and Hirschberg derived the recombination coefficients as a function of n_e in the range

10^{11}-10^{15} and in the T_e range 0.1-0.4 eV. They also studied the population densities, both theoretically and experimentally, from the afterglow emission intensities, and found that the experimental population densities compare well with the theory, taking only n=3,4,5 levels. Their calculations, however, did not take into account splitting of sublevels.

Johnson[13] has done experiments on afterglow and also on ohmic heating of discharges in the n_e range of 10^{12}-10^{13} and T_e of 0.25 and 4-14 eV. He used a collisional-radiative model with levels up to n=25 with separated sublevels up to n=8. He assumed that above n=25 Saha equilibrium is valid. He also calculated collisional-radiative recombination coefficient which he compared with experimental values. Johnson and Hinnov[14] have done experiments on afterglow with ohmic heating in the density range 10^{12}-10^{13} and T_e range 0.04-1 eV. Comparison with experimental results shows that the rate coefficient $K(2^3S \rightarrow 1^1S)$ cannot adequately account for the observed populations, a more likely path is through the process $2^3S \rightarrow 2^1S$ followed by deexcitation to the ground state. It may be mentioned here that in an earlier work Myers[15] had suggested that the mechanism of metastable cooling is through atom-atom collisions, ionization, followed by ion-molecule reactions.

In Collins and Robertson's[16] flowing afterglow experiments, at n_e of 5×10^{12} and maximum temperature of 0.15 eV, it was found that above n=6 Saha equilibrium exists and below this

level the population densities can be explained by the collisional-radiative model. They also concluded that the primary process of populating these levels is the collisional-radiative recombination of He^+ ions. Gusinow, Gerardo and Verdeyen[17] studied afterglow plasma at 2-8 Torr in the n_e range 10^{13}-10^{15} and T_e range 0.09 to 0.6 eV and used He-Ne laser interferrometric technique to measure n_e and T_e. They found that the experimental value of α is comparable to that calculated from the collisional-radiative model of Bates, Kingston and McWhirter. Born and Buser[18] studied afterglow phenomena from a condenser discharge in the pressure range 0.3-0.7 Torr, $n_e = 10^{12}$-10^{14}, T_e = 0.17 eV. According to them the decay of the metastable state 2^3S was not by usual deexcitations; diffusion to the wall is a more important cause for the observed temperature decay.

Of other kinds of experimental systems, Robben, Kunkel and Talbot[19] have done experiments in helium plasma jet at T_e range 0.15-0.3 eV and n_e range of 10^{12}-10^{14} and has shown that K(p,q), (p=q+1), values remain constant in the range of experimental conditions used and the measurements are consistent with Gryzinski's[20] values. Va Fugol, Pakhomer and Reznikov,[21] using high frequency discharge experiments at 1 Torr, T_e 12-4 eV, have shown that the metastable 2^3S lifetime is 2×10^{-4} sec and the metastables are responsible for He_2^+ formation as well as for the intense afterglow. Newton and Sexton[22] conducted

experiments on pulse discharges in the n_e range 8×10^{11}-1.8×10^{15} and pressure range 0.82-1.2 Torr. Their major conclusion is that the metastable atoms deactivate by volume deexcitation in the n_e range 10^{14}-10^{15}, but at lower densities wall deactivation is likely.

Ikee and Takeyama[23] have recently studied brush cathode plasmas in a magnetic field. They determined n_e and T_e from measurements of spectral intensities of the continuum spectrum which follows the series $2^3S \leftarrow n^3P$. From a plot of log $(\epsilon(\lambda)^5/\sigma_c)$ vs $1/\lambda$ (ϵ is the emission coefficient and σ_c is the photoionization cross-section) they determined T_e, and from the absolute value of $\epsilon(\lambda)$ the value of n_e. At a discharge current of 500 mA and a pressure of 0.9 Torr, T_e is 0.17 eV and n_e 1.8×10^{13}. The recombination rate calculated from the experimental results, which is equal to 2.2×10^{-10} cm^3 sec^{-1} at $T_e = 0.17$ eV and $n_e = 1.8 \times 10^{13}$, is in good agreement with that calculated from the collisional-radiative recombination theory of Bates, Kingston and McWhirter. The n_e was found to increase by one order of magnitude compared to n_e without the magnetic field.

Ikee and Takeyama[24] have also studied population densities of HeI excited states in brush cathode plasmas. They measured spectral line intensities for the transitions $2^1S \leftarrow n^1P$, $2^1P \leftarrow n^1D$, $2^3S \leftarrow n^3P$, $2^3P \leftarrow n^3S$ and $2^3P \leftarrow n^3D$ up to n=10 and determined the population densities of the excited states. They found that

for $n \geq 5$ the states are in thermal equilibrium and from Boltzmann plot determined the temperature, which was found compatible with the free electron temperature measured from recombination continuum. By interpolation of Saha increment values b_n as given by Drawin and Emard,[25] theoretical population densities were calculated for n_e, T_e values of the experiment. A comparison of the theoretical population densities with those obtained from the experiments on absolute intensity measurements show that the results match within the errors of interpolation of b_n and the experimental measurements.

Recently Otsuka, Ikee and Ishii[26] have made studies on helium plasma using their TPD (Test Plasma by Direct current discharge) machine. They made spectroscopic measurements of HeI and HeII line intensities at various points of the magnetized plasma column and also measured plasma parameters at the points of emission intensity measurements. The T_e range of their experiments was 0.2-8 eV, $n_e \sim 10^{14}$ and system pressure $\sim 10^{-3}$ Torr. From emission intensities, absolute population densities of the HeI states and HeII (n=4) states were determined. Estimates were made of n^{++} densities and these were applied to predict, using a collisional radiative model, the expected population densities for HeII (n=4) state. They also proposed a mechanism, for the observed phenomena in TPD machine, according to which He^{++} recombination is the major process upstream in the plasma column causing HeII excited states to be populated

by cascading of higher states. At downstream conditions, with lower electron temperatures, recombination of He^+ ions constitutes the major process causing higher levels of neutral helium to increase in population density which results in enhanced emission from such states.

Emission enhancement studies of HeII line 4686 Å have been made by Takeyama and Takezaki[27] in a longitudinal magnetic field in the pressure range 0.4-4 Torr and magnetic field intensity of 0-6 kilogauss. They find that the emission intensity has a maximum enhancement dependent on the pressure. The characteristic pressure for maximum intensity increases as the longitudinal field increases. They, however, do not offer any explanation for the emission enhancement. In a later work Takeyama and Takezaki[28] measured enhancement of helium neutral lines and found that the relative intensities belonging to $2^1P \leftarrow n^1D$ (6678, 4922, 4388 A) and $2^1S \leftarrow n^1P$ (3965 and 3614 A) series of HeI increase as the longitudinal field is increased. The enhancement becomes maximum at about 2 kilogauss. The lines belonging to the other four series $2^1P \leftarrow n^1S$, $2^3S \leftarrow n^3P$, $2^3P \leftarrow n^3S$ and $2^3P \leftarrow n^3D$ (except the line 5876 A) however do not show any enhancement, on the contrary, the relative intensities monotonically decrease as the field increases.

While some of the experimental work reported above involved calculations, there has been considerable work solely from theoretical side. D'Angelo[29] calculated the value of recombination

coefficient α in helium systems in the T_e range 0.26-0.9 eV and n_e range 10^{11}-10^{13} using a model of three body recombination and found the calculated values matched well with the large values of α obtained in Motley and Kuckes[10] experiments. Bates and Kingston[30] used approximate expressions for He^+-e elastic scattering cross-section to calculate quasi-equilibrium electron, ion temperatures and the corresponding collisional radiative recombination coefficient α and compared the calculated values, in the n_e range 10^9-10^{15}, with the experimental results of Hinnov and Hirschberg[12] on afterglows. Bates, Bell and Kingston[31] have also calculated the properties of a decaying optically thick plasma in the T_e range 0.09-1.4 eV and n_e range 10^8-10^{16} in which they took into consideration Penning ionization, and concluded that the primary process which determines the population of the first excited state is collisional-radiative recombination.

Drawin and coworkers have made extensive calculations of population densities in helium systems. Initially, Drawin[32] made some calculations of population densities of HeI states and in a recent work Drawin, Emard and Katsonis[5] have repeated the same calculations with refined atomic constants like term values, transition probabilities and cross-sections. The results are applicable to homogeneous stationary, transient and inhomogeneous diffusion dominated plasmas. The general model is similar to that of Bates, Kingston and McWhirter[4] but

for actual calculations they have taken a total of 51 levels, which include the 1^1S ground state, and the states 2^1S, 2^1P, 2^3S, 2^3P. The remaining 46 levels are equally divided between singlet and triplet series without special distinction between the sublevels, S, P, D etc. of the same principal quantum number, and going upto n=25. In the earlier work atom-atom exchange collisions between singlet and triplet levels had been incorporated, but in the recent work they are not included; which helps keep the rate equations linear. Instead, they have added electron-atom exchange collisions in the model and this partially makes up for the error involved in neglecting the atom-atom exchange interactions and, for degrees of ionization larger than 10^{-3}, the electron-atom collisions are much more efficient than atom-atom collisions. They made calculations for the limiting cases of optically thin and optically thick plasmas and also for intermediate cases where the degree of radiation trapping is intermediate between the extreme cases.

As indicated earlier, in homogeneous plasmas the rate equations simplify easily. Treatment of inhomogeneous or transient plasmas can be simplified if (a) for transient plasmas the relaxation times are short, and (b) for the inhomogeneous plasmas, the relaxation lengths are smaller than the smallest lateral dimension of the plasma in the direction of the gradients. In case of the latter, the system can be taken to be in quasi-homogeneous state and the divergence of the diffusion fluxes of

all the excited levels can be put equal to zero. Drawin and others[5] have given results of population density calculations in the electron density range 10^{10}-10^{20} and T_e range 0.09 to 11 eV for optically thin, optically thick and partially optically thick helium plasmas using explicit values of escape factors for various transitions involved. They also provide results for Saha decrements of ground state population and electron densities, and they find that trapping of resonance photons make significant changes in the ground state Saha decrements for electron densities $<10^{16}$. In all the cases of radiation trapping the Saha decrements are greater than unity for $n_e < 10^{17}$.

Drawin and others[5] have also applied the results of their calculations mentioned above to the experiment of Boersch, Geiger and Topschowsky[33] on He arc discharge. The latter experimenters did not provide a clear value for the electron temperature. Using the collisional-radiative model, Drawin and others[5] made calculations, for a range of T_e values and for a ground state population of 5.5×10^{15}, for the population of excited states using both inhomogeneous and the homogeneous stationary state model. In the n_e range 10^{12}-10^{13} and T_e = 2.8 eV good agreement between the measured and calculated values were found.

The above sample list of experiments and theoretical calculations on the helium system shows that work in both the categories has been numerous and widely varied, with overlaps in some

cases. Part of the difficulty in comparing one set of results with another however is that, in spite of special care, it is difficult to completely specify all experimental conditions in discharges, and sometimes unspecified parameters contribute significantly to the observed phenomena. But in principle, all experimental results should be explicable from one physical model, when appropriate allowances are made for different experimental conditions. No experiment or theoretical work referred above has explicitly undertaken such an extensive task. This is probably because a great deal more of experimental data is necessary, which implies that the understanding at this stage has necessarily got to be evolutionary in character, and gradually the gaps will be bridged. The present work was undertaken as an effort in this direction.

The purpose of the present study is to examine, experimentally, the applicability of the collisional-radiative model to low-temperature moderate density helium plasmas. The way it differs from some of the experiments reported earlier is that by varying some experimental parameters, a wide range of n_e, T_e conditions are realized in the plasma. The extended range of n_e, T_e provides a wider scope of testing this model. Specifically, the emission of HeI and HeII line radiation is studied under varying n_e, T_e conditions, and attempts made to understand the observed line intensities from application of a collisional radiative model.

Experimentally, the system that is used in the present work is a stationary state plasma system which has similarities to the positive column. Whereas in general the plasma electron density can be increased by injecting more power and more electrons into the plasma column, one alternative and convenient way to effect this is to gradually inhibit diffusion of the electrons to the wall containing the plasma by using a confining magnetic field. If the plasma is ignited in a cylindrical column and a longitudinal magnetic field is applied, the effect on the plasma charged particles is to confine the latter preferentially near the axial region with a consequent increase in electron density. Thus a much larger and efficient increase of electron density can be achieved in this manner concurrent with the reduction of transverse diffusion. Though the quantitative aspects of such inhibition of transverse diffusion[34-37] is a subject of considerable discussion and the exact dependence of the diffusion coefficient of the magnetic field is not entirely clear, the monotonic increase of the density is an experimentally observed fact.[38] Also known is the fact that with increase in field, the electron temperature decreases due to more frequent collisions with electrons and consequent loss of electron energy.[38] Thus in a plasma column subject to a longitudinal magnetic field, with change in magnetic field intensity the plasma column behaves as a reaction volume which moves through

a coupled variation of electron temperature and electron density and thus controls the excited state populations through detailed excitation-deexcitation processes. While the diffusion processes are unavoidably present, in a stationary state plasma soon a radial concentration profile is established for all the plasma species. For electrons and other charged particles one expects a maximum concentration on the axis. From a theoretical analysis of diffusion processes in cylindrical plasma columns it follows that the electron density radial profile is like a zero order Bessel function[39] $R(r) = R(0)J_o\ (2.405\ \frac{r}{a})$ where r is the distance from the axis and a is the tube radius (2.2 cm in the present case). This means that for a considerably wide zone near the axis, the electron density can be taken as practically invariant, e.g., within 10% variation, if $r \approx 0.35$ cm (size of the baffle in the present experiments). In this region the plasma resembles a homogeneous stationary state plasma. That the excited state populations follow somewhat similar distributions has been experimentally shown by Giannaris and Incropera.[9]

In the present work emission intensities of HeI and HeII lines are measured end-on from the near-axial region of a plasma column subjected to a longitudinal magnetic field. Plasma diagnostic measurements are carried out also in the same region. With increase in the magnetic field, the line emission intensities increase, and these emission enhancement

factors are experimentally measured. These emission enhancement results are then compared with the predictions of a collisional-radiative model, for both optically thin and optically thick plasma conditions. For application of the collisional-radiative model to stationary state plasmas and particularly to the emission enhancement results of the present investigation, independent calculations of population coefficients are also carried out. The results of these calculations are compared with those of other workers. Further, the model used in the present work is applied to some helium plasma experiments reported in recent literature.

Chapter II

EXPERIMENTAL

All the experiments are carried out in a long cylindrical discharge tube with conducting wall. The discharge is sustained by low energy electrons injected into the plasma column from an electron gun. The longitudinal magnetic field applied on the plasma is provided by a solenoid aligned coaxially with the discharge tube axis. The radiation from the plasma is taken out through a quartz window, collimated by a set of baffles external to the discharge tube and then analyzed using a grating monochromator.

The details of the discharge tube are schematically shown in Fig. 2.1. The tube is about 1 m in length and 2.2 cm in internal diameter. At both ends of the tube, chambers of internal diameter 9 cm and length 10 cm are connected and are used for mounting the electron gun, optical windows, vacuum gauges,

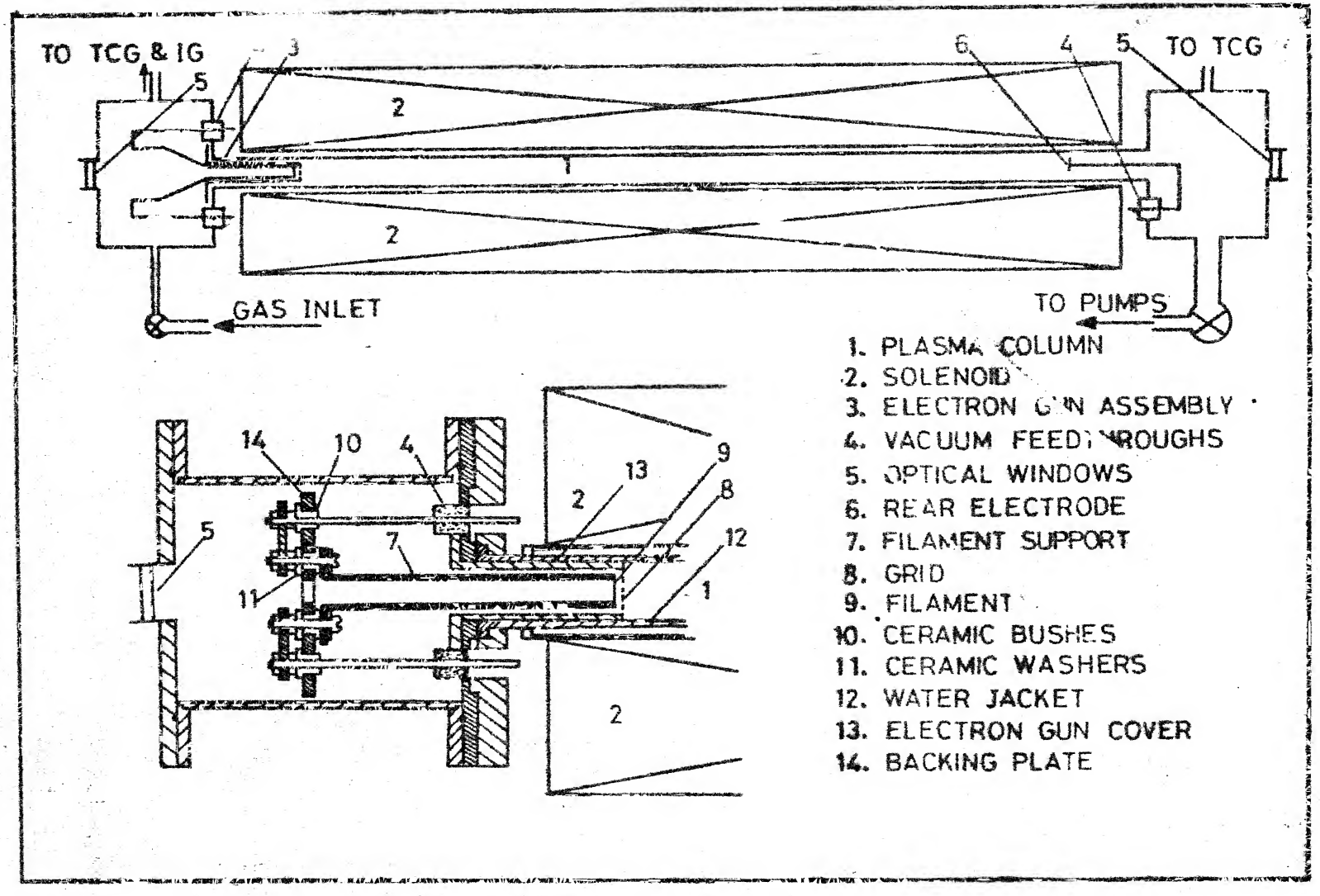

Fig. 2.1 Schematic diagram of the discharge tube

pumping line connections, gas inlet valve and electrical feed-throughs. The central tube as.well as the side chambers, made out of 304 non-magnetic stainless steel, are provided with water cooling jackets. The system is pumped by a 10 cm oil diffusion pump backed by a mechanical pump. There is an isolation valve between the diffusion pump and the discharge tube which permits, during an experiment, partial or total isolation of the system from the pumping line.

The outer cover of the electron gun consists of a 6 cm long 2.1 cm diameter stainless steel tube. The electron gun assembly is mounted on a 5 cm diameter stainless steel flange which itself is mounted on a 7.5 cm diameter backing plate using a set of 2.5 cm long ceramic insulators. A 0.5 mm diameter tungsten filament, shaped in the form of a 1 cm diameter circular ring is mounted on two 2 mm diameter tungsten rods, through which filament power is supplied.

The filament is located 2 mm inside the top end of the outer cover and inside a guard ring made of 1 mm tungsten wire wound in the form of a coil and mounted coaxially with the electron gun cover. The guard ring is electrically insulated from the outer wall of the gun and the filament. The top end of the gun has also a grid made of 0.25 mm tungsten wire placed 2 mm away from the plane of the filament. The grid which is in contact with the body of the gun, is also shorted to the discharge tube. The electron gun can be pushed inside the

discharge tube in such a manner that the backing plate rests on the electrical feedthroughs mounted on the collar of the central tube. There is a clearance of 1 cm diameter through the filament ring and the backing plate for end-on measurements of plasma radiation.

The magnetic field is provided by a solenoid mounted coaxially with the central discharge tube. The solenoid is wound with 20 SWG super-enamelled copper wire on a 95 cm long 4.2 cm diameter spool and is capable of generating about 250 gauss per ampere. The maximum current capability of the wire, with ambient air cooling, is about 4 amp.

The filament is biased 150 volts negative with respect to the discharge tube, the latter being kept at ground potential. The guard ring is at the same potential as that of the filament to minimize electron emission towards the wall. At the other end of the discharge tube a 1.5 cm diameter electrode or a stainless steel wire gauge disc, kept at ground potential, was placed, which constrained the 90 cm long plasma column to be free of external field. No observable difference in experimental results was found in these two modes of operation.

The electrical arrangement is shown in Fig. 2.2. The filament requires about 25 amp current (I_F) for 4 amp or electron emission current (i_e) and this is provided by a variable dc power supply. The drop across the filament is negligible compared to 150 V bias voltage. The bias voltage

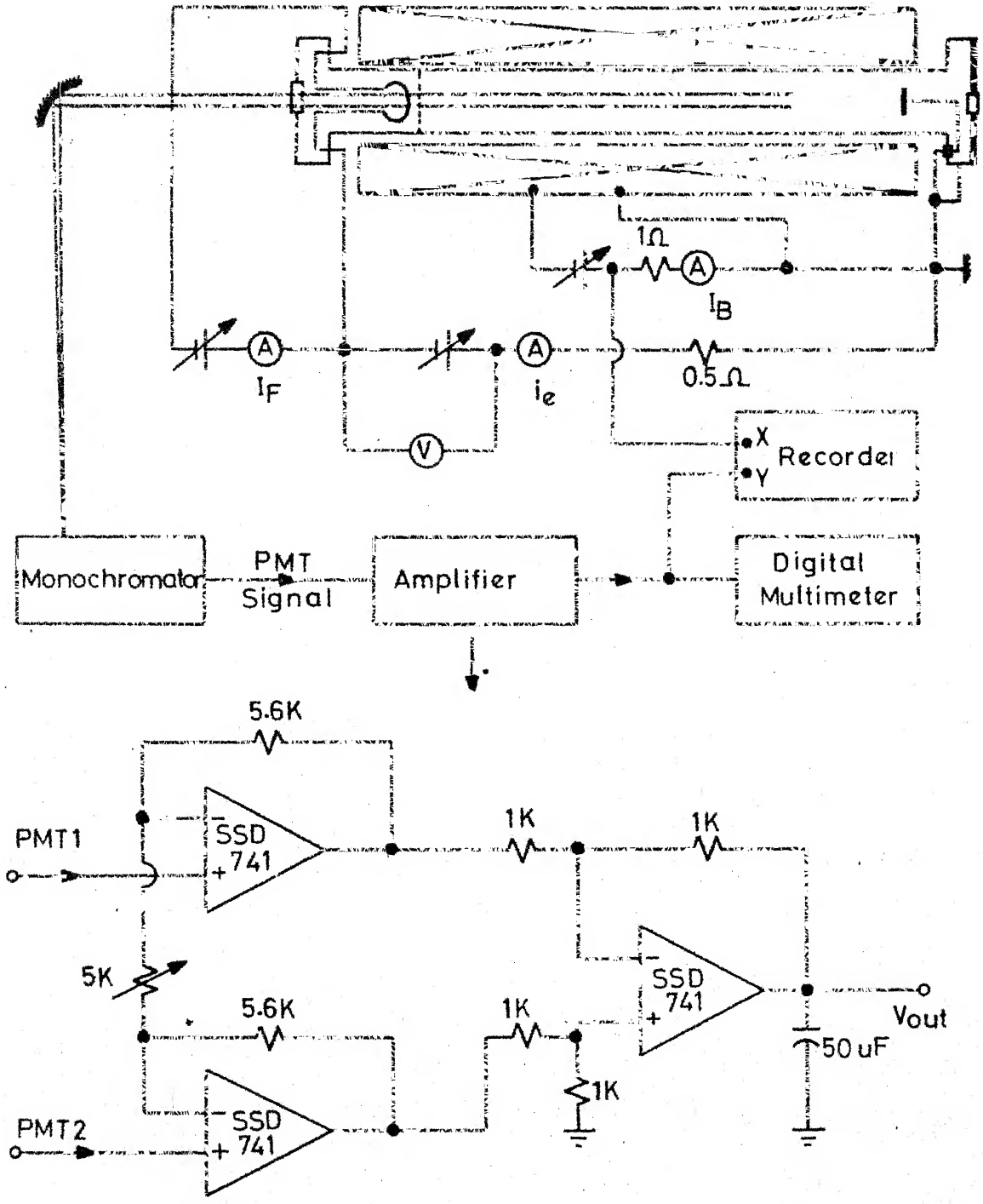

Fig. 2.2 Electrical arrangement in the expt.

is provided by a 200 volt 5 amp floating power supply through a 0.5 ohm limiting resistor and an ammeter for measurement of the electron emission current injected into the plasma column. The filament is located entirely inside the magnetic field and away from the rest of the mounting assembly. This assists the emitted electrons to be drawn into the plasma column. A 300 volts power supply is used for the solenoid and is connected through an ammeter and a 1 ohm (20 watt) resistor. The voltage sensed across this resistor provides a measure of the magnetic field applied.

The discharge system is pumped by a 10 cm oil diffusion pump backed by a mechanical pump to a pressure of 10^{-5} mm of Hg. From a careful study of leakage rates it was concluded that lower pressures could not be reached mainly because of the inefficiencies of the pumps and not due to any significant leakage. The pressure is measured by thermocouple and Bayard-Alpert ionization gauges. Both the gauges and their controls were calibrated against a Stokes McLeod gauge with helium gas in the system. Helium gas (Matheson, specified purity 99.99%) is introduced into the system through a needle valve. The required gas pressure (all experiments reported in the present work were carried out at 5×10^{-3} Torr) is maintained by controlling the flow rate through the valve. By concurrent control of the needle and isolation valves study could be done in a partially closed system to see the influence of flow rate on enhancements of radiation in magnetic field.

The radiation is observed along the axis of the discharge tube through the backing plate of the electron gun. To see that only parallel radiation from the plasma column along the axis is collected, the radiation is passed through two baffles of 0.7 cm diameter opening centred along the axis of the tube. The baffles are located such that they reject all radiation leaving the tube with an angle more than 0.5° with the axis. Measurements were also carried out with baffles .35 cm diameter without noticeable changes in experimental results, except the absolute intensities. The collimated beam is then focussed on the slit of the monochromator by a concave mirror which is placed 1 focal length away from the slit. A high resolution spectrometer built in our laboratory[40] is used as the monochromator (Appendix Fig. A.1). It uses a Bausch & Lomb 128x154 mm replica plane grating with 1200 grooves/mm blazed at 7500°A and employs Ebert-Fastie mounting in Czerny-Turner modification. The spectrometer can be operated either in 2.1 m or 6.4 m mode leading to a first order dispersion of 3.4 Å/mm and 1.12 Å/mm respectively. In the first order, the range of the spectrometer is 5040 to 12020 Å. The spectrometer is equipped with a camera for use with photographic plates as well as a set of two photomultiplier detectors for simultaneous measurements of 2 line intensities, if the lines are closely located. The slit width used for most measurements was 0.035 mm. The spectrometer was operated in 2.1 m mode for

the present experiments. The two photomultipliers (1P28, maximum response in 3400±500 A region) are mounted in two different housings, which have slit openings of .020-.030 mm x 25 mm located on the focal plane of the monochromator focussing elements. The dynodes of the photomultipliers are biased from a highly stabilised Fluke power supply (0.25% stability) and normally operated at 1000 volts. The photomultiplier anode currents are taken to an instrumentation amplifier operated in the difference mode as shown in Fig. 2.2. The amplified signal is taken to a digital voltmeter (sensitivity 0.1 mV) for direct readout or to an X-Y recorder.

Enhancement Experiments

The emission enhancement experiments were carried out as follows. The discharge system was first evacuated and helium admitted to the system through a needle valve to attain the required pressure. -150 volts bias was applied to the filament and the filament current was slowly increased till the desired emission current i_e was reached. The monochromator was set for the required emission line such that the slit of one of the photomultipliers is on the centre of the line while position of the other is adjusted on the continuum about 50 A away from the emission line. The output of the difference amplifier is recorded (which subtracts for the continuum intensity). The magnet current is then systematically increased

which permits measurement of line intensity at various magnetic field values. An intensity measurement in the absence of the field provides I_o. Enhancement ratios I_B/I_O can then easily be calculated.

Emission Intensity Ratios at Two Emission Currents: $(I_{i_1}/I_{i_2})_B$

These measurements are similar to those for simple emission enhancements in magnetic field. Here the information desired is the ratio of line emission intensities at two emission currents, at various magnetic fields. The magnetic field is first set to a desired value; the emission intensity of a given line is measured first at one emission current and then at the other. Independent zero corrections for the intensities are made by moving the photomultiplier to continuum, because the continuum intensity changes significantly with change in the emission current. Due to limitations of the biasing power supply an increase in the emission current results in lowering of the bias voltage, so every such change required readjustment of the bias voltage to -150 volts.

Langmuir Probe Measurements

A 2 mm long single probe was used, made of 1 mm diameter tungsten wire. The probe was provided with a glass shield at the base of the wire to reduce effects due to sputtering deposits. The conditions (i) the dimension of the probe < mean

free path of the ions, (ii) probe current << discharge current, and (iii) negligible disturbance of the plasma field by the probe were satisfied. The probe was introduced into the column from the pump end and the probe tip was located at the centre of the column. The nature of variation of probe characteristics as the probe position was varied along the axis was noted.

Measurement of HeI and HeII Line Intensity Ratios

In order to get an idea about the excited state populations of HeII using the line intensity ratio method, HeI 4713 A and HeII 4685 A lines were used. For this pair of lines, with a fixed setting of the grating (2nd order, 2.1 m operation) the detectors were moved for measuring the intensities, one after another. Appropriate continuum corrections were also made. Similarly, for determination of electron temperature, intensity ratios of singlet-triplet lines 5047 A to 4713 A and 4921 A to 4471 A were measured at various emission currents at different magnetic field value.

Chapter III

RESULTS

Emission Enhancements in Magnetic Field (I_B/I_o)

$n^{3,1}L \rightarrow 2^{3,1}(L\pm1)$ series of HeI lines were used for line intensity enhancement measurements in the presence of magnetic field. The details of the lines chosen are given in Fig. 3.1. In all, 16 HeI atomic lines were studied. They lie in the range 3000-7000 A and are easily accessible in the monochromator used. For the series $n^1D \rightarrow 2^1P$ (n = 3,4,5,6), plots of I_B/I_o, i.e., the ratio of the line intensity at a given magnetic field B to that at zero magnetic field as a function of the field are shown in Figs. 3.2, 3.3, 3.4 and 3.5. For each line I_B/I_o was measured at emission currents of 0.5 amp, 1 amp, 2 amp and 3 amp. In Figs. 3.7, 3.8 and 3.9, variations of I_B/I_o with magnetic field are shown for the triplet series $n^3S \rightarrow 2^3P$ (n = 3,4,5). In Figs. 3.6 and 3.10, the (I_B/I_o-B)

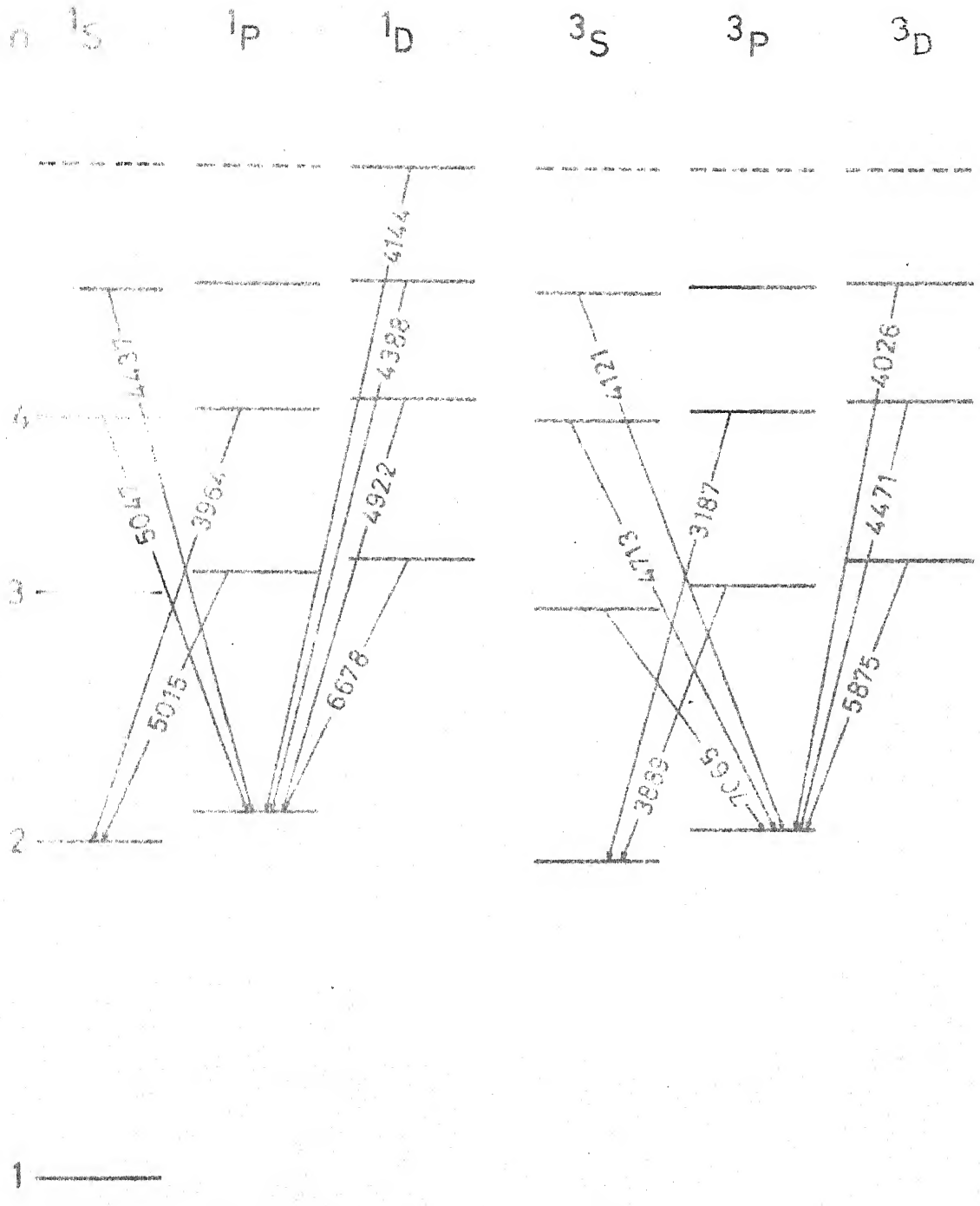

Fig. 3.1 He lines chosen for measurement (energy levels not to scale; wavelengths are in Å)

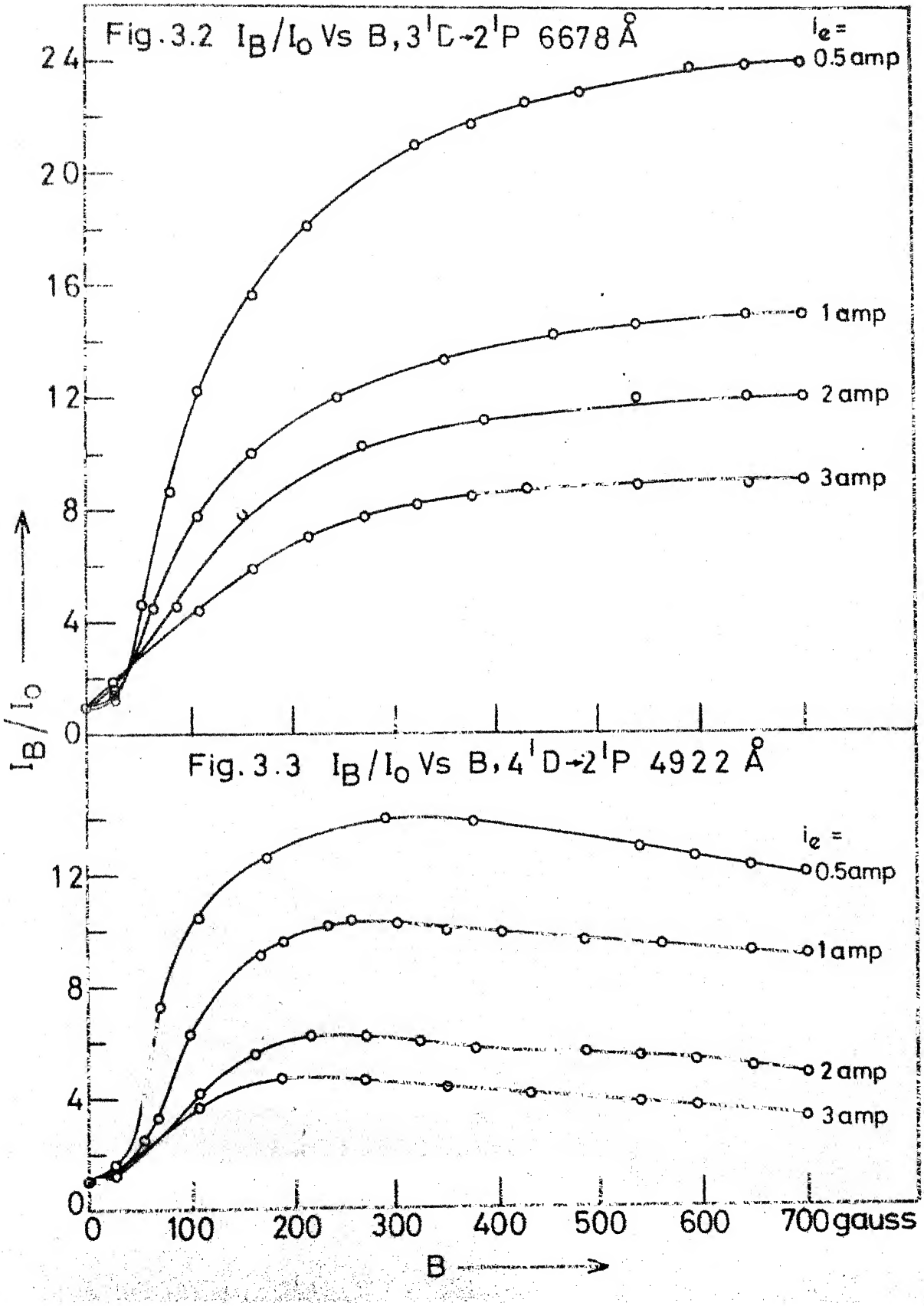
Fig. 3.2 I_B/I_o Vs B, $3^1D \rightarrow 2^1P$ 6678 Å
i_e =
0.5 amp
1 amp
2 amp
3 amp
I_B/I_o
0
4
8
12
16
20
24
Fig. 3.3 I_B/I_o Vs B, $4^1D \rightarrow 2^1P$ 4922 Å
i_e =
0.5 amp
1 amp
2 amp
3 amp
0
4
8
12
0
100
200
300
400
500
600
700 gauss
B

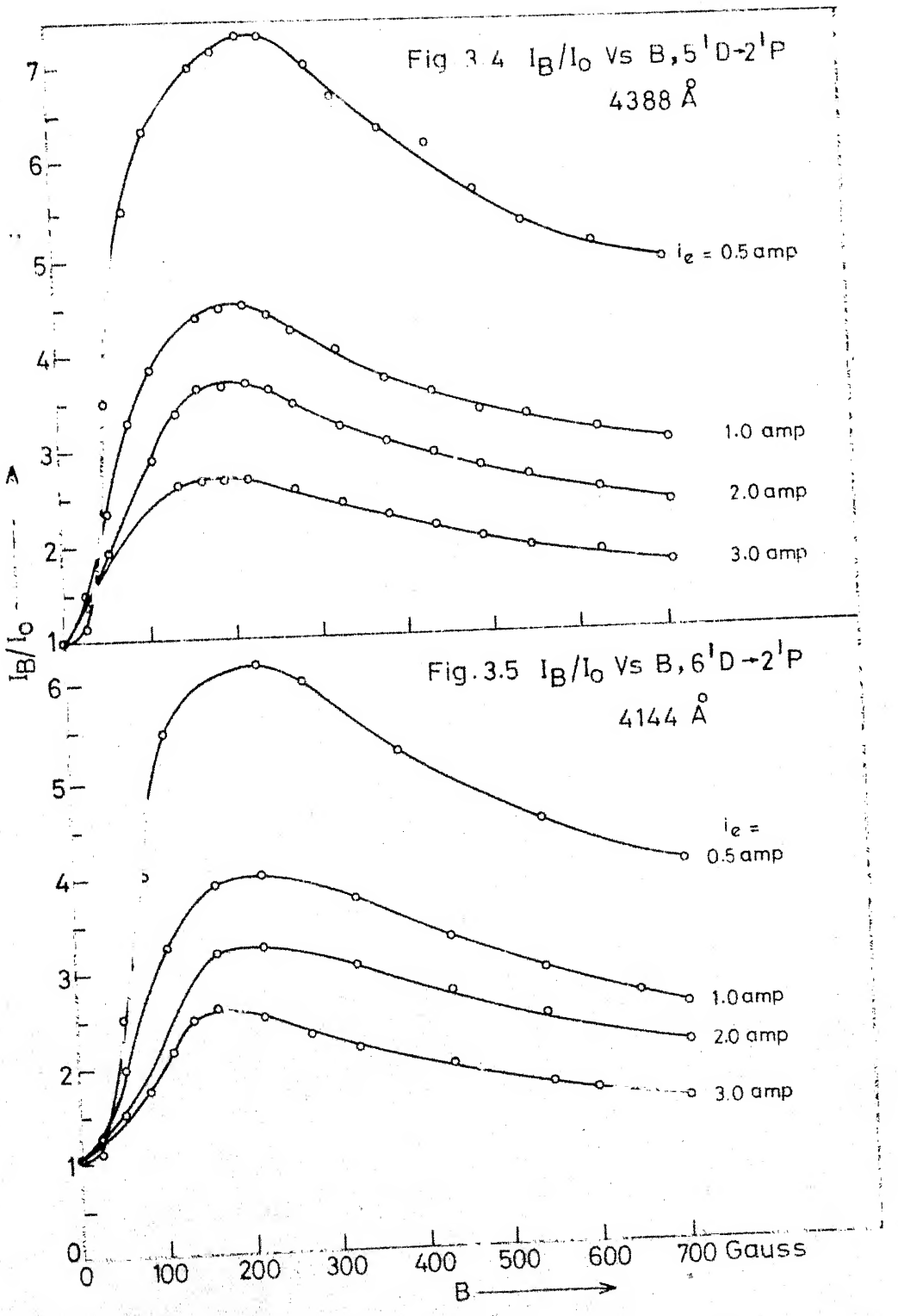
Fig 3.4 I_B/I_o Vs B, $5^1D \rightarrow 2^1P$
4388 Å
i_e = 0.5 amp
1.0 amp
2.0 amp
3.0 amp
I_B/I_o
Fig. 3.5 I_B/I_o Vs B, $6^1D \rightarrow 2^1P$
4144 Å
i_e =
0.5 amp
1.0 amp
2.0 amp
3.0 amp
0
100
200
300
400
500
600
700 Gauss
B

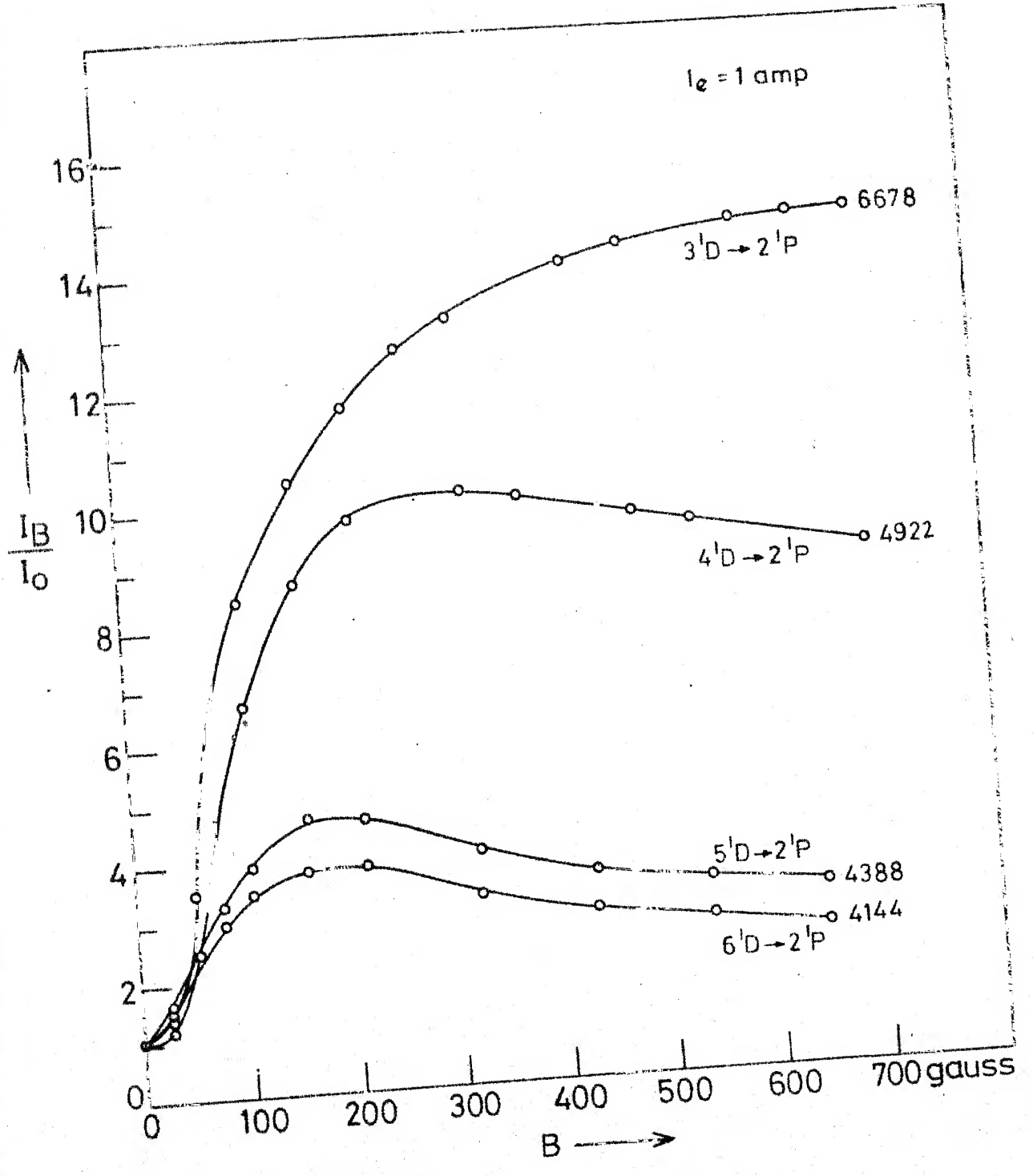

Fig. 3.6 Comparison of I_B/I_o for the series $n^1D \rightarrow 2^1P$ at 1amp emission current

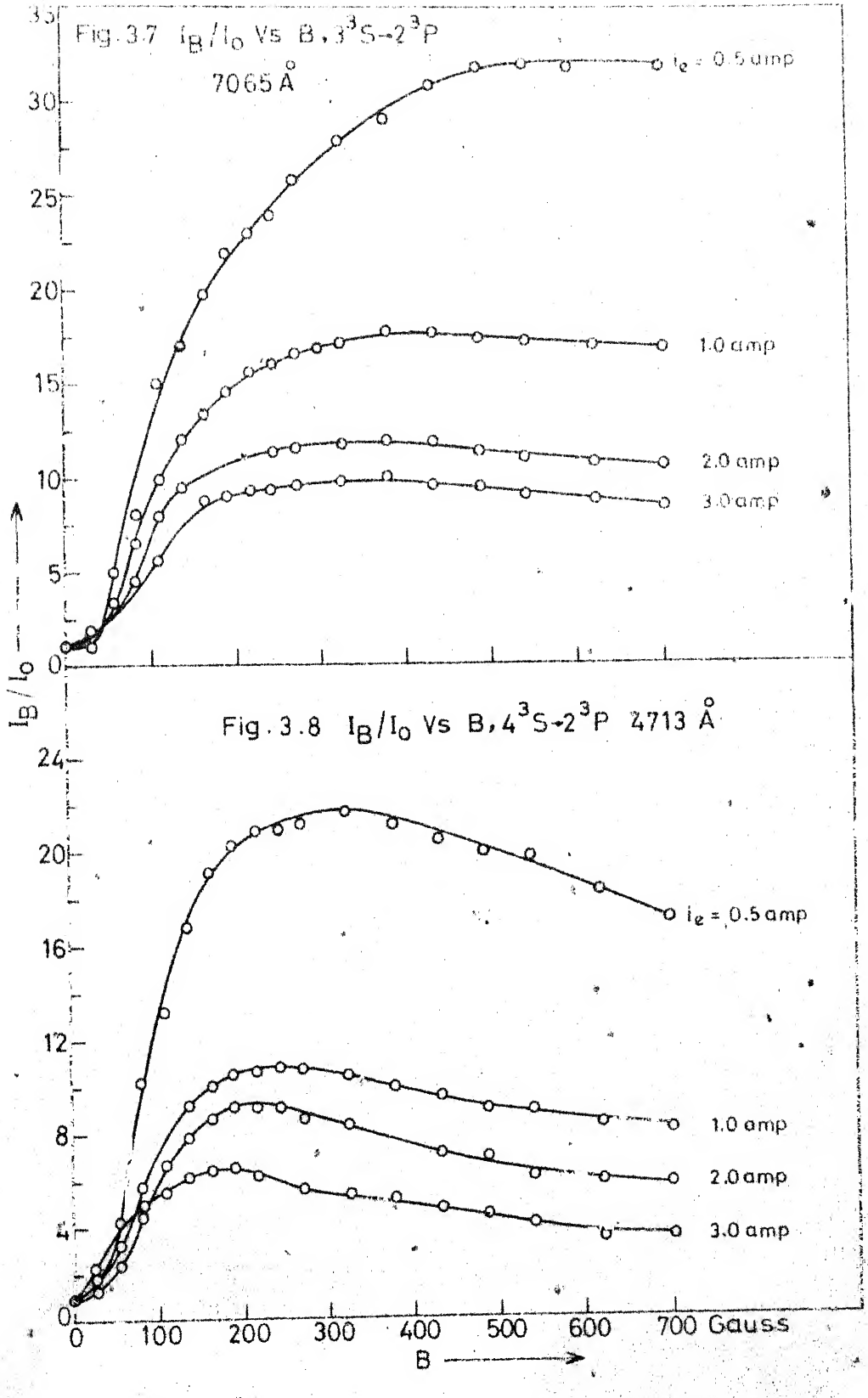
Fig. 3.7 I_B/I_o Vs B, $3^3S \rightarrow 2^3P$
7065 Å
i_e = 0.5 amp
1.0 amp
2.0 amp
3.0 amp
I_B/I_o
B
0
5
10
15
20
25
30
Fig. 3.8 I_B/I_o Vs B, $4^3S \rightarrow 2^3P$ 4713 Å
i_e = 0.5 amp
1.0 amp
2.0 amp
3.0 amp
0
4
8
12
16
20
24
0
100
200
300
400
500
600
700 Gauss

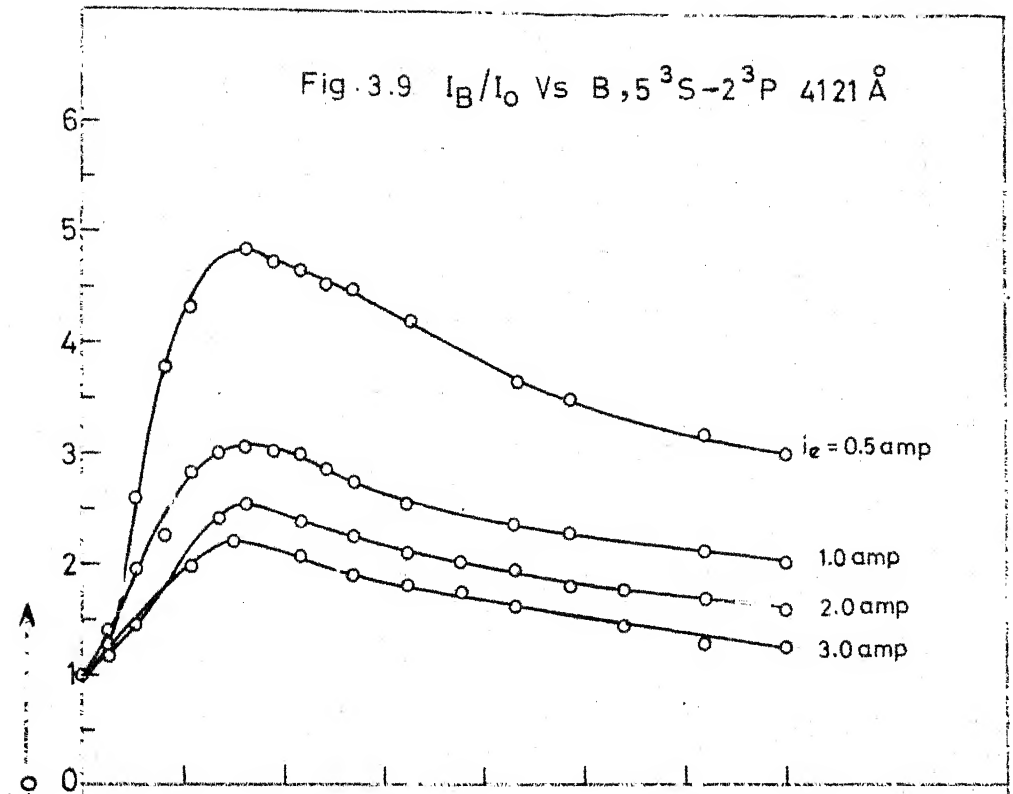

Fig. 3.10 Comparison of I_B/I_o for the series $n^3S \rightarrow 2^3P$ at 1amp. emission current

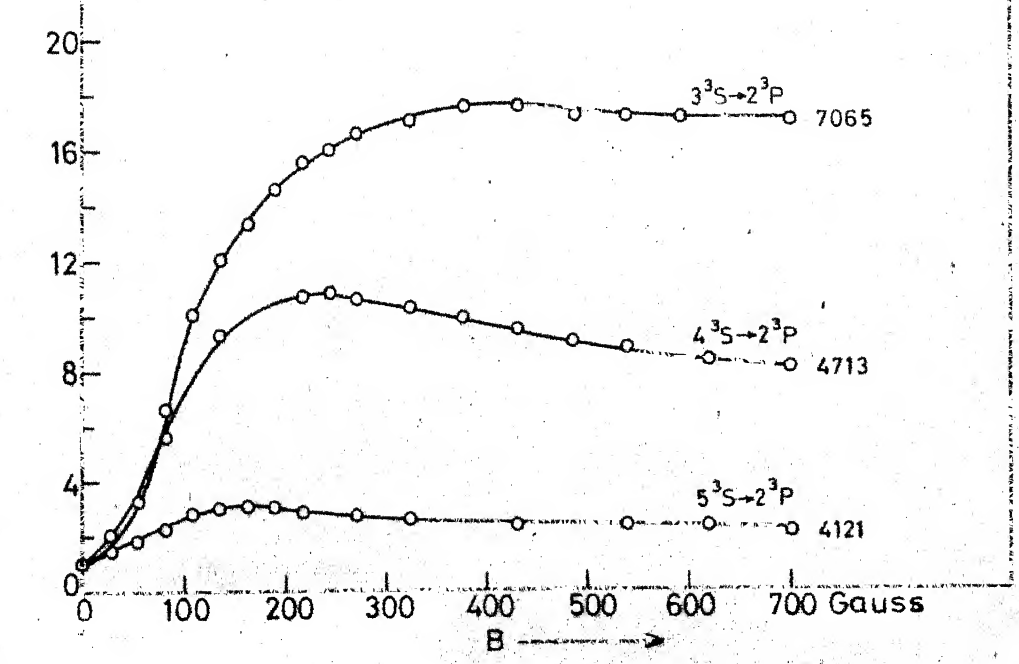

plots for the series $n^1D \rightarrow 2^1P$ and $n^3S \rightarrow 2^3P$ are compared at a constant emission current of 1 amp.

From the results shown in Figs. 3.2-3.5 and 3.7-3.9, the following general observations can be made.

(a) Lower the emission current, higher is the enhancement factor I_B/I_o.

(b) For the first line of any series, I_B/I_o increases rather rapidly in the lower magnetic field range (0-350 gauss), and then the increase is relatively less steep. For the other lines of the series, the enhancement factor increases, passes through a rather broad maximum, and slowly decreases at the highest magnetic fields.

(c) For a given line, as the emission current increases, the magnetic field at which a maximum in the enhancement factor is observed shifts to decreasing field values. This trend is somewhat less noticeable for higher lines of any series.

(d) From Figs. 3.6 and 3.10, it can be seen that at a given emission current, the magnetic field at which the maximum enhancement is observed decreases with increase in the energy of the emitting state. Sharp fall in the enhancement factor is observed for higher lines in the series.

Similar enhancement studies were carried out for all the four other series, viz., $n^3D \rightarrow 2^3P$ (n = 3,4,5), $n^3P \rightarrow 2^3S$ (n = 3,4),

$n^1S \rightarrow 2^1P$ (n = 4,5), $n^1P \rightarrow 2^1S$ (n = 3,4). For brevity, values of $(I_B/I_o)_{max}$, i.e., the maximum value of I_B/I_o attained, for all the lines of the above series and the corresponding magnetic field, at the four emission currents, are presented in Table 3.1. The Table also gives $(I_B/I_o)_{700}$, i.e., I_B/I_o value at 700 gauss. The general observations made above can also be verified from the Table.

The only measurable HeII line from the plasma, at 4686 Å (n=4→n=3), was used for emission enhancement measurements, and the results are shown in Fig. 3.11.

Figures 3.2 to 3.11 represent data from a single run. The range of variation of experimental I_B/I_o for the HeI lines (each measured at least 4 times, at time intervals sometimes of months) is given in Table 3.1. It is estimated that I_B/I_o values are dependendable within ±7%.

Error in I_B/I_o measured for 0.5 amps emission current is higher (∿15%) than those at higher emission currents because of extremely small signal observed at zero field. In general, i_e values are dependable within ±3%. Estimated variations in pressure are in the range $4\text{-}6\times10^{-3}$ Torr, but even when the pressure was increased up to 10 microns, changes in the I_B/I_o factors were found to be within the experimental error reported.

At lower pressures, experiments could not be conducted because of the limitations of the filament power supply and also due to inadequate cooling arrangements of the discharge tube.

TABLE 3.1

Emission Enhancement Factors $(I_B/I_o)_{max}$ (and the corresponding magnetic field) and (I_B/I_o) at 700 gauss

No.	Wavelength	Transition	i_e = 0.5 amp			i_e = 1 amp		
			$(I_B/I_o)_{max}$	B_{max}	$(I_B/I_o)_{700}$	$(I_B/I_o)_{max}$	B_{max}	$(I_B/I_o)_{700}$
1	5875	$3^3D \rightarrow 2^3P$	20.0± 1	600	17.5±2	13.5±1	600	12.0±1
2	4471	$4^3D \rightarrow 2^3P$	14.0± 0.5	350	12.0±0.5	11.0±0.5	300	9.5±0.5
3	4026	$5^3D \rightarrow 2^3P$	10.0± 0.5	200	4.5±0.5	7.0±0.5	170	3.5±0.3
4	3889	$3^3P \rightarrow 2^3S$	18.0± 1.0	700	18.0±1.0	9.5±1	650	9.0±1
5	3187	$4^3P \rightarrow 2^3S$	10.5± 0.5	370	9.5±1.0	6.0±0.3	370	5.0±0.3
6	7065	$3^3S \rightarrow 2^3P$	32.0± 2	700	32.0±3	17.5±1.5	450	16.0±1
7	4713	$4^3S \rightarrow 2^3P$	21.6± 2	320	17.0±1	11.0±1	250	8.0±0.5
8	4121	$5^3S \rightarrow 2^3P$	5.0±0.3	160	3.0±0.2	3.0±0.2	160	2.0±0.2
9	6678	$3^1D \rightarrow 2^1P$	24.0±1	700	24.0±3	14.5±1	700	14.5±1
10	4922	$4^1D \rightarrow 2^1P$	14.0±0.1	300	12.0±1	10.0±1	250	9.0±0.5
11	4388	$5^1D \rightarrow 2^1P$	7.0±0.4	260	4.8±0.3	4.5±0.5	200	3.0±0.2
12	4144	$6^1D \rightarrow 2^1P$	6.0±0.5	230	4.0±0.3	4.0±0.5	200	2.5±0.1
13	5047	$4^1S \rightarrow 2^1P$	6.0±0.5	170	2.8±0.2	3.5±0.4	170	2.0±0.1
14	4437	$5^1S \rightarrow 2^1P$	4.1±0.5	170	2.6±0.2	3.2±0.2	170	2.0±0.1
15	5015	$3^1P \rightarrow 2^1S$	8.0±0.5	700	8.0±0.5	4.0±0.3	700	4.0±0.2
16	3964	$4^1P \rightarrow 2^1S$	5.5±0.3	250	4.0±0.3	4.3±0.3	230	3.0±0.2

Table 3.1 (...Contd.)

No.	Wavelength	Transition	i_e = 2 amp $(I_B/I_o)_{max}$	B_{max}	$(I_B/I_o)_{700}$	i_e = 3 amp $(I_B/I_o)_{max}$	B_{max}	$(I_B/I_o)_{700}$
1	5875	$3^3D \rightarrow 2^3P$	9.5±0.5	600	9.5±0.5			
2	4471	$4^3D \rightarrow 2^3P$	7.5±0.5	300	6.0±0.5			
3	4026	$5^3D \rightarrow 2^3P$	5.0±0.5	170	2.5±0.2			
4	3889	$3^3P \rightarrow 2^3S$	7.0±0.3	430	7.0±0.3	5.2±0.2	430	5.0±0.3
5	3187	$4^3P \rightarrow 2^3S$	5.0±0.3	230	3.9±0.2	4.2±0.2	220	3.5±0.2
6	7065	$3^3S \rightarrow 2^3P$	12.0±1	400	10.5±1	10.5±0.5	300	8.0±1
7	4713	$4^3S \rightarrow 2^3P$	9.0±0.5	220	6.0±0.5	6.5±0.5	200	3.5±0.2
8	4121	$5^3S \rightarrow 2^3P$	2.5±0.1	150	1.7±0.2	2.3±0.1	150	1.25±0.1
9	6678	$3^1D \rightarrow 2^1P$	12.0±0.5	700	12.0±1	9.0±0.5	700	9.0±0.5
10	4922	$4^1D \rightarrow 2^1P$	5.8±0.3	220	4.8±0.2	4.8±0.3	200	3.0±0.2
11	4388	$5^1D \rightarrow 2^1P$	3.5±0.3	200	2.3±0.1	2.8±0.2	190	1.8±0.1
12	4144	$6^1D \rightarrow 2^1P$	3.2±0.2	200	2.0±0.1	2.5±0.1	160	1.5±0.1
13	5047	$4^1S \rightarrow 2^1P$	3.2±0.2	170	1.5±0.1			
14	4437	$5^1S \rightarrow 2^1P$	3.0±0.2	170	1.5±0.1			
15	5015	$3^1P \rightarrow 2^1S$	3.4±0.2	700	3.4±0.2			
16	3964	$4^1P \rightarrow 2^1S$	3.6±0.2	200	2.3±0.2			

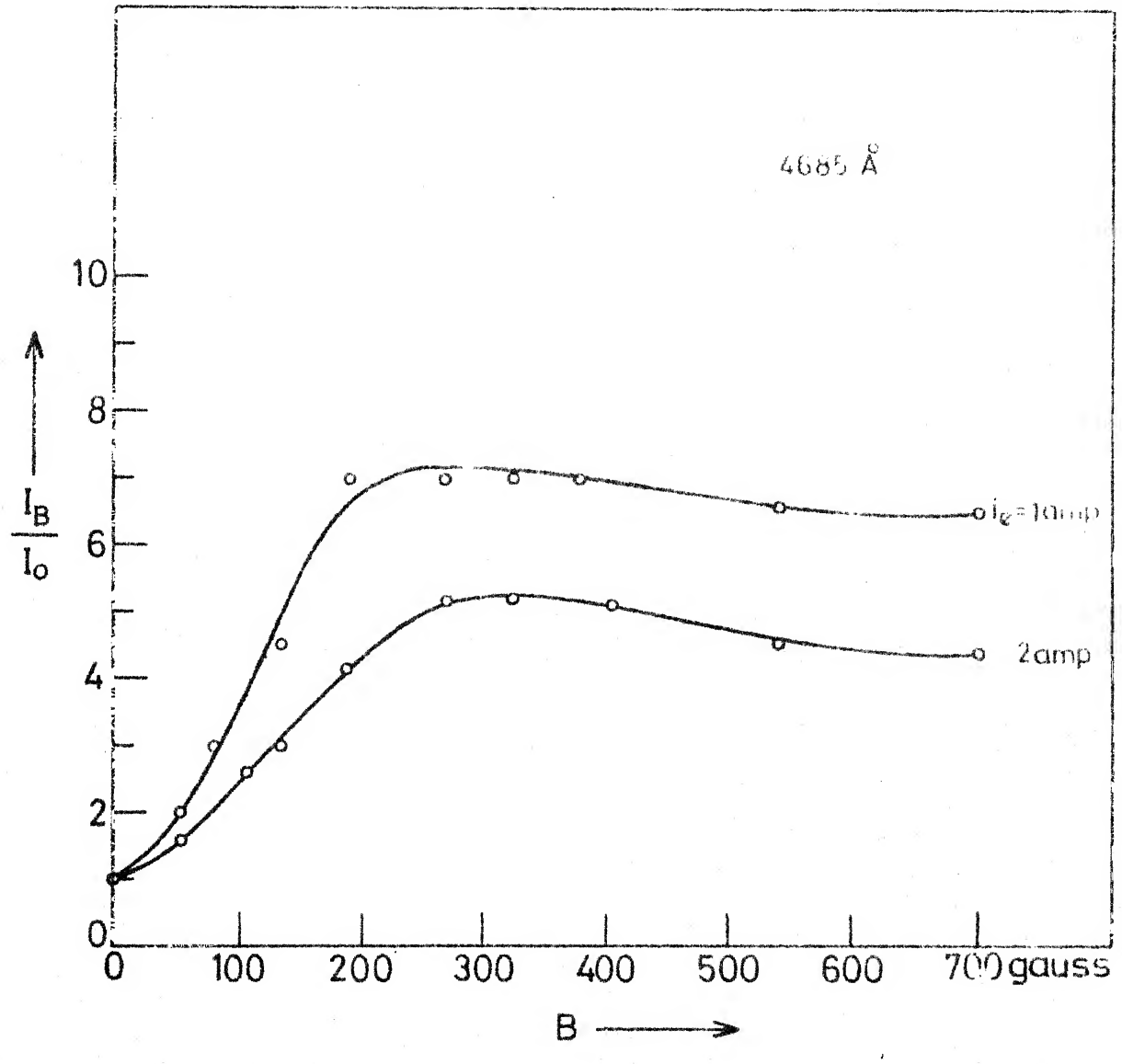

Fig. 3.11 I_B / I_o Vs B for He II n = 4 → n = 3 transition

On closing the isolation valve partially for a short time, no noticeable difference was found in the enhancement factors. This shows that enhancement factors are quite independent of the gas flow rate through the tube. Number of experiments at i_e=3 amp was limited, as at high currents heating of the plasma tube becomes significant.

Results of Ratio Measurements $I_B^{i_1}/I_B^{i_2}$

A typical plot of I_B^3/I_B^1, i.e., the ratio of the line intensity at 3 amp emission current to that at 1 amp emission current at a given magnetic field, versus the magnetic field is shown in Fig. 3.12 for the series $n^1D \rightarrow 2^1P$ (n = 3,4,5,6). In Fig. 3.13, the ratio of the line intensity at 2 amps to 0.5 amp emission current for the same series is plotted as a function of the magnetic field.

Similar measurements were made for other series and a typical plot for a triplet series is shown in Fig. 3.14 for a ratio of 3 amp to 1 amp emission current. These results are to be used later for electron density determination. Here again, a few generalisations can be made:

(a) The ratio is lower for higher lines at a given magnetic field.

(b) Ratio for the same line decreases with increase in the magnetic field.

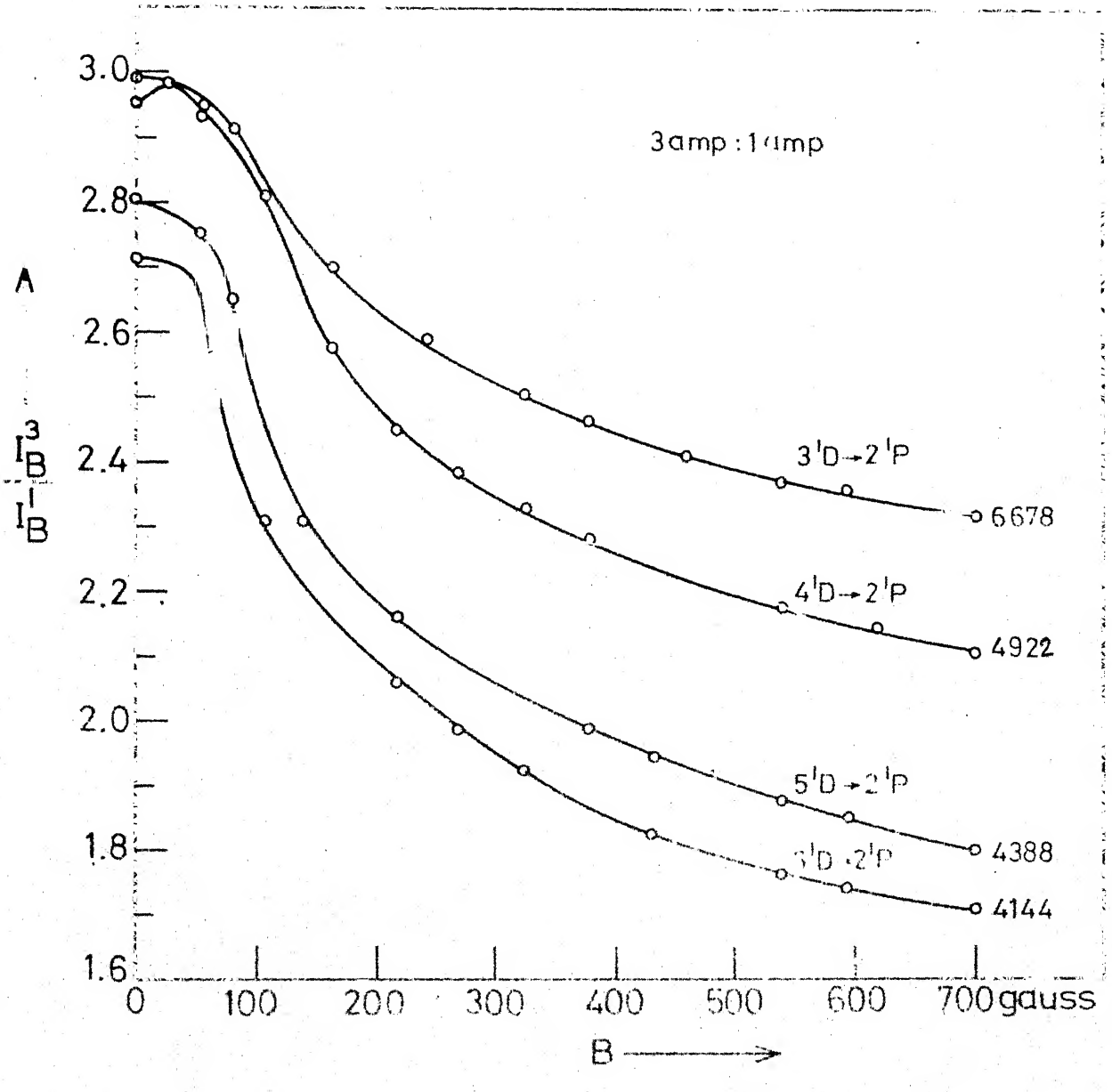

Fig. 3.12 Line intensity ratios at 3amp to 1amp emission current for $n^1D \rightarrow 2^1P$ series

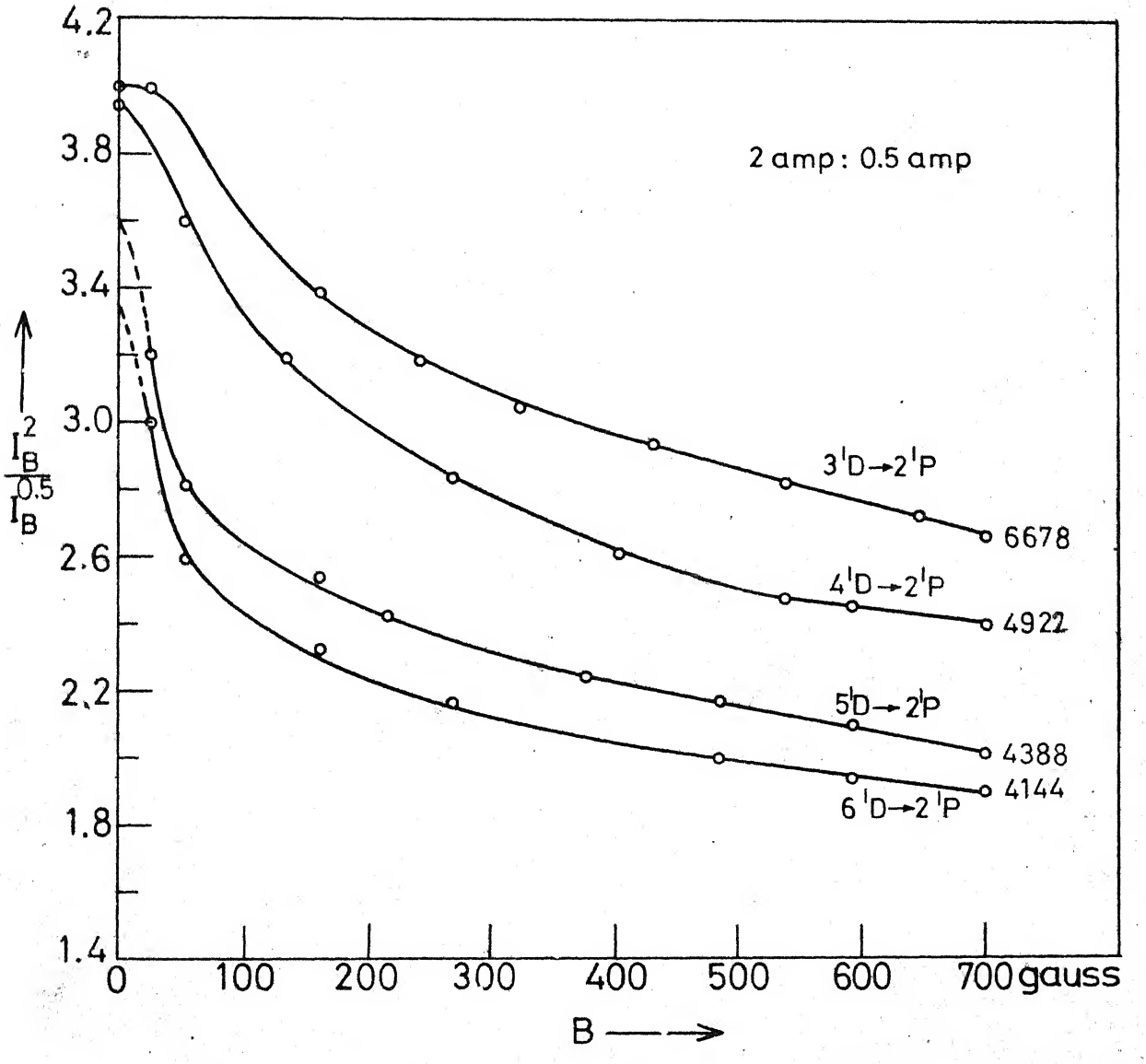

Fig. 3.13 Line intensity ratios at 2 amp to 0.5 amp emission current for $n^1D \rightarrow 2^1P$ series

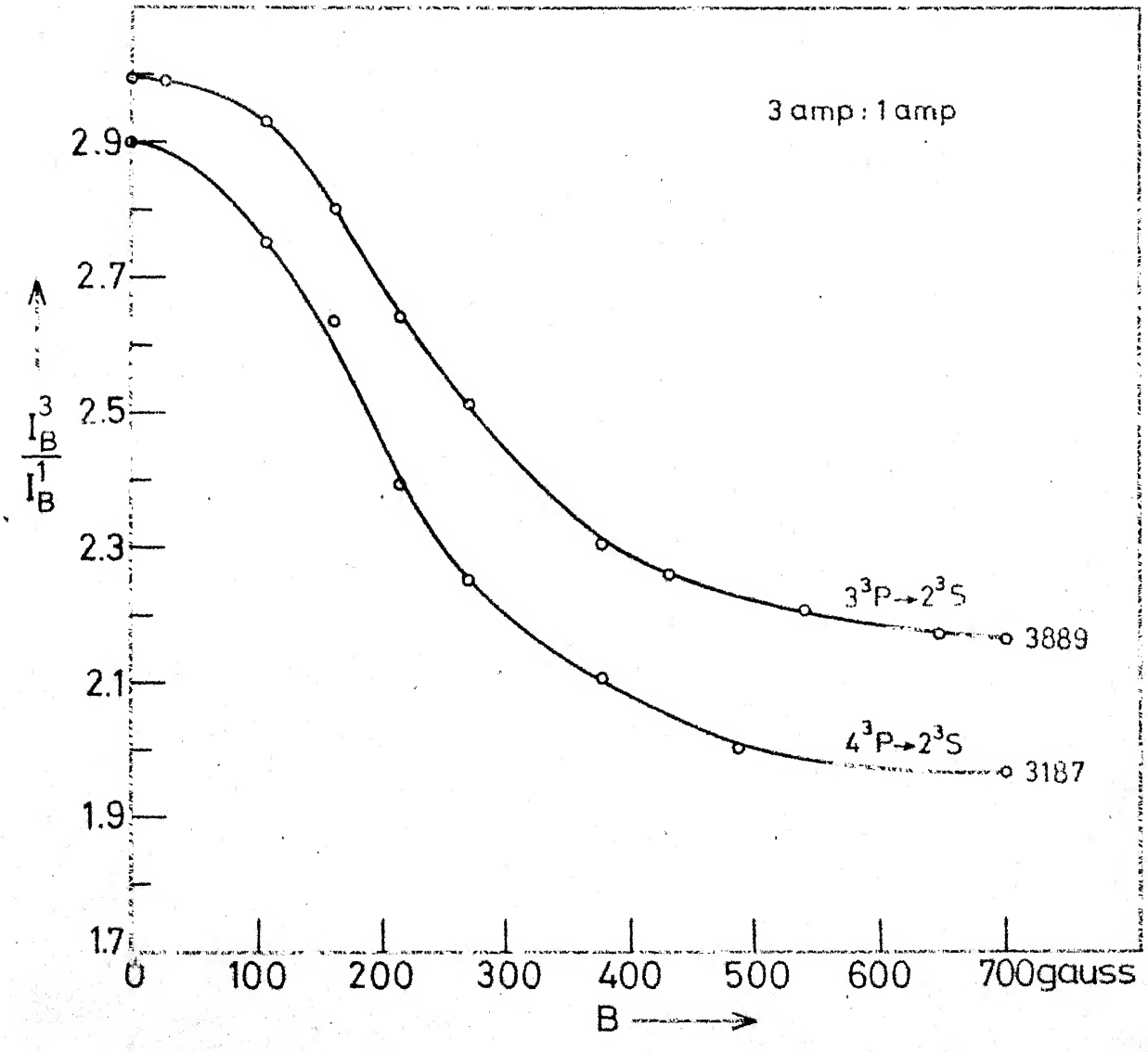

Fig.3.14 Line intensity ratios at 3 amp to 1 amp emission current for $n^3P \rightarrow 2^3S$ series

In Table 3.2, the line intensity ratios at two different emission current ratios (4 and 3) at zero and 700 gauss are given for all the lines studied. The observations made above on the basis of $n^1D \rightarrow 2^1P$ series generally hold good, as can be seen from Table 3.2. Studies were made with different sets of emission currents keeping the i_e ratios same. When 2.25 amp to 0.75 emission current ratio was chosen, the observed line intensity ratios were higher when compared with the values corresponding to 3 amp to 1 amp, at all magnetic field values.

The ratio measurements were made in a separate set of experiments and the data given in Table 3.2 are reproducible within 6%.

Temperature Measurements from Probe:

In Fig. 3.15, typical I-V characteristics of the probe at 1 amp of emission current are given. In Fig. 3.16 the plots of logarithm of electron current ($\ln i_{ep}$) against the probe voltage at various magnetic field and at 1 amp emission current is shown. Electron temperature obtained from the slopes of such curves at various magnetic field values is plotted in Fig. 3.19.

At zero magnetic field the probe current was extremely low and as such no dependable measurements could be made. At 50 gauss, the typical characteristics of a single probe were

TABLE 3.2

Emission intensity ratios at two emission currents $(I_B^{i_1}/I_B^{i_2})$

No.	Wavelength A	Transition	i_1/i_2=2 amp/0.5 amp=4 B=0 gauss	B=700 guass	i_1/i_2=2.25 amp/ 0.75 amp=3 B=0 gauss	B=700gauss
1	5875	$3^3D \rightarrow 2^3P$	4.0	2.60	2.9	2.10
2	4471	$4^3D \rightarrow 2^3P$	3.6	2.23	2.5	2.10
3	4026	$5^3D \rightarrow 2^3P$	3.1	2.02	2.25	1.5
4	5015	$3^1P \rightarrow 2^1S$	3.0	2.2	2.2	1.95
5	3964	$4^1P \rightarrow 2^1S$	3.1	2.18	2.33	1.82
6	5047	$4^1S \rightarrow 2^1P$	4.0	2.5		
7	4437	$5^1S \rightarrow 2^1P$	4.0	2.0		
					i_1/i_2 = 3 amp/1 amp = 3	
8	6678	$3^1D \rightarrow 2^1P$	4.0	2.62	3.0	2.32
9	4922	$4^1D \rightarrow 2^1P$	3.96	2.4	2.93	2.18
10	4388	$5^1D \rightarrow 2^1P$	3.85	2.0	2.80	1.80
11	4144	$6^1D \rightarrow 2^1P$	3.8	1.9	2.72	1.60
12	3889	$3^3P \rightarrow 2^3P$	4.0	2.9	3.0	2.10
13	3187	$4^3P \rightarrow 2^3S$	4.0	2.86	2.87	1.96
14	7065	$3^3S \rightarrow 2^3P$	4.2	2.36	3.00	1.76
15	4713	$4^3S \rightarrow 2^3P$	4.0	2.48	3.00	1.45
16	4121	$5^3S \rightarrow 2^3P$	3.0	2.55	2.35	1.48

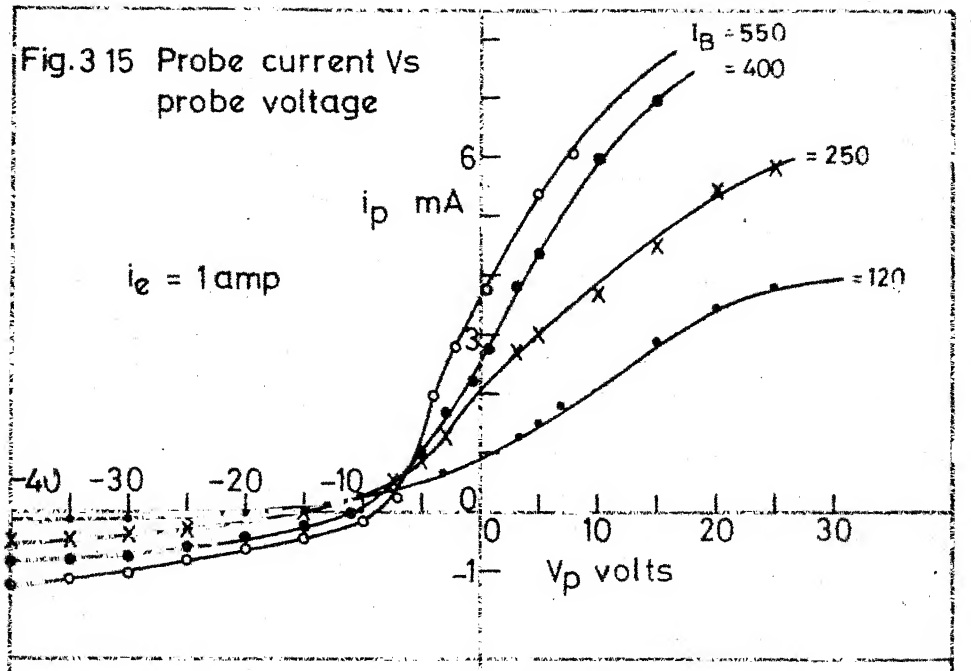

Fig. 3.15 Probe current Vs probe voltage

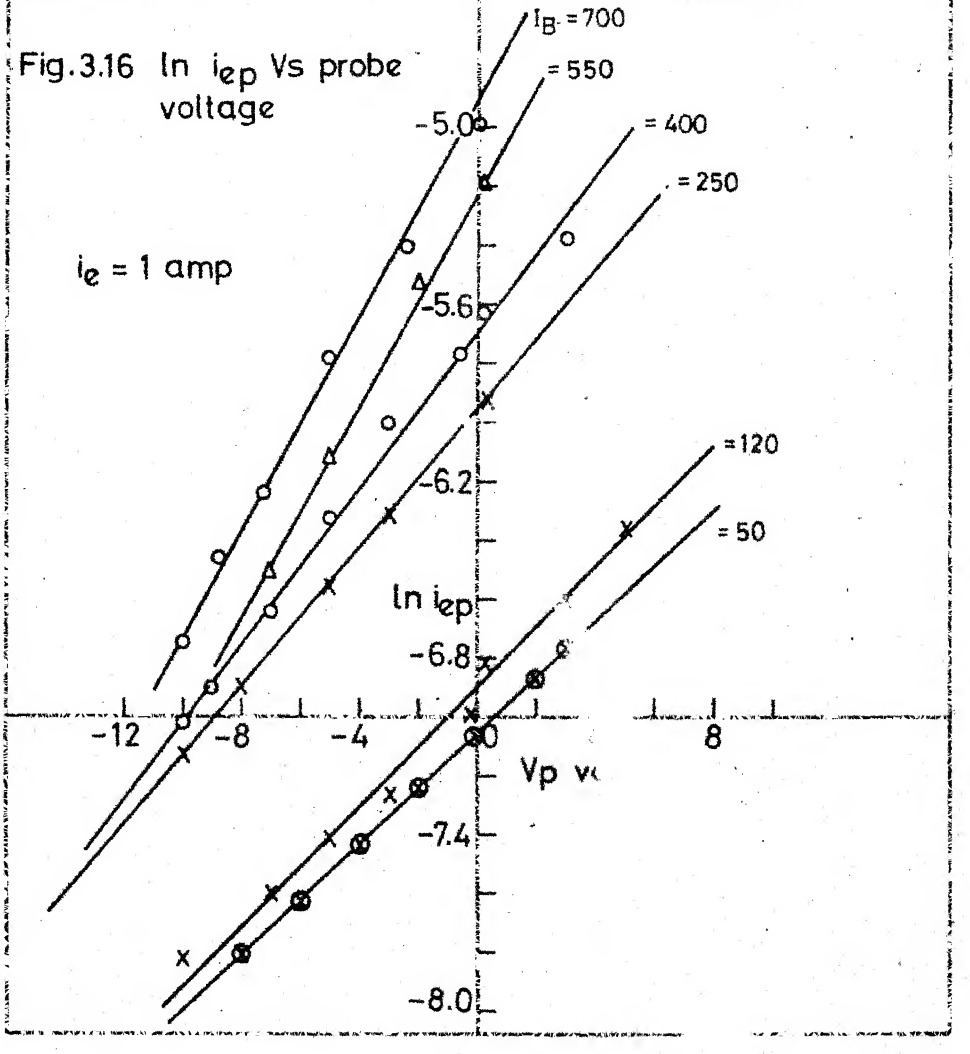

Fig. 3.16 ln i_{ep} Vs probe voltage

observed, i.e., ion as well as electron currents saturated. At higher magnetic field, the electron current did not reach saturation though ion saturation current could be measured. These observations are similar to those of some earlier workers.[38] At higher emission currents, the electron collection current was high and probe heating took place. In this region also measurements could not be made.

With the observations that could be made, the variations of electron temperature were from 10.0 eV to 5.6 eV in the range of 50-700 gauss. On extrapolation to zero field, T_e^o obtained was 11.4 eV.

A set of measurements was made at 0.5 amp emission current and the variation in the electron temperature in the range of 50 to 700 gauss was just about the same as shown in the T_e versus B plot in Fig. 3.19.

Density Measurements from Probe Data

Electron density was calculated using the equation

$$J_+ = 0.4\, n_+ e\, a \left(\frac{kT_e}{M_+}\right)^{1/2} \qquad (3.1)$$

given by Bohm and others,[37] where J_+ is the ion saturation current in amperes, e is the electron charge in coulombs, M_+ mass of helium ion, a - area of the probe and k is the Boltzmann constant. $n_+ (\simeq n_e)$ is calculated using T_e obtained

as above, variation of n_e was found to be from 6.8×10^9 cm^{-3} to 4.5×10^{11} over the magnetic field range 50 to 700 gauss as shown in Fig. 3.19.

It is to be mentioned here that axial variation of T_e was found to be within 10% at all magnetic field values. Further, at high and low fields, the ion saturation current was found to be practically invariant of the axial position. At medium magnetic field strengths the variation was found to be ~15%. with respect to the value at the centre of the column - with high values at the electron gun end and low values at the pump end.

Electron Temperature from Emission Intensity Ratio :

In Figs. 3.17 and 3.18 the experimentally observed intensity ratios of 5047 Å to 4713 and 4921 to 4471 Å lines are plotted against magnetic field at different emission currents. It shows that the intensity ratios and therefore the electron temperature, is independent of emission current at a given magnetic field. The plasma electron temperature from Fig. 3.17 is obtained by the following method.

It has been noticed that the electron impact excitations from the ground state to 4^1S and 4^3S states are strongly dependent on electron temperature. Considering the effects due to cascading from the higher to 4^1S and 4^3S states and excitation to these levels from the ground state, the intensity ratio of

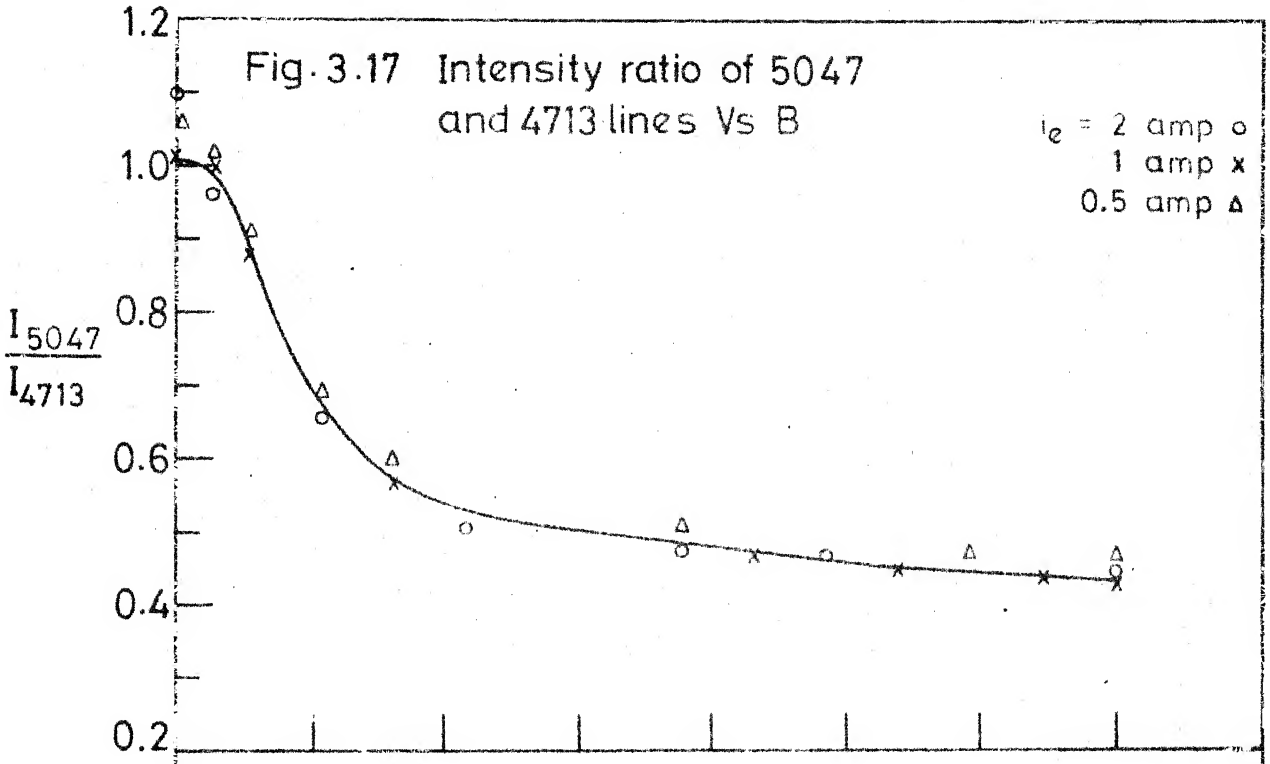

Fig. 3.17 Intensity ratio of 5047 and 4713 lines Vs B

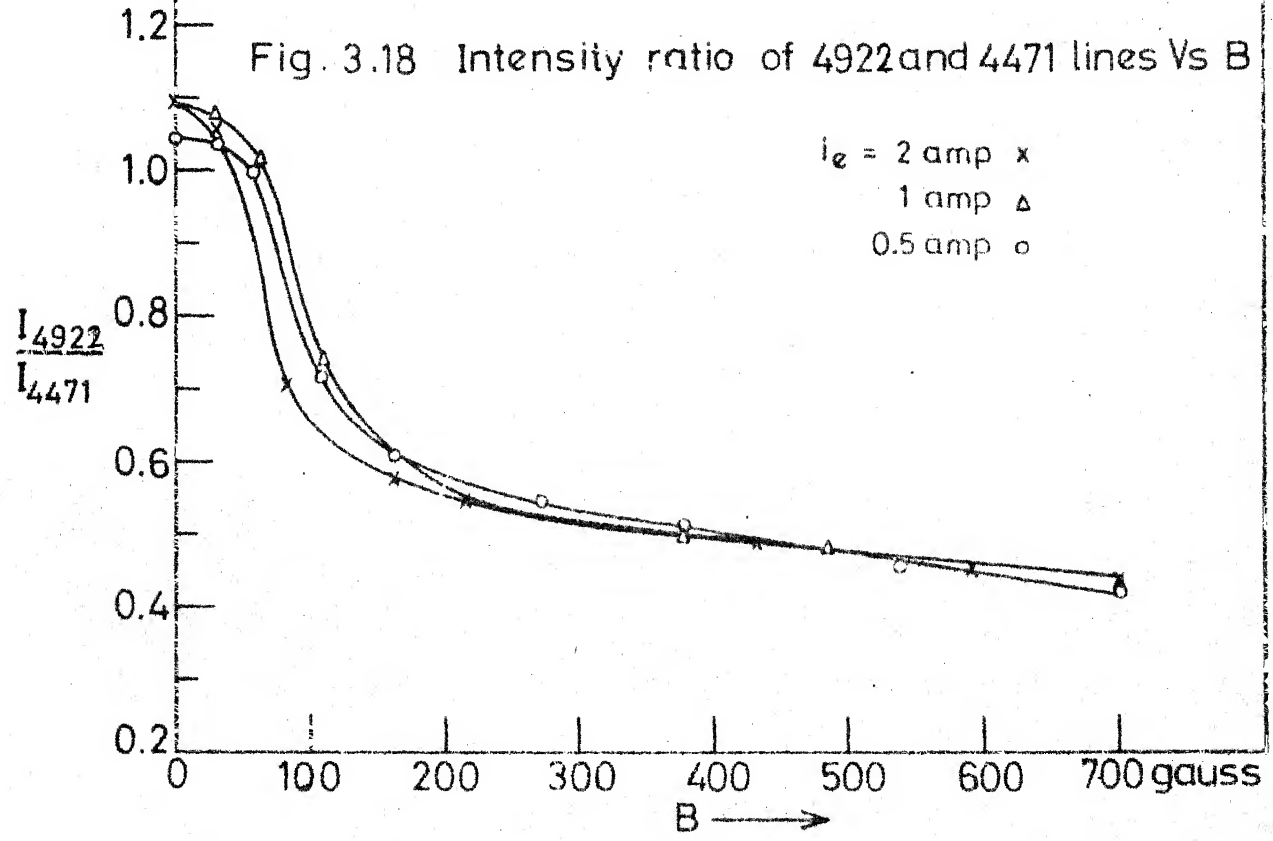

Fig. 3.18 Intensity ratio of 4922 and 4471 lines Vs B

5047 Å and 4713 Å lines given by Sovie[41] as

$$\frac{I_{5047}}{I_{4713}} = \frac{K\,(1^1S \rightarrow 4^1S)}{K\,(1^1S \rightarrow 4^3S)} \times \frac{\bar{A}\,(4^1S \rightarrow 2^1P)}{\bar{A}\,(4^3S \rightarrow 2^3P)} \cdot \frac{4713}{5047} \qquad (3.2)$$

where K's are collisional excitation coefficients, and $\bar{A}(p \rightarrow q) = A(p \rightarrow q) / \sum_q A(p \rightarrow q)$ where A's are spontaneous transition probabilities. Values of K's and A's used here will be described in detail in Chapter 4. Emission intensity ratios calculated from eq. 3.2 at various electron temperatures is then plotted against T_e. A comparison of this plot and, the experimentally observed line intensity ratios yield T_e values which are shown in Fig. 3.19. $(4^1D \rightarrow 2^1P)/(4^3D \rightarrow 2^3P)$ intensity ratios of Fig. 3.18 were not used for T_e measurements because these are known to be far less dependable than the $(4^1S \rightarrow 2^1P)/(4^3S \rightarrow 2^3P)$ line ratios.

Effect of variation of Aperture Size on I_B/I_o :

In Fig. 3.20, a plot of I_B/I_o vs B for 3889 Å line at 1 amp emission current is shown with different aperture sizes. As mentioned earlier baffle sizes varying from 0.3 cm to 0.7 cm diameter were used. To ensure collection of radiation from the axial region, 0.3 cm baffles were used at both ends of the tube for fine alignment, which give an angular divergence of $< 0.5^o$. But even then the same results were obtained.

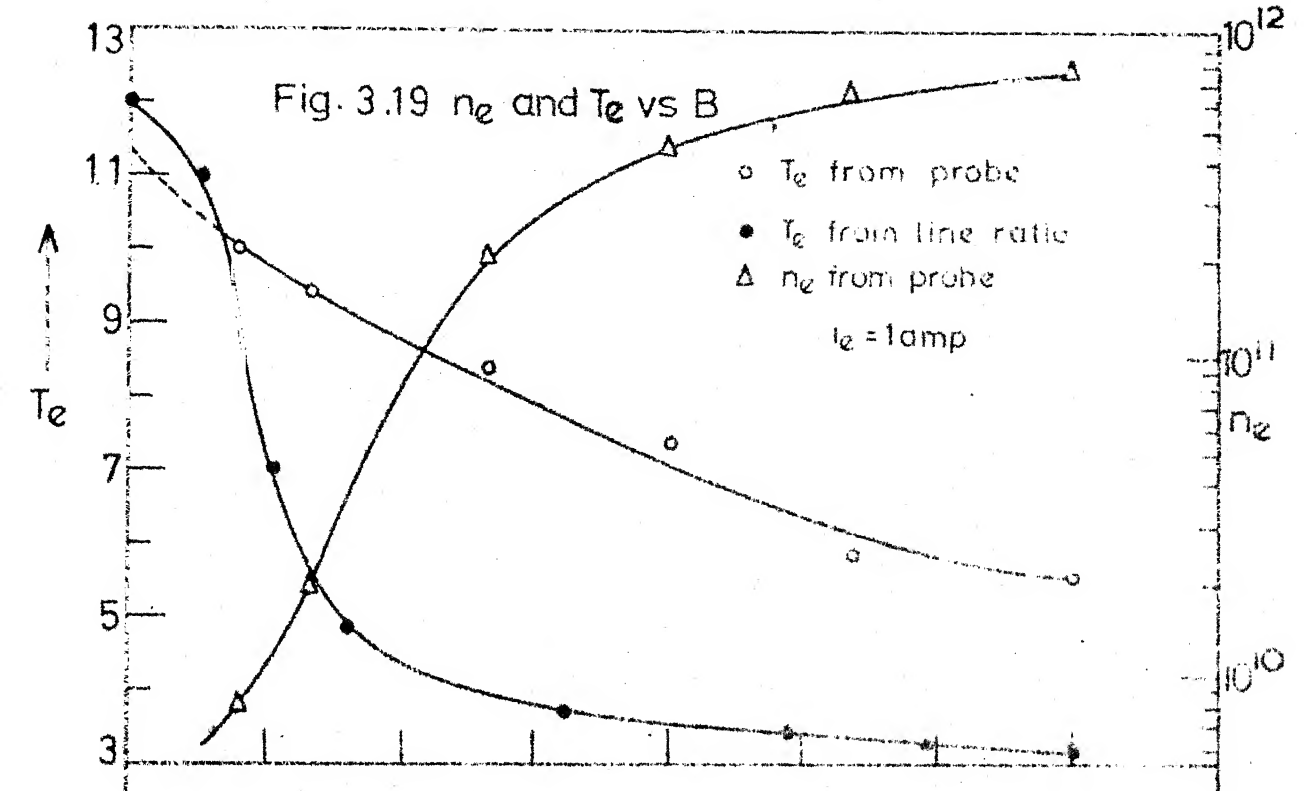
Fig. 3.19 n_e and T_e vs B
T_e
n_e
13
11
9
7
5
3
10^{12}
10^{11}
10^{10}
o T_e from probe
• T_e from line ratio
Δ n_e from probe
i_e = 1amp

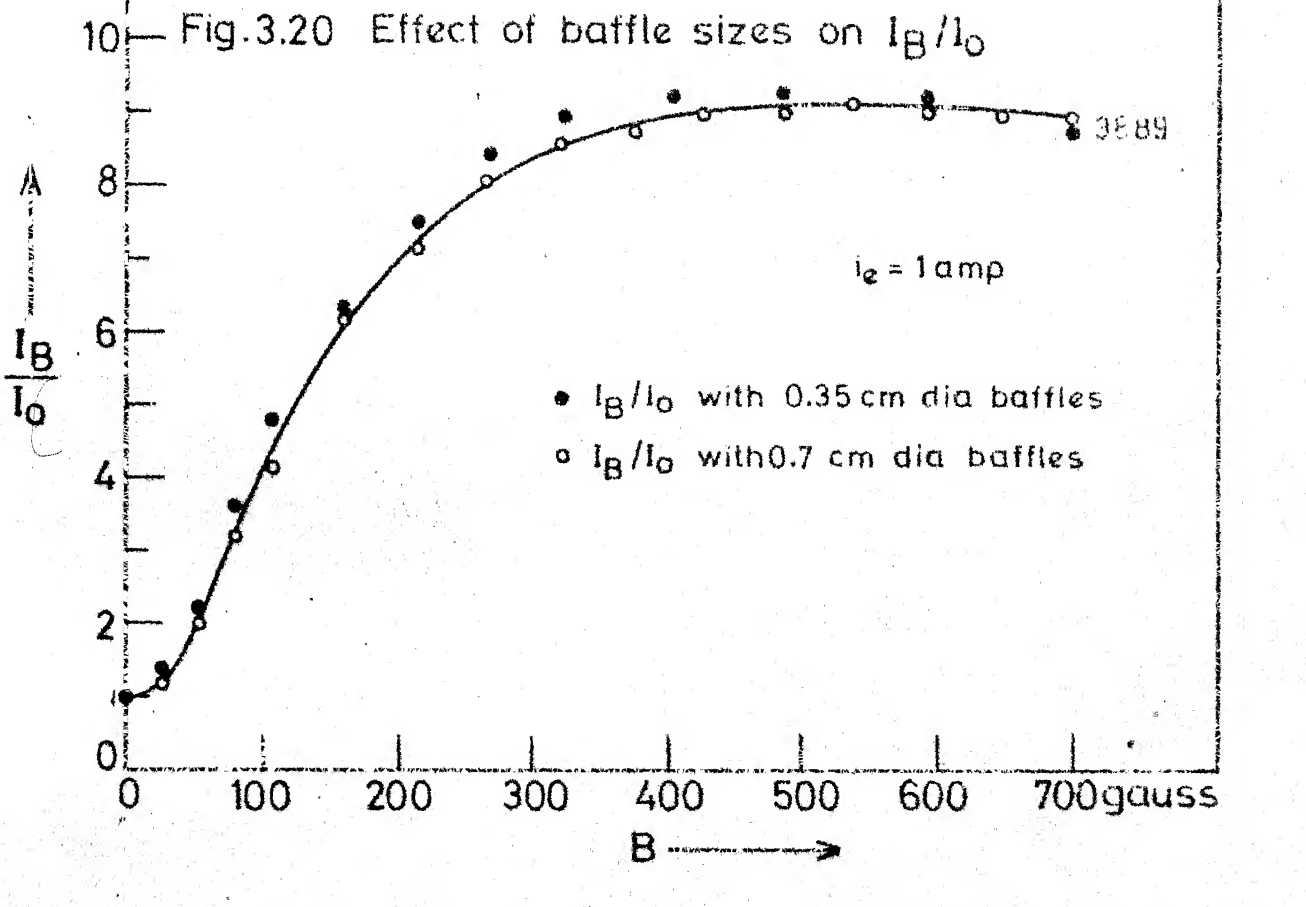
Fig.3.20 Effect of baffle sizes on I_B/I_o
$\frac{I_B}{I_o}$
10
8
6
4
2
0
0
100
200
300
400
500
600
700gauss
B
3889
i_e = 1amp
• I_B/I_o with 0.35cm dia baffles
o I_B/I_o with0.7 cm dia baffles

Chapter IV

ANALYSIS AND DISCUSSION

The primary purpose of the present work was to study emission enhancements in helium plasmas in presence of a magnetic field and correlate the experimental results with the fundamental population-depopulation processes occurring in the plasma. In the previous Chapter results of the emission enhancement studies for a number of HeI and HeII lines have been presented. In terms of the plasma parameters obtained, conservative estimates using eq. (1.1), or eq. (4) of Ref. 42, show that the plasma is under non-LTE condition throughout the entire range of magnetic field and emission current conditions of the experiment. Since explanation of observed emission intensities requires knowledge about population densities of excited states, and for non-LTE conditions theoretical population densities cannot be easily

obtained, a detailed collisional-radiative model applicable to inhomogeneous stationary state plasmas is necessary.

In this Chapter, (i) a collisional-radiative model is formulated which takes into account series of levels from both HeI and HeII systems; (ii) using this model, HeI and HeII population coefficient calculations are carried out for a wide range of n_e, T_e conditions, and the results presented; (iii) these results are then applied to the helium plasma investigated in the present work and comparison made between the experimental emission enhancement factors and those predicted theoretically. Later, (iv) the present experimental results are reviewed in the perspective of the population coefficients calculated by Drawin and the rate coefficients of Park, and (v) the collisional radiative model used in the present work applied to Stellarator C helium plasma experiments of Johnson and TPD machine experiments of Otsuka, Ikee and Ishii.

The Collisional Radiative Model Used in the Present Work:

The basic collisional radiative model has already been described in Chapter 1. The details of calculations differ on whether the system is optically thick or optically thin, the number of quantum levels taken into account for detailed balancing, and the choice of values of the rate coefficients $A(p,q)$, $K(p,q)$, $K(p,c)$, $\beta(p)$. For the HeI system, detailed

calculations for the excited state populations have been done by Johnson[13] and also by Drawin and Emard.[43] Calculations for the HeII system have been done by McWhirter and Hearn[6] and also by Drawin and Emard.[44] The HeI calculations of Johnson involve separated sublevels up to n=8 and upper limit of n=25 but their population densities are available in limited T_e and n_e combinations. Drawin and Emard's[43] calculations are for a wide range of temperature and density conditions and also for different values of optical thickness. But they have used grouped singlet and triplet levels above n=2. Experimental part of the present work uses HeI lines which involve individual sublevels of singlet and triplet states of n = 3,4,5,6 and therefore none of the above calculations are directly usable. As regards HeII excited states, simultaneous ionization-excitation processes needed to be included in the model to explain the observed population densities at the T_e, n_e range of the present experiments. Resort was therefore taken to an independent calculation of the non-LTE population densities of HeI and HeII excited states taking separated sublevels of HeI as are necessary for analyzing the emission enhancement data.

The levels used for detailed balancing are shown in Table 4.1. The salient features of the scheme are that it uses separated sublevels up to n=5, and all the sublevels above n=5 are combined together. The highest level taken

TABLE 4.1

Energy levels of HeI used in the collisional-radiative model

Level No. (p)	State	Energy (cm^{-1}) E_p	g_p	Level No. (p)	State	Energy (cm^{-1}) E_p	g_p
1	1^1S	0	1	17	$4^3F, 4^1F$	191452	28
2	2^3S	159856	3	18	4^1P	191493	3
3	2^1S	166278	1	19	5^3S	193347	3
4	2^3P	169078	9	20	5^1S	193663	1
5	2^1P	171135	3	21	5^3P	193801	9
6	3^3S	183237	3	22	5^3D	193917	15
7	3^1S	184865	1	23	5^1D	193919	5
8	3^3P	185656	9	24	$5^3F, 5^1F, 5^3G, 5^1G$	193921	64
9	3^3D	186102	15	25	5^1P	193943	3
10	3^1D	186105	5	26	6(n)	195251	144
11	3^1P	186210	3	27	7	196070	392
12	4^3S	190298	3	28	8	196595	512
13	4^1S	190940	1	29	9	196954	648
14	4^3P	191217	9	30	10	197213	800
15	4^3D	191445	15	31	11	197398	968
16	4^1D	191447	5	32	12	197543	1152

Energy levels of HeII used in the model

$i = 1$ to 13

$$E_i = 109677 \times 4 \left(1 - \frac{1}{i^2}\right) + 198311 \ cm^{-1}$$

and $g_i = 2i^2$

into consideration for HeI is n=12. It will be shown later that with further incorporation of higher levels the calculated population densities do not vary significantly. In addition, HeII levels up to n=13 are included to give a total of 45 levels. Sublevels of HeII are considered to be thermally distributed.

The following processes are included in the model. The HeI states are denoted by p's and q's and HeII states by i's and j's

$$He(p) + e \underset{K(q,p)}{\overset{K(p,q)}{<\!\!>}} He(q) + e \qquad (4.1)$$

$$He(p) + e \xrightarrow{K(p,i)} He^{+}(i) + e + e \qquad (4.2)$$

$$He(p) + e \xrightarrow{K(i,p)_{i=1}} He^{+}(1) + e + e \qquad (4.3)$$

$$He(p) \xrightarrow[p>q]{A(p,q)} He(q) + h\nu \qquad (4.4)$$

$$He^{+}(1) + e \xrightarrow{\beta(p)} He(p) + h\nu \qquad (4.5)$$

$$He(p) + He(1) \underset{KN(q,p)}{\overset{KN(p,q)}{<\!\!>}} He(q) + He(1) \qquad (4.6)$$

$$He(p) + He(1) \underset{KN(i,p)_{i=1}}{\overset{KN(p,i)_{i=1}}{<\!\!>}} He^{+}(1) + He(1) + e \qquad (4.7)$$

$$He^{+}(i) + e \underset{K(j,i)}{\overset{K(i,j)}{<\!\!>}} He^{+}(j) + e \qquad (4.8)$$

$$He^{+}(i) + e \underset{K(c,i)}{\overset{K(i,c)}{<\!\!>}} He^{++} + e + e \qquad (4.9)$$

$$He^{+}(i) \xrightarrow[i>j]{A(i,j)} He^{+}(j) + h\nu \qquad (4.10)$$

$$He^{++} + e \xrightarrow{\beta(i)} He^{+}(i) + h\nu \qquad (4.11)$$

Most of the above processes are commonly used in collisional-radiative models. Eq. (4.2) represents simultaneous ionization-excitation to HeII states and eqs. (4.6) and (4.7) describe neutral-neutral collisions for excitation and ionization respectively.

Since, in the T_e range of the present study, contribution even from the state HeII(1) towards the population density of HeI excited states is insignificant, contribution from HeII excited states to HeI levels is neglected.

In the above scheme only spontaneous decay processes are included. For optically thick conditions, reduced transition probabilities A(p,q), A(i,j) are used to take into account reabsorption of radiation from plasma. This is equivalent to inclusion of reverse processes of eqs. (4.4) and (4.10).

Putting $n_e/n^{+}(1) = X$ and $n_e/n^{++} = Y$, one has the following equilibrium relations:

$$K(p,q).n_E(p) = K(q,p).n_E(q) \qquad (4.12)$$

$$(n_e/X).K(i,p) = \sum_{i=1} K(p,i)\, n_E(p) \qquad (4.13)$$

$$K(i,j)\, n_E^{+}(i) = K(j,i)\, n_E^{+}(j) \qquad (4.14)$$

$$(n_e/Y)K(c,i) = K(i,c)\, n_E^{+}(i). \qquad (4.15)$$

$n(p)$ and $n^+(i)$ denote number densities of HeI and HeII states and n_e, n^{++} denote number densities of electron and doubly charged ions. $n_E(p)$ and $n_E^+(i)$ describe Saha equilibrium population densities respectively of HeI and HeII states given by eq. (1.7). Here c denotes the second continuum. For the above processes, time derivatives of excited state populations after incorporating equilibrium densities can be written as

$$\begin{aligned}\frac{\dot{n}(p)}{n_E(p)} &= -\rho(p)\{n_e[\sum_{i=1}^{13} K(p,i) + \sum_{q\neq p}^{32} K(p,q)] \\ &+ n(1)\sum_{q\neq p}^{32} KN(p,q) + \sum_{p>q} A(p,q) + n(1)\,KN(p,1)\} \\ &+ \sum_{p\neq q}^{32} \rho(q)\,KN(p,q).n(1).\frac{n_E(q)}{n_E(p)} + \sum_{p\neq q}^{32} \rho(q)K(p,q).n_e \\ &+ \sum_{q>p} \rho(q).A(q,p)\frac{n_E(q)}{n_E(p)} + n_e.K(p,i)_{(i=1)} + \frac{n_e^2}{\chi n_E(p)}\beta(p) \\ &+ \frac{n_e^2}{\chi n_E(p)}\cdot n(1)\,KN(i,p) \qquad (4.16)\end{aligned}$$

and

$$\begin{aligned}\frac{\dot{n}^+(i)}{n_E^+(i)} &= -\rho^+(i)\{n_e[K(i,c) + \sum_{i\neq j}^{13} K(i,j)] + \sum_{i>j} A(i,j)\} \\ &+ \sum_{i\neq j}^{13} \rho^+(j)\,K(i,j).n_e + \sum_{j>i} \rho^+(j)\frac{n_E^+(j)}{n_E^+(i)}.A(j,i) \\ &+ \sum_{p=1}^{32} \rho(p).n_e.\frac{n_E(p)}{n_E^+(i)}K(p,i) + n_e\,K(i,c) + \frac{n_e^2}{\gamma n_E^+(i)}\beta(i) \\ &[\rho(p) = n(p)/n_E(p);\ \rho^+(i)=n^+(i)/n_E^+(i)] \qquad (4.17)\end{aligned}$$

It is assumed that loss due to diffusion to the walls for all the excited states of HeI and HeII is negligible. In that case eqs. (4.16) and (4.17) represent the controlling equations for all HeI and HeII excited states. The eqs. (4.16) and (4.17), after equating the right hand side to zero (for $p \neq 1$, $i \neq 1$), can be combined to give a set of 43 linear simultaneous equations. The inhomogeneous stationary state solution, in terms of the local ground state population densities of HeI and HeII (which have contributions from diffusion losses), can be written as

$$\rho(p) = r_o(p) + r_1(p) \cdot \rho(1) \qquad (4.18)$$

$$\rho^+(i) = r_o^+(i) + r_1^+(i)\ \rho(1) + r_2^+(i) \cdot \rho^+(1) \qquad (4.19)$$

It is to be noted that $n_E(p)/n_E^+(i) = \frac{g_p}{g_i} \cdot \frac{n^+(1)}{n^{++}} \cdot \exp((E_p - E_j)/kT_e)$, and in order to solve the set of linear equations, an explicit value of this ratio $n^+(1)/n^{++}$ is required. The solution is therefore obtained in terms of n_e, T_e, T_g and $n^+(1)/n^{++}$, and given these parameters, population densities of all the excited states can be determined in terms of $n(1)$ and $n^+(1)$. In eq. (4.18), $r_o(p)$ gives the contribution towards $\rho(p)$ from the first continuum and $r_1(p) \cdot \rho(1)$ is the contribution from the ground state of HeI. In Eq. (4.19), $r_o^+(i)$ is the contribution from the second continuum towards $\rho^+(i)$, $r_1^+(i)\rho(1)$ gives the contribution from the ground state of HeI while $r_2^+(i)\ \rho^+(1)$ gives the contribution from the ground state of HeII.

Effect of autoionization processes is assumed to be relatively less significant. Population of He^+ ground state due to autoionization will not change the results of the present calculations since HeII(i) and HeI(p) population densities are calculated on the basis of assumed values of He^+ ground state population (i.e., $n^+(1) \simeq n_e$). Further, radiative decay from the autoionizing states populate the very high excited states of HeI preferentially. Atom-atom collisions are included in the general programme although at neutral densities and electron temperatures of the present experiments it makes little contribution.

Diffusive losses of the metastable states are neglected for the following reasons.[45] The total relaxation frequency for the metastable states can be written as $\nu = 1/\tau = n(1)\,\sigma_d \langle v \rangle + K_m n(1) + n_e \sum_q K(m,q)$ where τ is the relaxation time, $n(1)$ is the ground state population density, σ_d is the momentum transfer cross-section, $\langle v \rangle$ the average velocity of the ground state particles, K_m the rate coefficient for neutral-metastable collisions and $K(m,q)$ the rate coefficient for excitation-deexcitation by electronic collisions. For worst case calculations, at neutral densities of the present experiments, i.e., 2×10^{14}, $T_g \sim 1000$ K, $\sigma_d = 2.4 \times 10^{-15}$ cm^2, $n_e = 10^{10}$ $T_e \sim 11$ eV, the second term of the above equation is negligible and the first and third terms are of the same order, $\sim 5 \times 10^4$ sec^{-1}. At all higher n_e values, the third term becomes so

dominant that diffusive losses of the metastable population density may be neglected in comparison with volume deactivation. It may be added here that, in some recent calculations[46] also, metastable diffusive losses have been neglected.

Choice of Atomic Parameters :

The various collisional and radiative rate coefficients used in the calculations are obtained as follows.

Spontaneous transition probability A(p,q) values for HeI are taken from the tables of Wiese, Smith and Glennon.[47] A(i,j) values for HeII are obtained from the tables of Green, Rush and Chandler.[48]

For calculation of collisional ionization rate coefficients $K(p,i)_{i=1}$, Gryzinski's[49] formulation is used. Ionization cross-sections for HeI states is then given by

$$He_e Q^{He^+}(E_e/E_p) = \frac{2\pi e^4}{E_p^2} g_p(E_e/E_p), \qquad (4.20)$$

where E_p is the ionization potential of the pth level and E_e is the energy of the colliding electron. Putting $E_e/E_p = x$, $g_p(x)$ is given by

$$g_p(x) = \frac{1}{x}\left(\frac{x-1}{x+1}\right)^{3/2}\left[1 + \frac{2}{3}\left(1 - \frac{1}{2x}\right)\ln\left(2.7+(x-1)^{1/2}\right)\right] \qquad (4.21)$$

Ionization rate constant K(p,i) for the pth level is obtained by averaging the corresponding cross-sections over Maxwellian

distribution of velocity of the colliding electron, i.e.,

$$K(p,i) = \int_{v^*}^{\infty} He_e Q^{He^+} (E_e/E_p)\, f(v).v.dv, \qquad (4.22)$$

where

$$f(v)dv = (2/\pi)^{\frac{1}{2}} (m/kT_e)^{3/2} \exp(-\tfrac{1}{2} mv^2/kT_e).v^2.dv$$

and $v^* = (2E_p/m)^{\frac{1}{2}}$. With the simplification $\frac{1}{2} mv^2 = E_e$, and substitution of the values of the atomic constants,

$$K(p,i) = \frac{2.918}{T_e^{3/2}} \int_1^{\infty} g_p(x)\, e^{-\alpha x}\, x\, dx,$$

where $\alpha = E_p/kT_e$. This can also be written substituting for $q_p(x)$,

$$K(p,i) = (2.918/T_e^{3/2}) \exp(-\alpha) \int_o^{\infty} f(z)\, e^{-z}\, dz \qquad (4.23)$$

after putting $(x-1) = y$ and $\alpha y = z$. The above equation is integrated numerically using Gaussian quadrature method as follows:

$$\int_o^{\infty} f(z).e^{-z}dz = \sum_{i=1}^{n} H_i\, f(a_i) \qquad (4.24)$$

where H_i's and a_i's are weight factors and zeros of nth order Laguerre polynomial. Typical values of ionization rate coefficients for HeI are given in Table 4.2.

For collisional excitation coefficients K(p,q), the following cases arise for HeI system.

TABLE 4.2

Values of HeI ionization rate coefficients K(p,i) i=1 in $cm^3 sec^{-1}$ at T_e = 11.2 eV and 5.9 eV

Level No.*	11.2 eV	5.9 eV	Level No.	11.2 eV	5.9 eV
1	1.53^{-9}	1.34^{-10}**	17	4.08^{-6}	4.05^{-6}
2	2.12^{-7}	1.20^{-7}	18	4.12^{-6}	4.09^{-6}
3	3.09^{-7}	1.92^{-7}	19	6.42^{-6}	6.69^{-6}
4	3.71^{-7}	2.41^{-7}	20	7.03^{-6}	7.39^{-6}
5	2.27^{-7}	2.87^{-7}	21	7.39^{-6}	7.80^{-6}
6	1.22^{-6}	1.01^{-6}	22	7.58^{-6}	8.03^{-6}
7	1.47^{-6}	1.26^{-6}	23	7.59^{-6}	8.04^{-6}
8	1.62^{-6}	1.41^{-6}	24	7.59^{-6}	8.04^{-6}
9	1.71^{-6}	1.51^{-6}	25	7.64^{-6}	8.10^{-6}
10	1.72^{-6}	1.51^{-6}	26	1.22^{-5}	1.35^{-5}
11	1.74^{-6}	1.53^{-6}	27	1.82^{-5}	2.07^{-5}
12	3.26^{-6}	3.14^{-6}	28	2.54^{-5}	2.95^{-5}
13	3.68^{-6}	3.60^{-6}	29	3.38^{-5}	4.00^{-5}
14	3.89^{-6}	3.83^{-6}	30	4.36^{-5}	5.22^{-5}
15	4.08^{-6}	4.04^{-6}	31	5.42^{-5}	6.56^{-5}
16	4.08^{-6}	4.04^{-6}	32	6.64^{-5}	8.11^{-5}

* Refer to Table 4.1 for the HeI states

** Read 1.34^{-10} as 1.34×10^{-10}, etc.

(i) Optically allowed transitions: (2^1P-1^1S, 3^3P-2^3S, etc.)
The expression for excitation cross-section $q_{p,q}(E_e)$ used by Drawin[50] is as follows:

$$q_{p,q}(E_e) = 4\pi a_o^2 \left[1 - \frac{E_1^H}{E_{p,q}}\right]^2 f(p,q)\, g(x) \qquad (4.25)$$

where a_o is the Bohr radius, $E_1^H = 13.59$ eV, $E_{pq} = E_q - E_p$, $f(p,q)$ is the absorption oscillator strength, E_e the electron energy, and $g(x) = \alpha_{pq} \frac{x-1}{x^2} \ln (1.25\, \beta_{p,q}\, x)$, (here x is equal to $E_e/E_{p,q}$); α and β are constants close to unity. Using $f(p,q)$ values from the Tables of Wiese and others[47] and integrating the cross-section expression over Maxwellian electron energy distribution, excitation rate coefficients $K(p,q)$ are obtained.

(ii) Optically forbidden transitions without change in multiplicity: (1^1S-2^1S, 2^1P-2^1D, etc.)
The excitation function given by Drawin[50] is

$$q_{p,q}(E_e) = 4\pi a_o^2 \Omega_{p,q} \frac{1}{x}\left(1 - \frac{1}{x}\right) \qquad (4.26)$$

where x is defined as in (i) and $\Omega_{p,q}$ is a constant for a given transition and tabulated by Drawin.[50]

(iii) Optically forbidden transitions with change in multiplicity:
(a) Drawin[50] has given the following expressions for cross-section for transitions involving the ground state

(1^1S-2^3S, 1^1S-2^3P etc.)

$$q_{p,q}(E_e) = 4\pi\, a_o^2\, Q_{p,q}\, \frac{x^2-1}{x^5}, \qquad (4.27)$$

and (b) those not involving the ground state (2^3S-2^1S, 2^1S-3^3P etc.)

$$q_{p,q}(E_e) = 4\pi\, a_o^2\, Q_{p,q}\, x^{-1}. \qquad (4.28)$$

$Q_{p,q}$ values as given by Drawin are used.

(iv) Excitation cross-sections which were not given by Drawin for the case iii(b) were obtained from the compilations of Moiseiwitsch.[51] As in (i), the rate coefficients are obtained by usual integration over Maxwellian energy distribution.

Typical values of K(p,q) calculated according to the cross-sections above are given in Table 4.3.

The radiative recombination coefficient $\beta(p)$ values for HeI are obtained by appropriate integration of the recombination cross-section given by Kramers[52]:

$$q(v) = \frac{128}{3\sqrt{3}}\, \frac{\pi^4\, Z^4\, e^{10}}{c^3\, h^4\, m_e\, v^2\, n^3}\, g(\nu) \qquad (4.29)$$

where v is defined by $h\nu = h\nu_o + \frac{1}{2} m_e v^2$, ν is the frequency of radiation, ν_o the threshold frequency and $g(\nu)$ free-bound Gaunt factor, and Z is the nuclear charge, equal to 2. Typical values of $\beta(p)$ obtained from eq. (4.29) are given in Table 4.4.

TABLE 4.3

Typical values of HeI collisional excitation coefficients K(p,q) and collisional deexcitation coefficients K(q,p) in cm^3 sec^{-1} at T_e = 11.2 eV and 5.9 eV

p	q	11.2 eV	5.9 eV	p	q	11.2 eV	5.9 eV
$1^1S(1)$	$-2^1P(5)$	1.54^{-10}*	5.91^{-11}	$2^3S(2)$	$-3^3P(8)$	5.30^{-9}	7.42^{-9}
		3.45^{-10}**	2.37^{-10}			2.35^{-9}	2.07^{-9}
	$-3^1P(11)$	3.17^{-11}	3.33^{-12}		$-4^3P(14)$	1.29^{-9}	8.11^{-10}
		8.42^{-11}	5.73^{-11}			6.11^{-10}	5.24^{-10}
	$-4^1P(18)$	1.26^{-11}	1.36^{-12}		$-5^3P(21)$	5.42^{-10}	3.29^{-10}
		3.82^{-11}	2.59^{-11}			2.64^{-10}	2.24^{-10}
$2^1S(3)$	$-3^1P(11)$	2.46^{-8}	1.84^{-8}	$2^3S(2)$	$-2^1S(3)$	3.08^{-8}	3.98^{-8}
		1.03^{-8}	9.34^{-9}			9.93^{-8}	1.37^{-7}
	$-4^1P(18)$	4.81^{-9}	3.30^{-9}		$-3^1S(7)$	6.43^{-9}	6.91^{-9}
		2.12^{-9}	1.88^{-9}			2.55^{-8}	3.52^{-8}
	$-5^1P(25)$	1.59^{-9}	1.05^{-9}		$-4^1S(13)$	5.01^{-9}	5.07^{-9}
		7.20^{-10}	6.28^{-10}			2.13^{-8}	2.93^{-8}
$1^1S(1)$	$-2^3S(2)$	2.66^{-11}	7.14^{-12}	$2^3S(2)$	$-3^1D(10)$	5.67^{-9}	8.72^{-9}
		5.27^{-11}	6.98^{-11}			4.56^{-9}	9.12^{-9}
	$-2^3P(4)$	1.82^{-11}	4.40^{-12}		$-4^1D(16)$	2.03^{-9}	3.00^{-9}
		1.33^{-11}	1.74^{-11}			1.73^{-9}	3.51^{-9}
	$-3^3S(6)$	1.26^{-11}	2.59^{-12}		$-5^1D(23)$	8.76^{-9}	1.23^{-9}
		3.23^{-11}	4.16^{-11}			7.68^{-10}	1.31^{-9}
n=6 (26)	n=7(27)	1.21^{-5}	1.40^{-5}				
		4.47^{-6}	5.22^{-6}				
n=11(31)	n=12(32)	1.70^{-4}	2.09^{-4}				
		1.43^{-4}	1.76^{-4}				

* Upper values denote excitation coefficients K(p,q)

**Lower values denote deexcitation coefficients K(q,p)

The numbers in the parentheses represent the level number.

TABLE 4.4

Typical values of HeI radiative recombination coefficients $\beta(p)$ in $cm^3\ sec^{-1}$ at T_e=11.2 eV and 5.9 eV

Level No. (p)	11.2 eV	5.9 eV	Level No. (p)	11.2 eV	5.9 eV
1	1.07^{-12}	1.48^{-12}	17	6.21^{-15}	8.56^{-15}
2	1.03^{-13}	1.43^{-13}	18	6.16^{-15}	8.48^{-15}
3	7.48^{-14}	1.03^{-13}	19	3.78^{-15}	5.21^{-15}
4	6.38^{-14}	8.72^{-14}	20	3.42^{-15}	4.71^{-15}
5	5.64^{-14}	7.74^{-14}	21	3.23^{-15}	4.45^{-15}
6	2.14^{-14}	2.94^{-14}	22	3.14^{-15}	4.32^{-15}
7	1.78^{-14}	2.45^{-14}	23	3.13^{-15}	4.32^{-15}
8	1.62^{-14}	2.23^{-14}	24	3.13^{-15}	4.32^{-15}
9	1.53^{-14}	2.10^{-14}	25	3.11^{-15}	4.28^{-15}
10	1.53^{-14}	2.10^{-14}	26	1.81^{-15}	2.40^{-15}
11	1.51^{-14}	2.07^{-14}	27	1.13^{-15}	1.55^{-15}
12	7.90^{-15}	1.09^{-14}	28	7.53^{-16}	1.04^{-15}
13	6.84^{-15}	9.59^{-15}	29	5.29^{-16}	7.28^{-16}
14	6.54^{-15}	9.02^{-15}	30	3.84^{-16}	5.29^{-16}
15	6.22^{-15}	8.57^{-15}	31	2.91^{-16}	4.01^{-16}
16	6.22^{-15}	8.57^{-15}	32	2.24^{-16}	3.09^{-16}

$\beta(i)$, the radiative recombination coefficient values for hydrogenic ion HeII are obtained from Seaton's[53] formulation

$$\beta(i) = 5.197 \times 10^{-14} Z x_i^{3/2} S_n(D) \qquad (4.30)$$

where $D = 157890\ Z^2/T_e$ and $x_i = D/i^2$. $S_n(D)$ values are obtained by interpolation using Seaton's table. Typical values of $\beta(i)$ are given in Table 4.5.

Rate coefficients for collisional excitation and ionization for HeII are obtained by using expressions used by Bates, Kingston and McWhirter.[4] The HeII excitation coefficient is given by

$$K(i,j) = \frac{4.75 \times 10^{-5}}{Z^2} \frac{i^2 j^2}{j^2 - i^2} \frac{f_{ij}}{T_e^{1/2}} \exp(-E_{ij}/kT_e) \qquad (4.31)$$

where f_{ij} is the absorption oscillator strength and $E_{ij} = E_j - E_i$. Oscillator strength values are obtained from the table of Green, Rush and Chandler.[48]

HeII ionization coefficients are given by

$$K(i,c) = \frac{1.4 \times 10^{-5}}{Z^2 T_e^{1/2}} i^2 \exp\left(\frac{-E_{ic}}{kT_e}\right) \qquad (4.32)$$

where E_{ic} is the ionization potential of ith state. Typical values of $K(i,j)$ and $K(i,c)$ are given in Table 4.6.

The collisional deexcitation coefficients $K(q,p)$, $K(j,i)$ and three-body recombination coefficient $K(i,p)$ and $K(c,i)$ are obtained from eqs. (4.12)-(4.15).

TABLE 4.5

Typical values of HeII radiative recombination coefficient $\beta(i)$ cm^3 sec^{-1} at T_e = 11.2 eV and 5.9 eV

i	11.2 eV	5.9 eV
1	3.29^{-13}	6.94^{-13}
2	1.50^{-13}	2.29^{-13}
3	7.44^{-14}	1.25^{-13}
4	4.12^{-14}	7.69^{-14}
5	2.80^{-14}	5.03^{-14}
6	1.92^{-14}	3.63^{-14}
7	1.41^{-14}	3.53^{-14}
8	1.03^{-14}	2.09^{-14}
9	8.01^{-15}	1.90^{-14}
10	6.26^{-15}	1.22^{-14}
11	4.93^{-15}	1.1^{-14}
12	4.10^{-15}	8.2^{-15}
13	3.33^{-15}	7.4^{-15}

TABLE 4.6

Values of excitation K(i,j) and ionization K(i,c) coefficients of HeII at T_e = 11.2 eV and 5.9 eV

	11.2 eV	5.9 eV
	K(i,j) cm^3 sec^{-1}	
K(1,2)	4.95^{-10}	2.57^{-11}
K(1,3)	4.04^{-11}	1.15^{-12}
K(1,10)	4.52^{-13}	8.28^{-15}
K(2,3)	7.85^{-8}	5.90^{-8}
K(2,4)	8.57^{-9}	5.21^{-9}
K(2,10)	1.67^{-10}	8.10^{-11}
K(8,9)	1.79^{-5}	2.40^{-5}
K(9,10)	2.79^{-5}	3.80^{-5}
	K(i,c) cm^3 sec^{-1}	
K(1,c)	1.50^{-10}	2.64^{-12}
K(2,c)	2.30^{-8}	1.06^{-8}
K(5,c)	3.98^{-7}	4.62^{-7}
K(10,c)	1.85^{-6}	2.44^{-6}
K(13,c)	3.18^{-6}	4.28^{-6}

Ionization-excitation coefficients K(p,i) for transitions HeI(p) → HeII(i) are calculated using the following empirical expression for excitation cross-section

$$q_{pi}(x) = 2\pi\, a_o^2 \left[\frac{E_1^H}{E_{pi}}\right]^2 g(x) \qquad (4.33)$$

where $g(x) = \frac{x-1}{x^2} \ln(1.25\,x)$, $x = E_e/E_{pi}$, and $E_{pi}=E_i-E_p$. (4.34)

Ionization-excitation cross-section value q_i calculated from eq. (4.33) matches closely the cross-section presented for the case He(1) + e → He^+(4)+e+e by Drawin.[50] It should be pointed out here that cross-sections for simultaneous Ionization-excitation of HeII states from HeI ground state was studied by Dalgarno and McDowell[54] and their cross-sections are more than one order of magnitude lower than those predicted by eq. (4.33). Detailed analysis of the results given later, however, show that excitation function used here yield reasonable matching of theoretical and experimental results. Typical values of K(p,i) obtained from eq. (4.33) are presented in Table 4.7.

Rate coefficients of excitation, deexcitation, ionization for processes involving collisions between the excited states of HeI and the ground state HeI(1) and the reverse processes, viz., KN(p,q), KN(q,p), KN(p,i), KN(i,p), are calculated using expressions given by Drawin, Klan and Ringler.[46] Typical values of these coefficients are given in Table 4.8.

TABLE 4.7

Values of ionization-excitation coefficients K(p,i) He(p) →HeII(i) cm^3 sec^{-1} at T_e=11.2 eV and 5.9 eV

(p,i)	11.2 eV	5.9 eV
1^1S-1	7.73^{-10}	7.2^{-11}
1^1S-2	2.56^{-12}	8.10^{-15}
1^1S-3	1.03^{-12}	1.77^{-15}
1^1S-12	5.30^{-13}	5.74^{-10}
2^3S-1	1.00^{-7}	5.67^{-8}
2^3S-2	3.26^{-11}	5.18^{-13}
2^3S-3	1.20^{-11}	1.02^{-13}
2^3S-12	5.80^{-12}	3.14^{-13}
2^1S-1	1.47^{-7}	9.07^{-8}
2^1S-2	3.63^{-11}	6.16^{-13}
2^1S-3	1.33^{-11}	1.21^{-13}
2^1S-12	6.41^{-12}	3.70^{-14}
n=10-1	2.54^{-5}	2.94^{-5}
n=10-2	6.19^{-11}	1.44^{-12}
n=10-3	2.20^{-11}	2.75^{-13}
n=10-12	1.05^{-11}	8.24^{-14}

TABLE 4.8

Values of neutral-neutral collision coefficients KN(p,q), KN(q,p), KN(p,i) and KN(i,p)

T_g = 0.09 eV and T_e = 11.2 eV, n(1) = 2×10^{14} cm^{-3}

p	q	KN(p,q) $cm^3 sec^{-1}$	KN(q,p) $cm^3 sec^{-1}$
26 (n=6)	27 (n=7)	1.38^{-9}	1.20^{-8}
26 (n=6)	28 (n=8)	1.79^{-10}	4.39^{-9}
26 (n=6)	32 (n=12)	1.24^{-11}	2.68^{-9}
30 (n=10)	31 (n=11)	5.15^{-8}	8.14^{-8}
30 (n=10)	32 (n=12)	7.93^{-8}	1.16^{-7}

p	KN(p,i) cm^3 sec^{-1} $i=1$	KN(i,p) cm^6 sec^{-1} $i=1$
25 (5^1p)	4.12^{-14}	1.07^{-29}
26 (n=6)	1.85^{-11}	1.30^{-24}
27 (n=7)	2.38^{-10}	3.48^{-23}
28 (n=8)	8.49^{-10}	1.36^{-22}
32 (n=12)	1.73^{-8}	4.57^{-21}

Optical Escape Factors :

Holstein[3] has given the following simple expression for calculation of escape factors:

$$\Lambda_{pq} = \frac{1.6}{\tau(p,q)\ (\pi \ln \tau_{pq})^{\frac{1}{2}}} \qquad (4.35)$$

where $\tau(p,q)$ is the optical depth.

Drawin and Emard[55] have considered optical escape factors in detail and included effects due to Stark broadening, inelastic and superelastic collisions suitable to collisional radiative model, and derived expressions for $\Lambda_{p,q}$ and $\tau_{p,q}$ in terms of 2^1P-1^1S transition for HeI. But in the present study, electron density being low (10^{10}-10^{13}) for Stark broadening to become important, only Doppler broadening is taken into account and accordingly the following expression for optical depth is applicable:

$$\tau_{p,q} = \tau_{12} \frac{f_{pq}}{f_{12}} \frac{\lambda^2_{pq}}{\lambda^2_{12}} \frac{(\Delta\lambda_D)_{pq}}{(\Delta\lambda_D)_{12}} . \qquad (4.36)$$

where $$(\Delta\lambda_D)_{pq} = \frac{\lambda_{pq}}{c} \left(\frac{2kT_g}{M}\right)^{1/2}, \qquad (4.37)$$

and $$\tau_{12} = \frac{e^2}{m_e c^2} f_{12}\, n(1)\, L \frac{\lambda^2_{12}}{(\Delta\lambda_D)_{12}} \qquad (4.38)$$

Here (1,2) indicates the first resonance transition (1^1S-2^1P), f_{pq} is the absorption oscillator strength, λ_{pq} is the wavelength of the line radiation, T_g is the gas temperature, M and m_e are the atomic and electronic masses, and L is the

average length through which the light travels.

Λ_{1q} values calculated from τ_{1q} (from eq. (4.35)) are used in the calculations wherein A(q,1) are replaced by $\Lambda_{1,q}$ A(q,1).

Plasma Parameters Used in CR Model Calculations:

From probe data, axial variation of T_e was found to be within 10% at all magnetic field values. Further, at high and low field values, the ion saturation current was found to be practically invariant of the axial position. At median magnetic field strengths the variation was found to be ∿15% with respect to the value at the centre of the column — with high values at the electron gun end and low values at the pump end. On the basis of these observations it was concluded that, although some axial variation exists, reasonable values of average population densities can be obtained using the n_e, T_e values at the centre of the column.

n_e Determination from Current Ratio Method

In Chapter 3 results were presented on measurements of emission intensity ratios at pairs of emission currents for a number of HeI lines. On the basis of these ratios and collisional-radiative model calculations, it is possible to derive electron density variations in the plasma as has recently been

applied to hydrogen plasma.[56] Examination of the r_o and r_1 coefficients given in Table 4.10 as well as those in Ref. 43 will show that r_o coefficients, in the temperature and electron density range of the present experiments, has negligible contributions to the population densities of excited states in comparison with contributions from r_1. Neglecting thus the contribution of r_o in eq. (4.18), the ratio of r_1 values at two electron densities n_{e_2} and n_{e_1} is given by

$$\frac{r_1^{n_{e_2}}(p)}{r_1^{n_{e_1}}(p)} = \frac{n^{n_{e_2}}(p)}{n^{n_{e_1}}(p)} = \frac{I^{n_{e_2}}(p)}{I^{n_{e_1}}(p)} \qquad (4.39)$$

where $I^{n_{e_1}}(p)$, $I^{n_{e_2}}(p)$ refer to emission intensities of a given transition at the two electron densities. The second equality in eq. (4.39) is valid because of cancellation of the common transition probability appearing both in the numerator and the denominator. The above equation can be used for deriving the plasma electron densities.

Table 4.9 shows that the ratio of r_1 values at two electron densities n_{e_1} andn_{e_2} is dependent only on the magnitude of electron densities and is insensitive to changes in electron temperature. Thus a certain ratio of $r_1^{n_{e_2}}/r_1^{n_{e_1}}$ is unique to a certain n_{e_2}/n_{e_1} ratio and the n_{e_1} (or n_{e_2}) value. If a plot is made of this r_1-ratio versus the electron density n_{e_1} (or n_{e_2}), and it is assumed that the plasma electron density n_e's are proportional

TABLE 4.9

Values of the ratio of $r_1^{n_{e_2}}/r_1^{n_{e_1}}$ for the HeI 3^3P state at various electron temperatures

n_{e_1}	n_e ratio $= n_{e_2}/n_{e_1}$	T_e (eV) 11.4	9.5	8.0	5.8	3.17
1.0^{10}	3	2.98	2.99	2.99	2.99	2.99
	4	3.97	3.97	3.98	3.98	3.98
5.0^{10}	3	2.93	2.94	2.94	2.95	2.95
	4	3.87	3.88	3.89	3.90	3.98
1.0^{11}	3	2.88	2.89	2.89	2.91	2.92
	4	3.77	3.78	3.79	3.82	3.96
5.0^{11}	3	2.62	2.61	2.62	2.67	2.90
	4	3.30	3.29	3.30	3.39	3.39
1.0^{12}	3	2.41	2.40	2.41	2.42	2.42
	4	2.96	2.92	2.95	3.04	3.09
1.0^{13}	3	1.51	1.49	1.49	1.49	1.50
	4	1.62	1.60	1.59	1.60	1.63

to the emission current i_e's (i_e as defined in Ch. 2), the electron density at which the r_1-ratios match with the experimental emission intensity ratios $I^{i_{e_2}}(p)/I^{i_{e_1}}(p)$ is the electron density of the plasma at emission current i_{e_1} (or i_{e_2}). By using emission intensity ratios at emission currents 3 amp to 1 amp and also 2 amp to 1/2 amp, plasma electron densities were derived. The r_1 ratio plots for the states 3^1D, 4^1D, 5^1D and 3^3P, 4^3P are given in Figs. 4.1, 4.2 and 4.3. In these figures r_1^4/r_1^1 (or r_1^3/r_1^1) represents the ratio of r_1 values at $4n_{e_1}$ (or $3n_{e_1}$) to that at n_{e_1}. Figures 4.1, 4.2 and 4.3 in conjunction with Figs. 3.12, 3.13 and 3.14, are used to derive electron densities. Electron densities, derived in this manner versus the field plot is given in Fig. 4.4. r_1-Ratio plots of Figs. 4.1, 4.2 and 4.3 can be made with any collisional-radiative model results, but in this case, r_1 values obtained from the collisional-radiative model calculations in the present work have been used.

It is necessary, for calculation of population densities, to have knowledge about the plasma parameters n_e and T_e. However, the n_e values deduced from the ratio method as above, and n_e from probe data are at variance. The same is true for T_e obtained from probe method and that from ratio of singlet-triplet emission intensities, as shown in Fig. 3.19. Rather than making collisional-radiative model calculations for all such plasma parameter conditions as shown in Fig. 3.19 and Fig. 4.4, a reverse approach is adopted, wherein n_e, T_e profiles are evolved from concurrent considerations of the

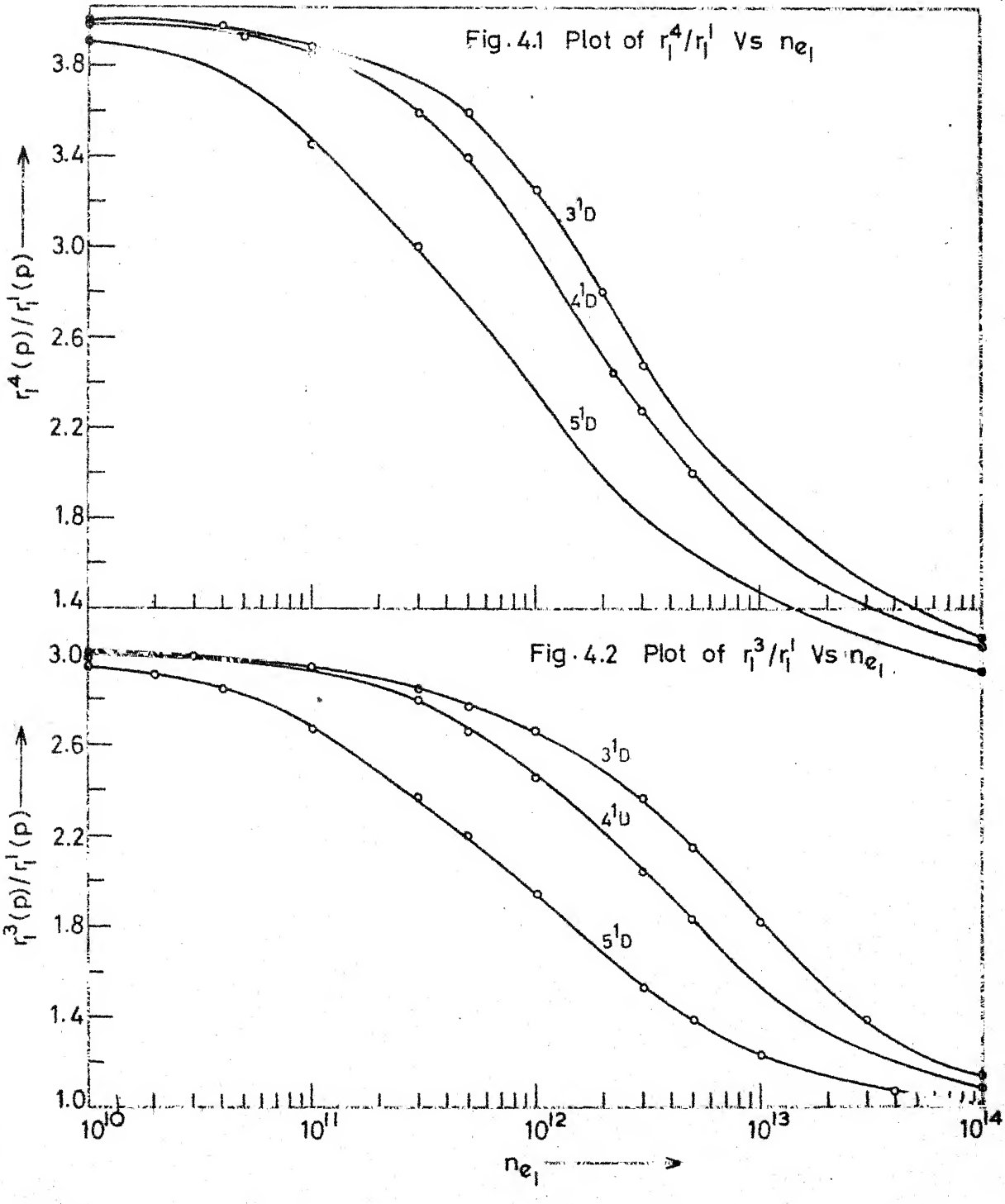
Fig. 4.1 Plot of r_l^4/r_l^1 Vs n_{e_l}
$r_l^4(p)/r_l^1(p)$
3.8
3.4
3.0
2.6
2.2
1.8
1.4
3^1D
4^1D
5^1D
Fig. 4.2 Plot of r_l^3/r_l^1 Vs n_{e_l}
$r_l^3(p)/r_l^1(p)$
3.0
2.6
2.2
1.8
1.4
1.0
3^1D
4^1D
5^1D
10^{10}
10^{11}
10^{12}
10^{13}
10^{14}
n_{e_l}

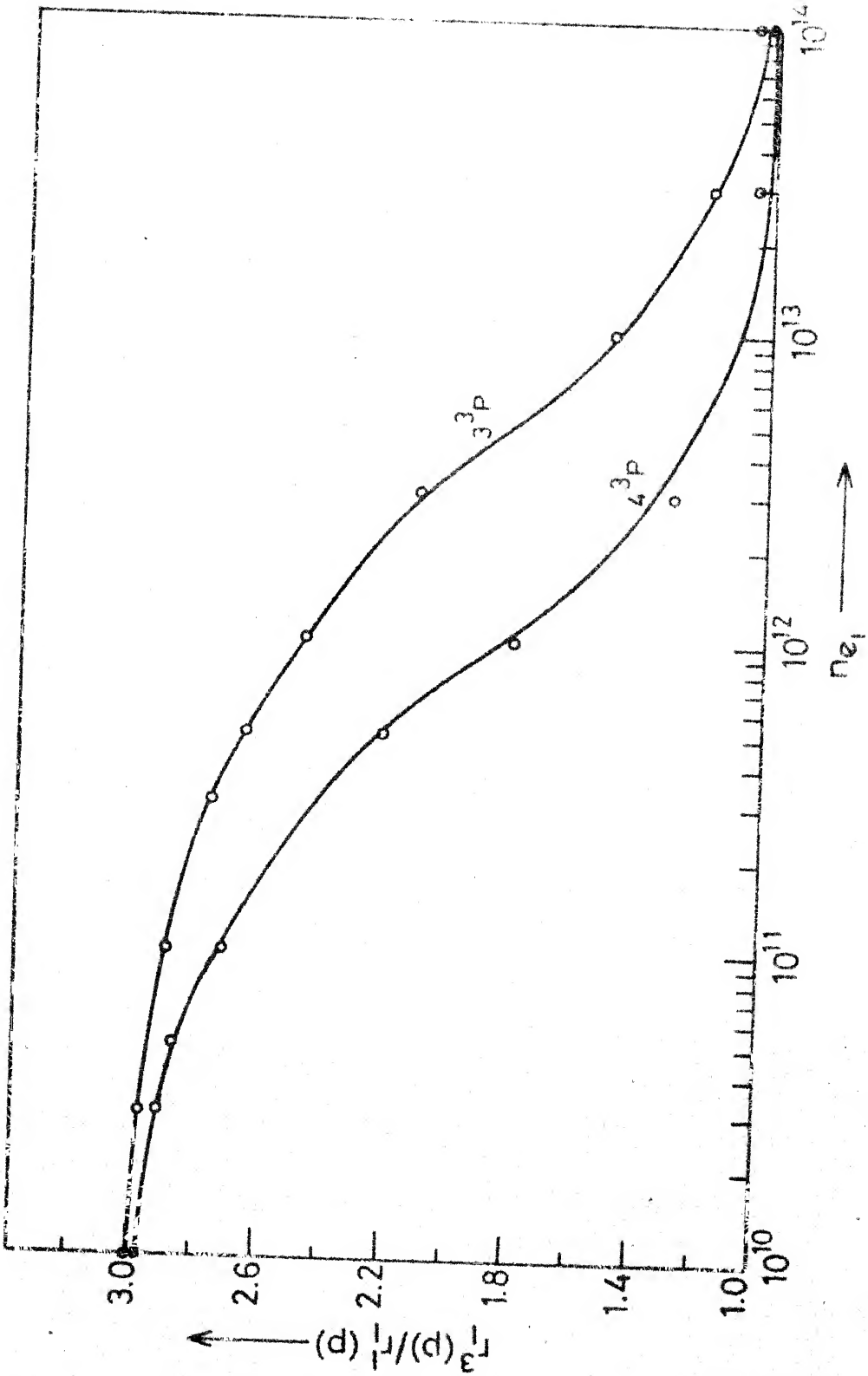

Fig. 4.3 Plot of r_1^3/r_1^1 as a function of n_{e_1}

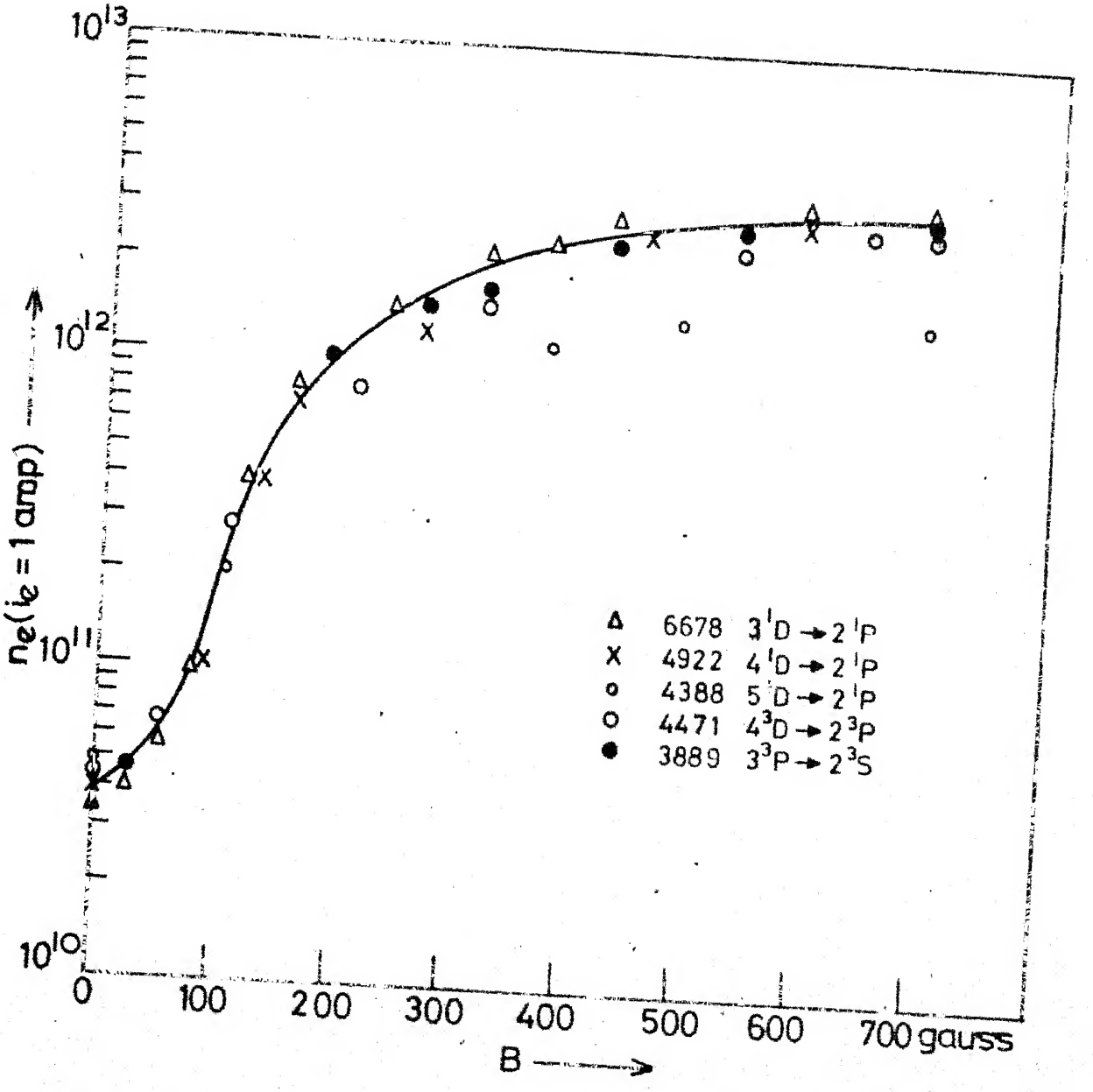

Fig.4.4 n_e from the current ratio method

observed enhancement factors and the predictions from the model. Specifically at B=0, $n_e=4x10^{10}$, T_e = 11.2 eV and at B = 700, n_e = 3.2 x 10^{12}, T_e = 5.9 eV are used. The n_e, T_e profile (as a function of the magnetic field B) adopted in the intermediate region is shown in Fig. 4.15. Later, such n_e, T_e profiles are compared with those obtained from experimental measurements of plasma parameters and reasonableness of the n_e, T_e profiles used in the calculations are discussed.

Calculation of Enhancement Factors and Comparison with Experimental Results:

As pointed out earlier, 43 equations involving the populations of HeI and HeII were solved simultaneously, using IBM 7044/1401 computer, to give final r_o, r_1, r_o^+, r_1^+ and r_2^+ coefficients from which populations of various HeI and HeII states could be calculated from eqs. (4.18) and (4.19). Calculations were made for an electron temperature range of 3 eV-14 eV at every 0.5 eV interval, an electron density range of 10^9-10^{17} with 5 values (1,3,5,7,9) for every decade, neutral densities of 10^{14} to 4 x 10^{14}, at gas temperatures T_g = 500, 1000, 1500 and 2000°K, and $He^+(1)/He^{++}$ ratios 1, 10, 1000, 10^4, 10^5. Calculations were made for three sets of HeI optical escape factors: (i) for all radiation Λ_{pq} = 1, i.e., plasma optically thin, (ii) plasma partially optically thick for resonance radiation with $\Lambda_{1,5}$ = 0.0009, $\Lambda_{1,11}$ = 0.006, $\Lambda_{1,18}$ = 0.014, $\Lambda_{1,25}$ = 0.03, $\Lambda_{1,26}$ = 0.07, $\Lambda_{1,27}$ = 0.15, $\Lambda_{1,28}$ = 0.35;

the rest $\Lambda_{pq} = 1$, (iii) plasma partially optically thick for resonance radiation with $\Lambda_{1,5} = 0.0095$, $\Lambda_{1,11} = 0.075$, $\Lambda_{1,18} = 0.15$, $\Lambda_{1,25} = 0.35$, $\Lambda_{1,26} = 0.7$ and rest $\Lambda_{pq} = 1$. (Note that p, q refer to level numbers given in Table 4.1.) The case (ii) corresponds to L $\sim$ 40 cm and (iii) to L $\sim$ 6 cm in eq. (4.38). For HeII, Lyman radiation (i) completely optically thick for all lines, i.e., $\Lambda_{1j} = 0$, (ii) $\Lambda_{12} = 0.001$, $\Lambda_{13} = 0.01$, $\Lambda_{14} = 0.06$, $\Lambda_{15} = 0.1$ and rest $\Lambda_{ij} = 1$ corresponding to L $\sim$ 6 cm. Calculations were made for all possible combinations of n_e, T_e, $n(1)$, T_g, $n^+(1)/n^{++}$, and various optically thick conditions detailed above.

Some typical values of r_o, r_1 are given in Table 4.10. For HeI(p) population density calculations, the ground state HeI(1) density is taken as $\sim 2 \times 10^{14}$. It will be observed that the population of HeI levels given by eq. (4.18) is dominated by the second term which contains the population coefficient r_1, since contribution from r_o values are negligible in the entire range of electron densities involved in the experiment. r_1 values for 1 set of conditions involving the five series of transitions are presented here, in Figs. 4.5-4.9. The conditions used are $n(1) = 2 \times 10^{14}$, $T_g = 1000^oK$, $T_e = 5.9$ and 11.2 eV, $n^+(1)/n^{++} = 10^4$, and plasma partially optically thick $\Lambda_{1,5} = 0.0095$, $\Lambda_{1,11} = 0.075$, $\Lambda_{1,18} = 0.15$, $\Lambda_{1,25} = 0.35$, $\Lambda_{1,27} = 0.7$ and all other $\Lambda_{p,q} = 1$.

TABLE 4.10

Values of $r_o(p)$, $r_1(p)$ coefficients and contributions from $r_o(p)$ and $r_1(p)$ to population densities of some HeI excited states

Partially optically thick case (Λ_{pq}'s as in column 3 of T.4.11), $n^+ \sim n_e$

T_e = 11.2 eV, n(1) = 2.0^{14} cm^{-3}

n_e	p	$r_o(p)$	$r_1(p)$	$r_o.n_E(p)$ A	$\frac{r_1(p).n_E(p).n(1)}{n_E(1)}$ B	n(p)=A+B (cm^{-3})
10^{10}	6 (3^3S)	5.5	2.34^{-8}	3.64^{-3}	1.82^6	1.82^6
	9 (3^3D)	3.2	1.80^{-9}	5.6^{-2}	6.79^5	6.79^5
	11(3^1P)	3.3	2.10^{-8}	1.1^{-2}	1.58^6	1.58^6
	15(4^3D)	3.8	1.04^{-9}	6.3^{-2}	3.70^5	3.70^5
	22(5^3D)	2.3	9.89^{-10}	2.2^{-2}	3.40^5	3.40^5
10^{14}	6	1.7	1.78^{-5}	6.18^5	1.38^9	1.38^9
	9	1.1	2.34^{-6}	1.93^6	8.82^8	8.83^8
	11	1.7	2.28^{-5}	5.98^5	1.72^9	1.72^9
	15	0.97	6.38^{-7}	1.6^6	2.27^8	2.28^8
	22	0.98	1.40^{-7}	1.57^6	4.83^7	4.98^7
			T_e = 5.9 eV, n(1) = $2x10^{14}$ cm^{-3}			
10^{10}	6	0.36	3.29^{-8}	3.99^{-3}	4.12^5	4.12^5
	9	2.00	2.78^{-9}	1.04^{-1}	1.63^5	1.63^5
	11	0.14	2.48^{-8}	1.42^{-3}	2.91^5	2.91^5
	15	1.24	1.63^{-9}	5.70^{-2}	8.56^4	8.56^4
	22	1.47	1.52^{-9}	6.48^{-2}	7.57^4	7.57^4
10^{14}	6	1.85	2.42^{-5}	2.03^6	3.00^8	3.02^8
	9	1.14	3.89^{-6}	5.93^6	2.29^8	2.34^8
	11	1.88	2.25^{-5}	1.95^6	2.64^8	2.65^8
	15	1.00	8.91^{-6}	4.65^6	4.68^7	5.13^7
	22	0.99	1.78^{-7}	4.34^6	8.86^6	1.30^7

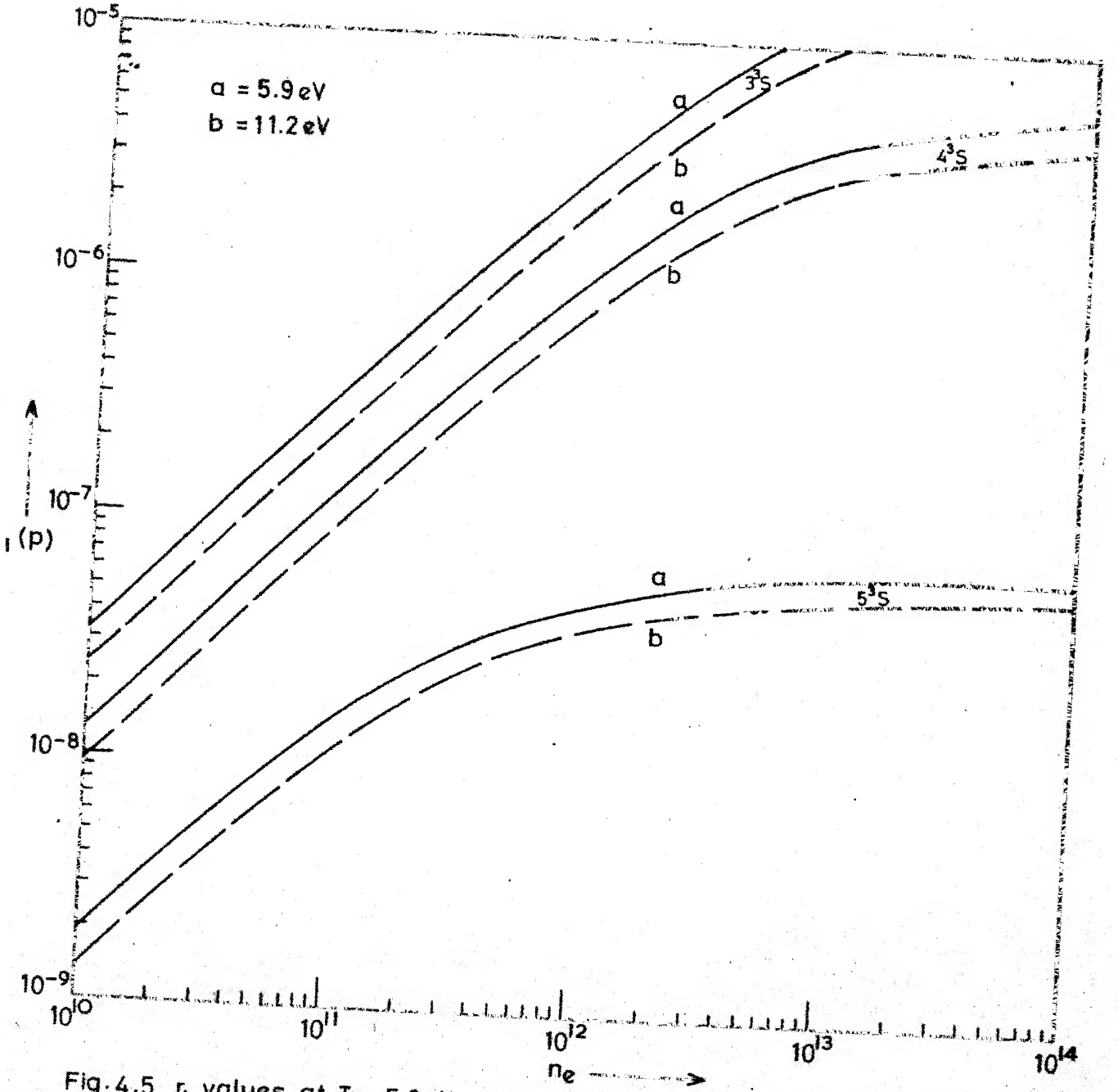

Fig. 4.5 r_1 values at $T_e = 5.9$ eV and 11.2 eV for HeI states 3^3S, 4^3S, 5^3S

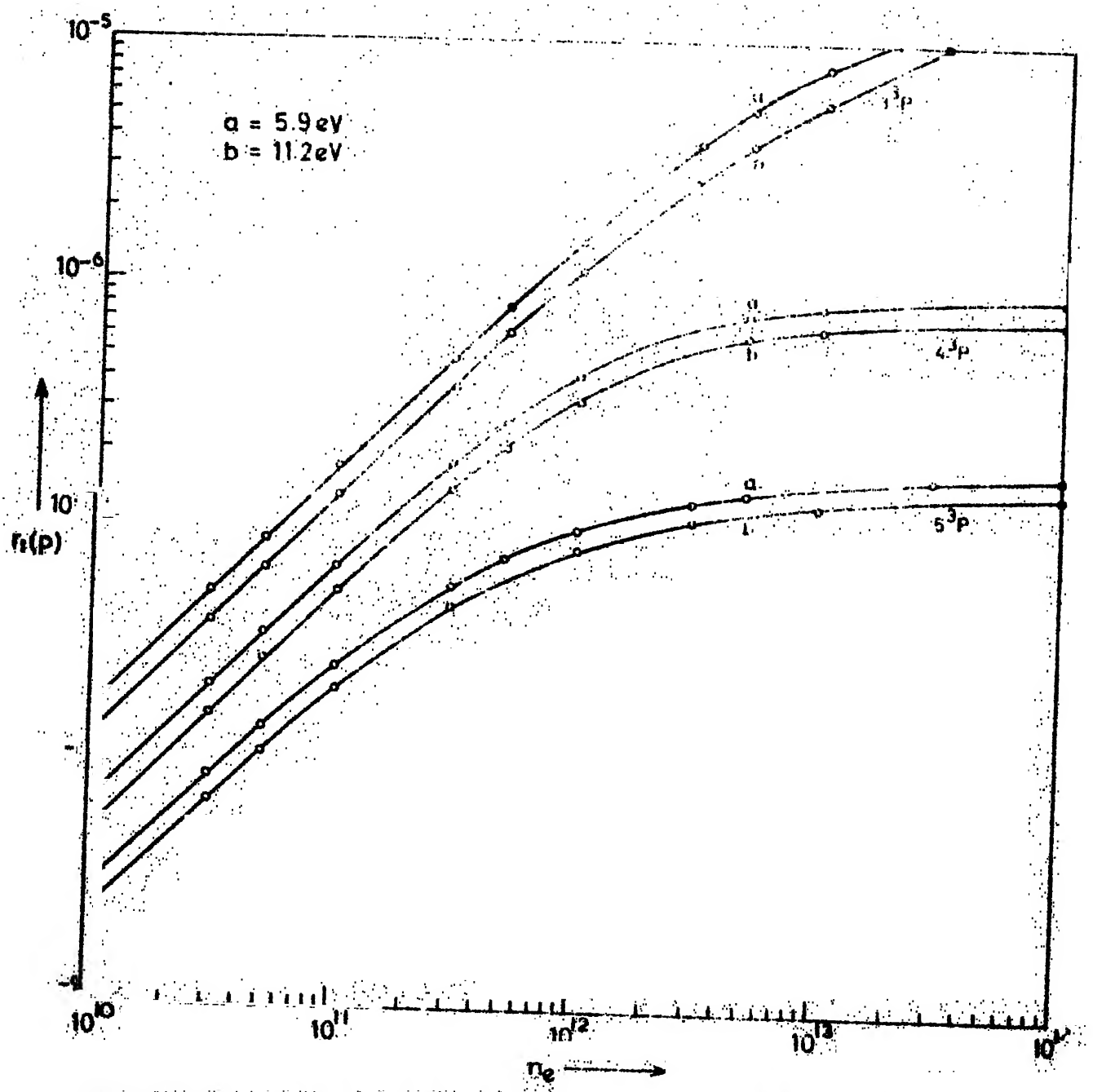

Fig. 4.6 r_i values at T_e=5.9eV and 11.2eV for He I states 3^3P, 4^3P, 5^3P

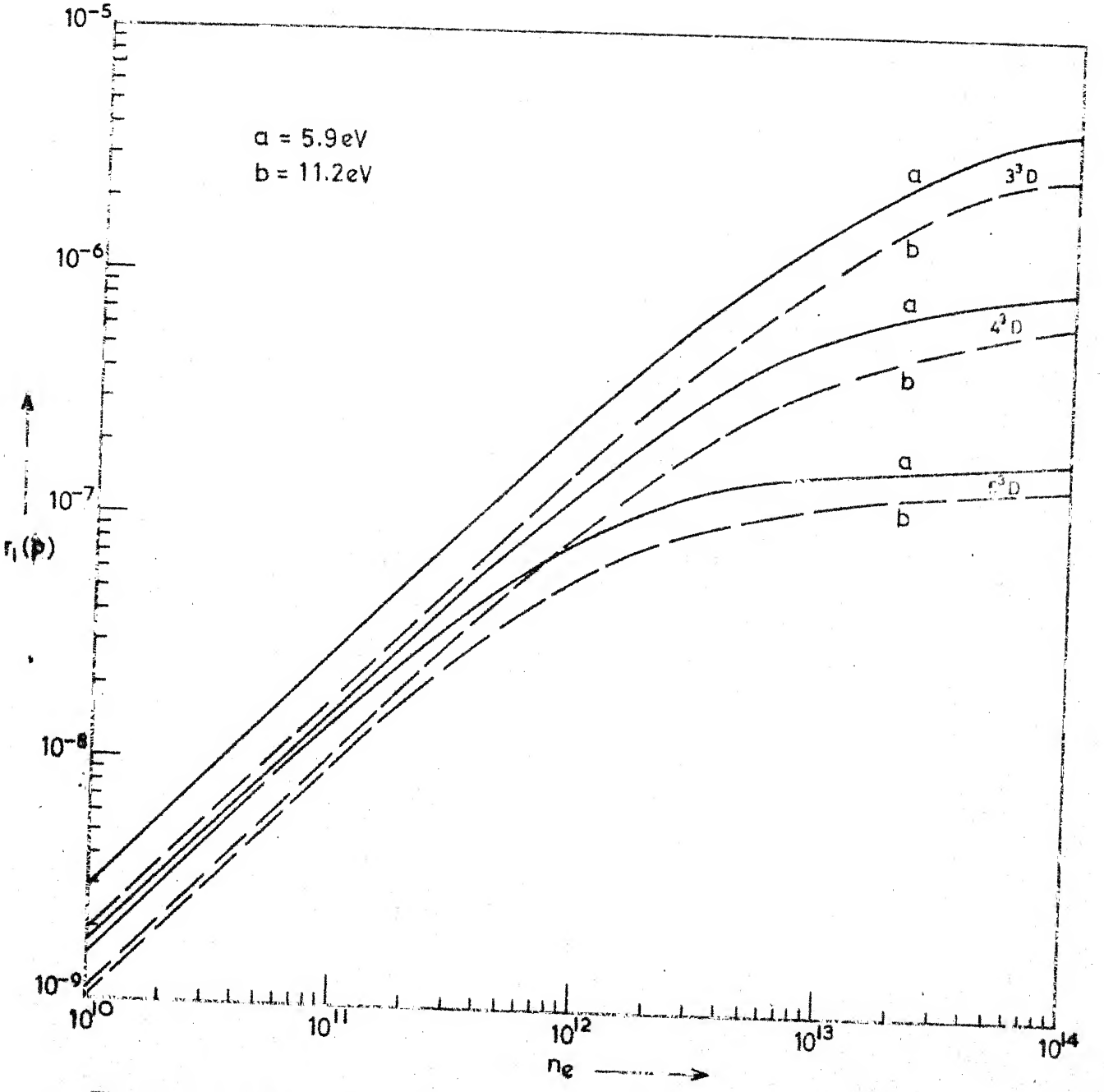

Fig. 4.7 r_1 values at $T_e = 5.9$ eV and 11.2 eV for He I states $3^3D, 4^3D, 5^3D$

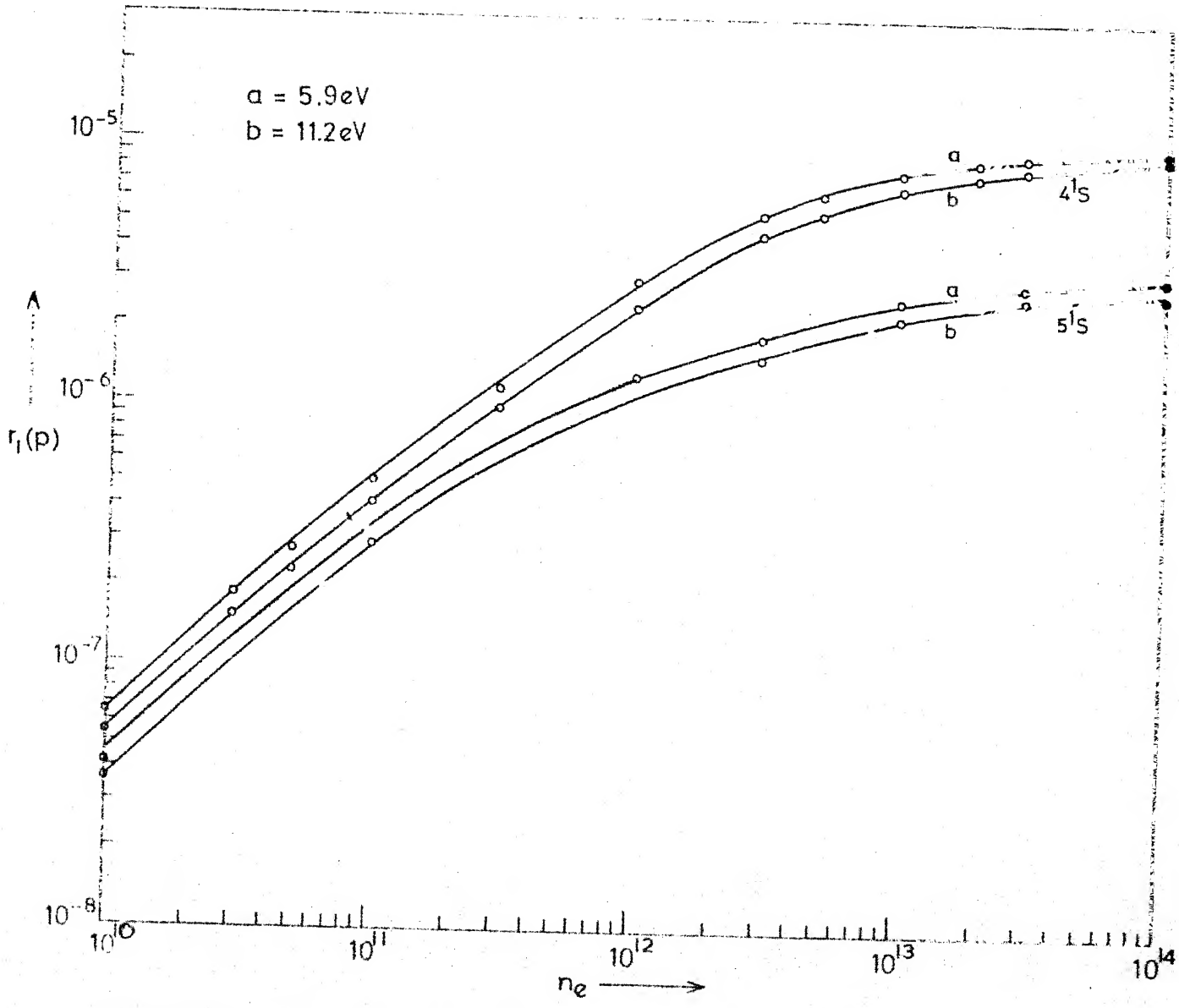

Fig. 4.8 r_i values at T_e = 5.9eV and 11.2 eV for He I states 4^1S, 5^1S

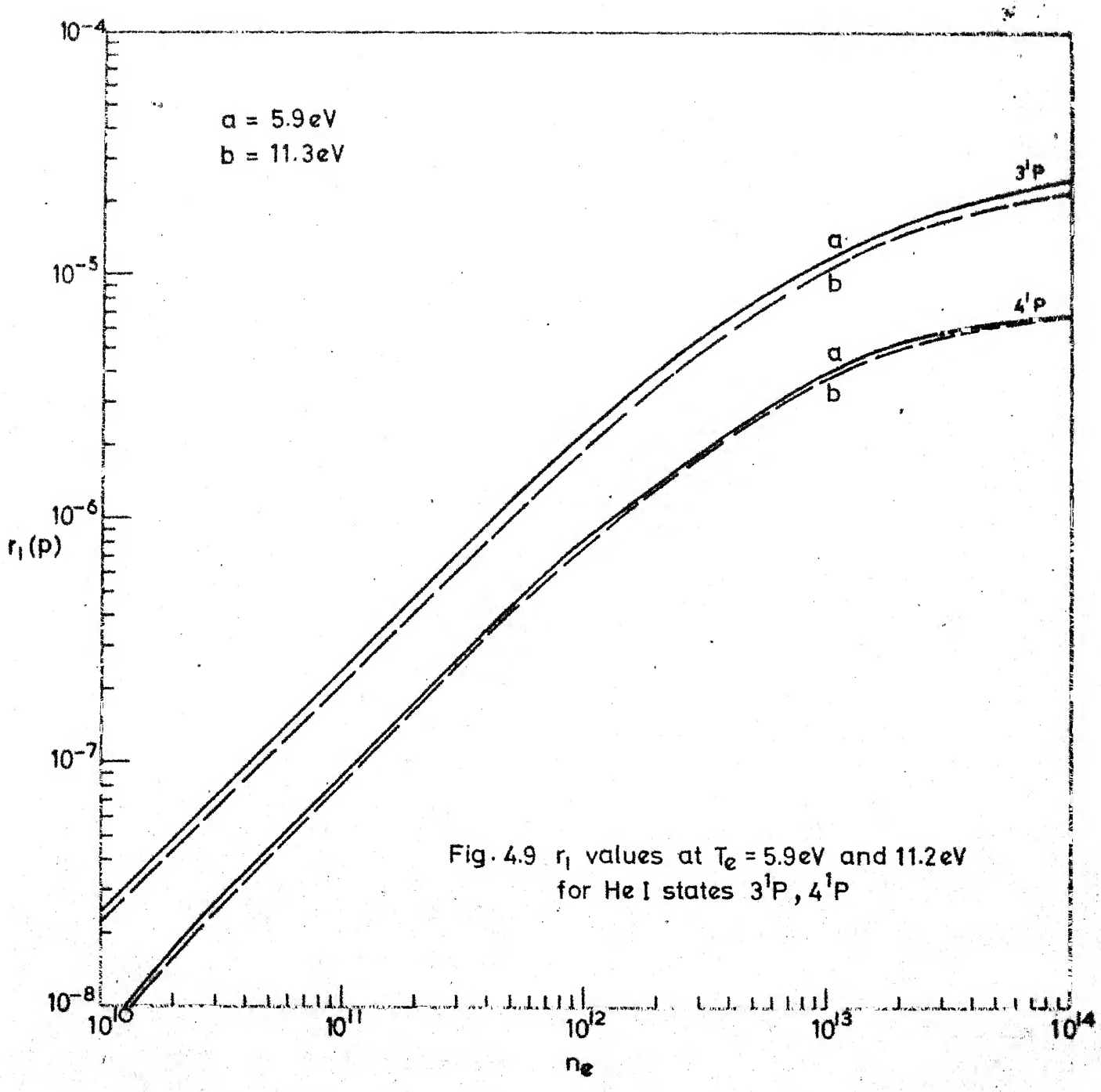

Fig. 4.9 r_l values at T_e = 5.9eV and 11.2eV for He I states 3^1P, 4^1P

The emission enhancement factor of a line, i.e., the ratio of emission intensity at field B to that in absence of field is given, from a consideration of eq. (4.18) and neglecting r_o contribution, by the following equation:

$$\frac{I_B(p)}{I_o(p)} = \frac{n_B(p)}{n_o(p)} = \frac{r_1(n_e^B, T_e^B)}{r_1(n_e^o, T_e^o)} \exp\left(-E_p\left(\frac{1}{kT_e^B} - \frac{1}{kT_e^o}\right)\right) \quad (4.40)$$

where T_e^B and T_e^o represent the electron temperatures at field B and that in the absence of field and E_p are as given in Table 4.1. Whereas in general such enhancement factors can be written for any two fields B_1 and B_2, we present here the enhancement factors wherein one of the intensities is at zero field.

In order to evaluate such enhancement factors predicted by the model, it is necessary therefore to consider two r_1 plots, one for T_e at B=0 and the other for T_e at B=700 gauss. According to the discussion presented in the previous section we use $T_e(B=0)$ = 11.2 eV and T_e(B=700 gauss) = 5.9 eV. This means that r_1 plots at 11.2 eV and 5.9 eV are needed to evaluate the enhancement factors. However, if theoretical estimates of enhancement factors for the entire range of magnetic field variation is required, it is necessary to use the electron temperature profile as the magnetic field is varied and then use the appropriate series of r_1 curves. In Table 4.11 the theoretical enhancement factors $I_{B=700}/I_{B=0}$ are presented for various conditions and then these are compared with the corresponding experimentally observed values.

TABLE 4.11

Comparison of observed and calculated $(I_B/I_o)_{700}$ for 1 amp emission current

Line Å	Transition	Expt. $(I_B/I_o)_{700}$ (Table 3.1)	Theoretically calculated $(I_B/I_o)_{700}$		
			Optically thin $\Lambda_{pq} = 1$	Partially* optically thick without reduced $^1P \rightarrow {}^1D$ coeff.	Partially** optically thick with reduced $^1P \rightarrow {}^1D$ coeff.
			1	2	3
5047	$4^1S \rightarrow 2^1P$	2.0	4.7	5.1	5.0
4437	$5^1S \rightarrow 2^1P$	2.0	2.0	2.6	2.0
7065	$3^3S \rightarrow 2^3P$	16.0	13.0	14.4	13.8
4713	$4^3S \rightarrow 2^3P$	8.0	9.3	9.7	9.2
4121	$3^3S \rightarrow 2^2P$	2.0	2.2	1.9	1.9
5875	$3^3D \rightarrow 2^3P$	12.0	12.7	15.4	13.2
4471	$4^3D \rightarrow 2^3P$	9.5	10.3	11.6	9.8
4026	$5^3D \rightarrow 2^3P$	3.5	4.4	5.2	3.0
3889	$3^3P \rightarrow 2^3S$	9.0	8.5	16.0	10.0
3187	$4^3P \rightarrow 2^3S$	5.0	4.7	4.6	4.5
6678	$3^1D \rightarrow 2^1P$	14.5	10.8	32.0	12.2
4922	$4^1D \rightarrow 2^1P$	9.0	6.0	19.5	9.4
4388	$5^1D \rightarrow 2^1P$	3.0	3.0	4.8	2.9
5015	$3^1P \rightarrow 2^1S$	4.0	17.0	6.6	9.0
3964	$4^1P \rightarrow 2^1S$	3.0	13.8	6.0	6.0

* $\Lambda_{1,5} = 0.0009$, $\Lambda_{1,11} = 0.006$, $\Lambda_{1,18} = 0.014$, $\Lambda_{1,25} = 0.03$ $\Lambda_{1,26} = 0.07$, $\Lambda_{1,27} = 0.15$, $\Lambda_{1,28} = 0.35$, Rest $\Lambda_{pq} = 1$.

** $\Lambda_{1,5} = 0.0095$, $\Lambda_{1,11} = 0.075$, $\Lambda_{1,18} = 0.15$, $\Lambda_{1,25} = 0.35$, $\Lambda_{1,26} = 0.7$, Rest $\Lambda_{pq} = 1$.

For these calculations n_e (B=0) = 4×10^{10}, n_e(B=700) = 3.2×10^{12}; T_g = 1000 K, $n^+(1)/n^{++} = 10^4$.

In Table 4.11, the first column of theoretical values is for the optically thin condition. It will be noted that the theoretical values of the ratio is within 9% except for the transitions $4^1S \rightarrow 2^1P$, $3^1D \rightarrow 2^1P$, $4^1D \rightarrow 2^1P$, $3^1P \rightarrow 2^1S$ and $4^1P \rightarrow 2^1S$, out of which the last two lines show very large variations. Criteria for application of optically thick condition have been discussed in the previous section, and such condition is applicable to the results of the present experiments. Results of calculations using partially optically thick condition with $\Lambda_{1,5} = 0.0009$, $\Lambda_{1,11} = 0.006$, $\Lambda_{1,18} = 0.014$, $\Lambda_{1,25} = 0.03$, $\Lambda_{1,26} = 0.07$, $\Lambda_{1,27} = 0.15$, $\Lambda_{1,28} = 0.35$ and the rest of transitions $\Lambda_{pq} = 1$ are shown in the second column of theoretically predicted results.

The immediate effect of application of optically thick condition is to increase the populations of 3^1P and 4^1P at low electron densities without significantly affecting the populations at high electron densities, and this leads to a lowering of emission intensity enhancement factors. But this condition simultaneously increases the populations of the 3^1D and 4^1D states for moderate and high densities and hence very large enhancement factors result. In this case the average variation of the theoretical I_B/I_o values with respect to the experimental ratios is within 15% except for the lines $4^1S \rightarrow 2^1P$, $3^1D \rightarrow 2^1P$ and $4^1D \rightarrow 2^1P$.

While exploring possible conditions which might further bridge the gap between the experimental and the theoretical ratios, one notes that use of optically thin condition and higher values of collisional excitation coefficients from 1^1S to n^1P would also lead to lower values of emission enhancement factors for the lines $3^1P \rightarrow 2^1S$ and $4^1P \rightarrow 2^1S$. However, not only does this not take care of the requirement of partially optically thick condition as previous discussion indicates, but the rate coefficients of the resonance transitions 1^1S-n^1P are quite well studied, and the values seem to be reasonably accepted. On the other hand, if partially optically thick condition is used as shown in the column 2 of the theoretical results, additional considerations are necessary which will at least lead to lower values of the enhancement factors for the lines $3^1D \rightarrow 2^1P$ and $4^1D \rightarrow 2^1P$. In this regard, two changes can be incorporated, primarily with the idea of finding conditions which makes the theoretical and experimental ratios match closer, (i), which involves making the plasma less optically thick compared to that used for calculations of column 2, and (ii), which uses reduced values of the excitation rate coefficients of $^1P-^1D$ transitions. Specifically, the plasma is considered partially optically thick with $\Lambda_{1,5}=0.0095$, $\Lambda_{1,11} = 0.075$, $\Lambda_{1,18} = 0.15$, $\Lambda_{1,25} = 0.35$, $\Lambda_{1,26} = 0.5$ and the rest $\Lambda_{pq} = 1$, and the $K(p,q)$ used for $^1P-^1D$ transitions are 1/2 of the values that can be calculated using eq. (4.25).

The results of such calculations are shown in column 3 of theoretical results in Table 4.11. Among the three sets of theoretical results presented, the last set of calculations given in column 3 provides the best match with the experimental enhancement factors giving an average deviation or 7%, except the lines, $3^1P \rightarrow 2^1S$ and $4^1S \rightarrow 2^1P$.

While Table 4.11 shows the emission enhancement factors I(B=700)/I(B=0), emission enhancement profiles for the entire range of magnetic field variation, calculated by using the conditions of column 3 of Table 4.11, and n_e, T_e profiles of Fig. 4.13 are presented in Figs. 4.10-4.12 for the transitions $3^1D \rightarrow 2^1P$, $4^1D \rightarrow 2^1P$ and $5^1D \rightarrow 2^1P$, $3^3P \rightarrow 2^3S$ and $4^3P \rightarrow 2^3S$, $3^3D \rightarrow 2^3P$, $4^3D \rightarrow 2^3P$ and $4^3D \rightarrow 2^3P$.

It is to be mentioned here that the fit of the theoretical and experimental enhancement profiles is not significantly inferior from Figs. 4.10-4.12 if partially optically thick conditions of column 2 are used, except for the lines $3^3P \rightarrow 2^3S$, $3^1D \rightarrow 2^1P$, $4^1D \rightarrow 2^1P$. This, however, shows up also in Table 4.11.

All the experimental results presented in Table 4.11 are for an emission current of 1 amp. Enhancement factors were also measured at emission currents of 1/2 amp, 2 amp and 3 amp. The experimental emission enhancement factors have already been presented in Table 3.1. It has been shown that the electron densities are proportional to emission currents from data on electron collection current in the plasma

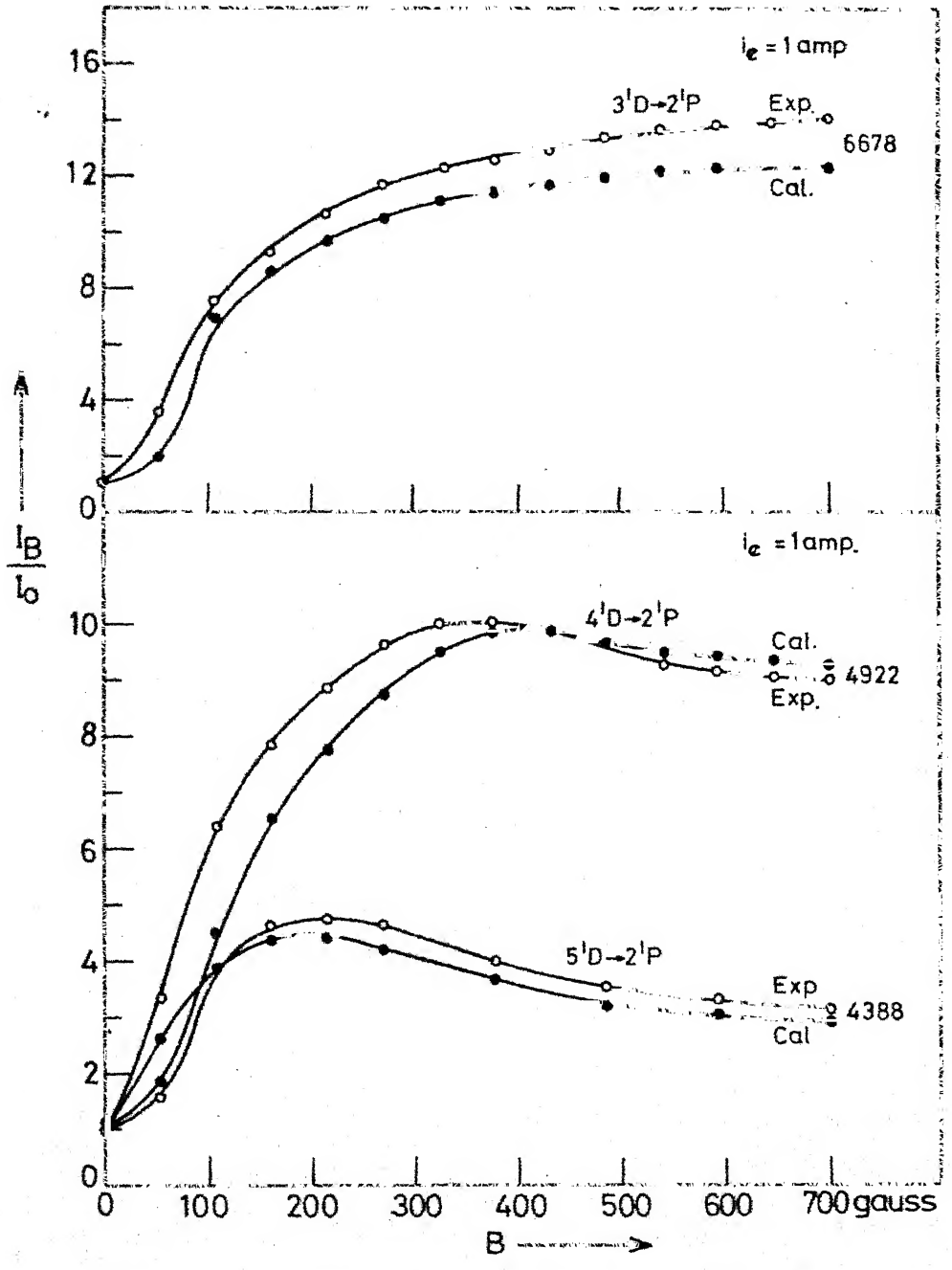

Fig. 4.10. Comparison of experimental and theoretical emission enhancement profiles

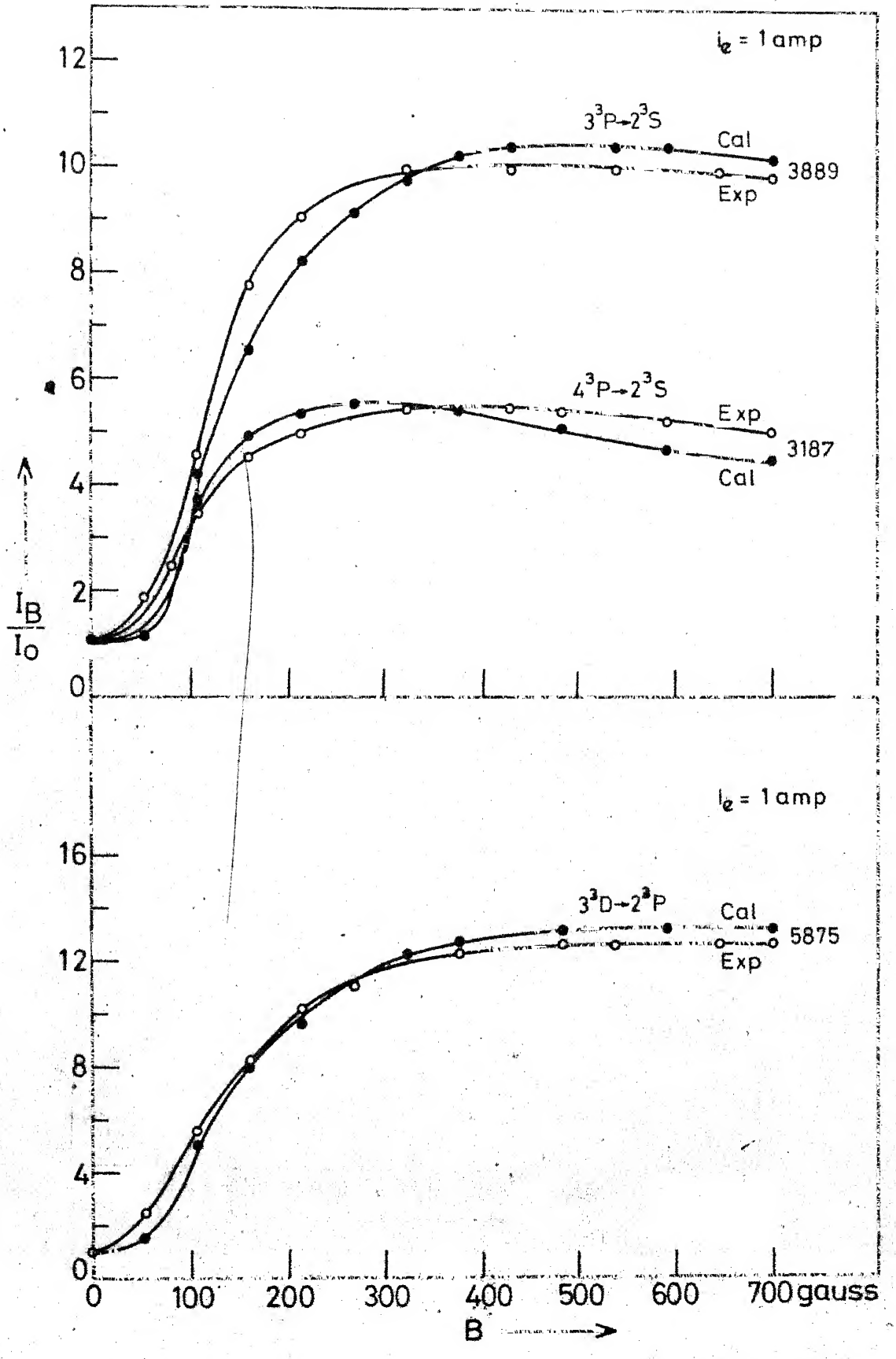

Fig. 4.11 Comparison of experimental and theoretical emission enhancement profiles

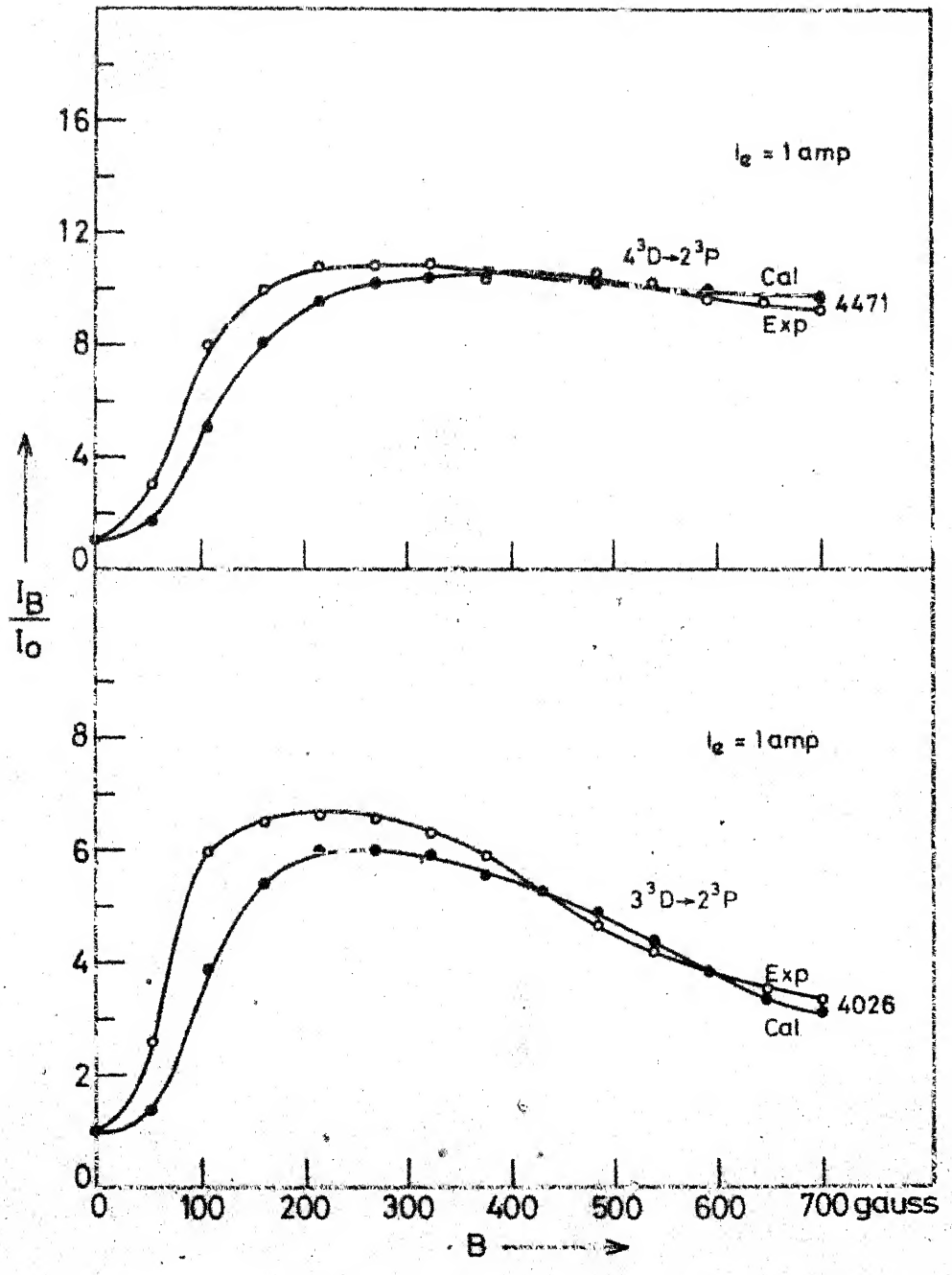

Fig. 4.12 Comparison of experimental and theoretical emission enhancement profiles

column, and also from probe data. The ion saturation current was in the ratio of ½:1:2:3 for emission currents of ½ amp: 1 amp:2amp:3amp. Theoretical emission enhancement factors for other emission currents therefore can be calculated using electron densities in proportion to that used for calculations at 1 amp of emission current. Electron temperatures are also necessary for calculation of populations. In longitudinal magnetic field electron temperature may be considered[39] to be independent of electron density. Experimental relative intensity measurements using He lines $4^1S/4^3S$ and $4^1D/4^3D$ to obtain T_e, as shown in Fig. 3.17 and 3.18, bear this out. Though the absolute values obtained are somewhat different, it is clear that at a particular B, T_e does not have n_e dependence in the experimental n_e range. One, therefore, may use the same T_e range for ½,2,3 amp of emission currents as has been used for 1 amp of emission current. Results of such theoretical calculations of enhancement factors I(B=700)/I(B=0) are shown in Table 4.12. Some enhancement profiles are shown in Fig. 4.13 which are evaluated in the same manner as enhancement factors at 1 amp of emission current. It must be mentioned that, here also, when the results are compared to the profiles corresponding to the conditions of column 2 of Table 4.11, the major variation from experimental curves arises for the lines 3^3P-2^3S, 3^1D-2^1P and 4^1D-2^1P.

TABLE 4.12

Comparison of experimentally observed and calculated $(I_B/I_0)_{700}$ for 0.5 amp, 2 amp and 3 amp emission currents

Emitting State	Line Å	i_e = 0.5 amp Cal	Obs	i_e=2 amp Cal	Obs	i_e = 3 amp Cal	Obs
3^3S	7065	20	32	10.7	10.5	7.4	8.0
4^3S	4713	14	17	6.2	6.0	3.9	3.5
5^3S	4121	2.8	3	1.5	1.7	1.1	1.2
3^3P	3889	14.0	18.0	7.3	7.0	5.2	5.0
4^3P	3187	10.04	9.5	3.6	3.9	2.2	3.5
3^1D	6678	16.2	24	10.5	12.0	9.5	9.0
4^1D	4922	13.0	11.0	4.4	4.8	3.6	3.0
5^1D	4388	5.2	4.8	2.5	2.3	2.1	1.8
3^3D	5875	16.0	17.5	10.5	9.5	8.0	
4^3D	4471	12.7	12.0	7.5	6.0	5.2	
5^3D	4026	6.0	4.5	2.7	2.5	2.1	
4^1S	5047	6.2	2.8	2.2	1.5	2.0	
5^1S	4437	3.0	2.6	1.7	1.5	1.5	
3^1P	5015	10.8	8.0	7.5	3.4	5.7	
4^1P	3964	8.0	4.0	4.8	2.3	3.0	

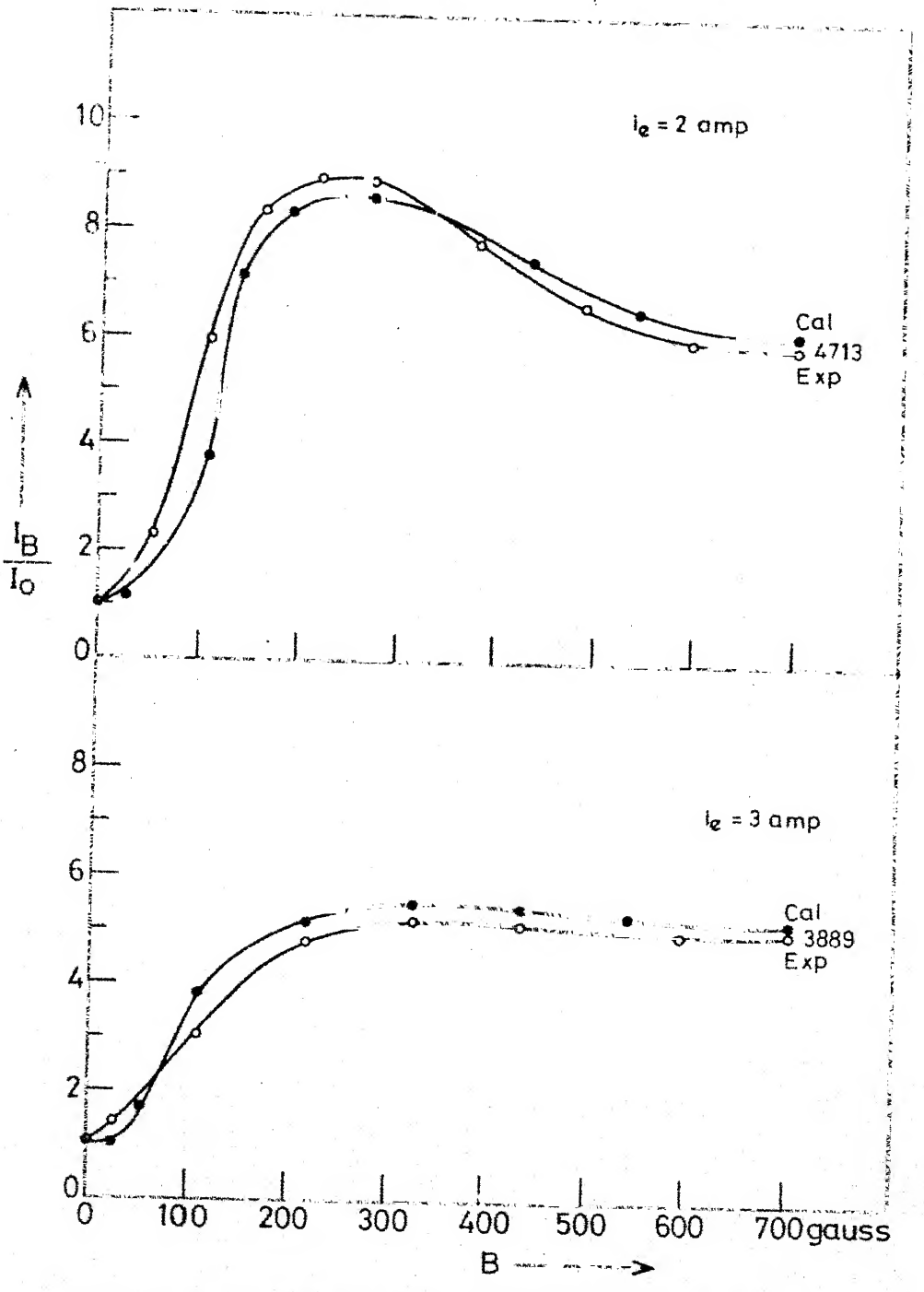

Fig.4.13 Comparison of experimental and theoretical emission enhancement profiles

Population of HeII levels also can be determined in a manner similar to that of HeI, i.e. using r_o^+, r_1^+ and r_2^+ coefficients (obtained by simultaneously solving the HeII equations with HeI ones) and assuming HeII(1) $\approx n_e$ and HeI(1) $\sim 2 \times 10^{14}$. Typical values of r_o^+, r_1^+ and r_2^+ coefficients and some population values are shown in Table 4.13. Enhancement factors I(B=700)/I(B=0) are also shown in Table 4.13. Enhancement profile for i=4, calculated by using the T_e and n_e profiles of Fig. 4.15, in the range B=0 and B=700, is shown in Fig. 4.14.

Now that the experimental and calculated emission profiles have been compared using the n_e, T_e profiles of Fig. 4.15, it is proper to discuss these plasma parameter profiles in the perspective of experimental plasma diagnostics data. Electron densities measured using probes is found to be 7-8 times lower than those observed from current ratio method although the pattern of variation from low field to high field is the same. Although the probe data gives an order of magnitude check of n_e, the probe n_e is likely to be less reliable for density determinations due to uncertainties of the probe theory in the magnetic field. Studies of Shaw and Kino[57] show that ion collection at the probe is normally lower in a magnetic field, corresponding to the plasma of the same density in absence of the field, and point out that it is difficult to get complete ion saturation. That the adopted

TABLE 4.13

$r_o^+(4)$, $r_1^+(4)$ and $r_2^+(4)$ of HeII (i=4) at 11.2 eV and 5.9 eV

n_e	$r_o^+(4)$		$r_1^+(4)$		$r_2^+(4)$	
	11.2 eV	5.9 eV	11.2 eV	5.9 eV	11.2 eV	5.9 eV
10^{10}	0.34	0.20	2.94^{-8}	2.06^{-10}	5.7^{-10}	6.5^{-10}
10^{12}	0.36	0.23	2.92^{-6}	2.05^{-8}	5.6^{-8}	6.2^{-8}
10^{14}	0.60	0.40	2.0^{-4}	1.8^{-6}	4.0^{-6}	4.8^{-6}

T_e eV	n_e	Optical thickness	n(1)	$n^+(4)$
11.2	4.0^{10}	Optically thin	2.0^{14}	9.97^3
5.9	3.2^{12}	Partially* optically thick	2.0^{14}	4.84^4

Observed $(I_B/I_O)_{700}$ = 6.3 at 1 amp

Calculated $(I_B/I_O)_{700} = \frac{4.84^4}{9.97^3}$ = 4.85

* Λ_{12} = 0.001, Λ_{13} = 0.01, Λ_{14} = 0.06, Λ_{15} = 0.1, & Λ_{ij} = 1.

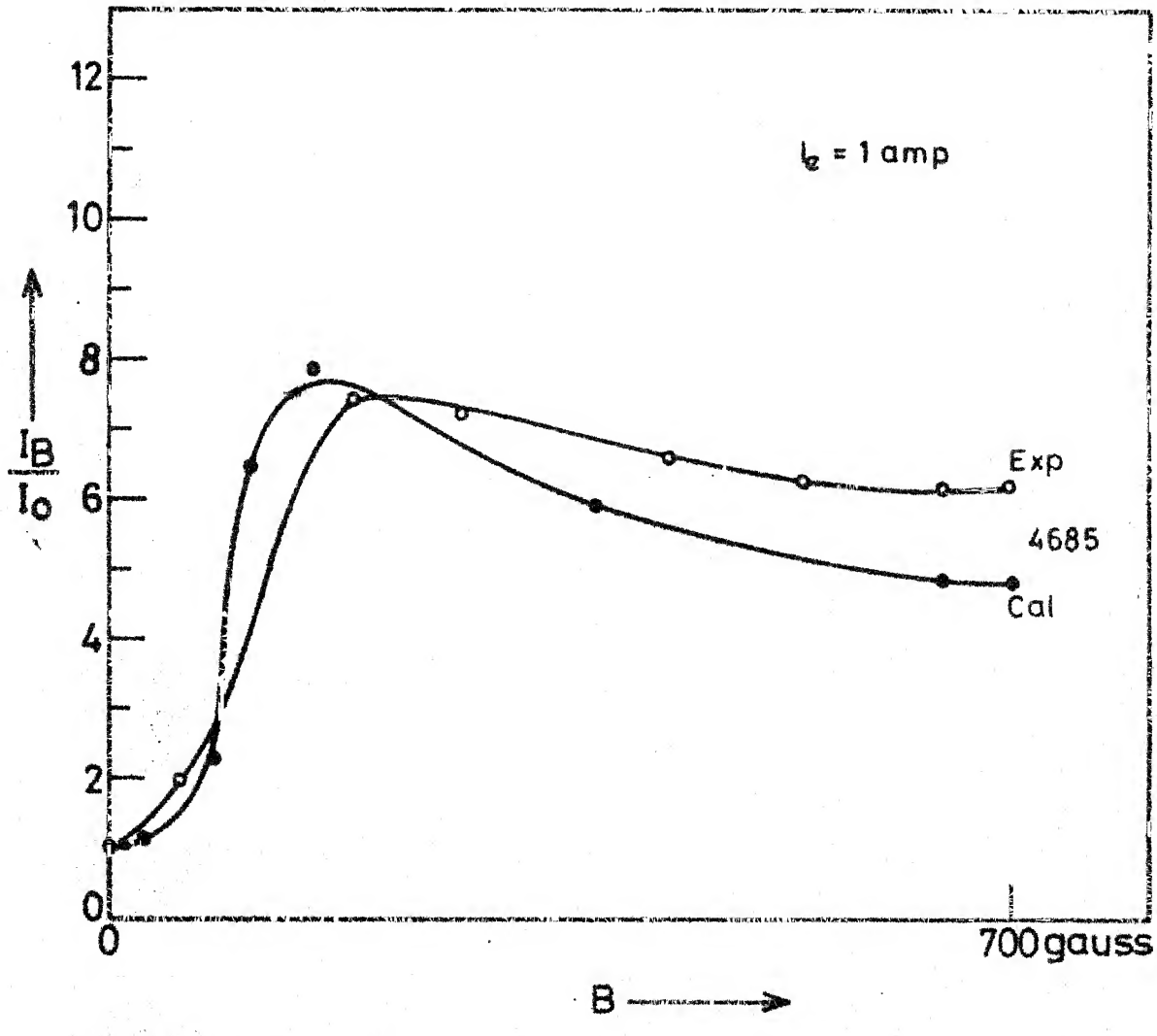

Fig.4.14 Comparison of calculated and observed I_B/I_o for He^+ line

n_e profile in Fig. 4.15 is located higher than the probe n_e profile, is compatible with these observations. An inspection of Fig. 4.15 shows the remarkable similarity between probe n_e profile and the n_e profile used in calculations as well as that obtained from emission current ratio method. It may be noted that if the effective collection area is lower than the geometric area used in n_e evaluation, significant improvement in n_e will result.

The electron temperature profile adopted for collisional-radiative model calculations is closer to T_e profile obtained from electric probes but considerably off from T_e profile obtained through singlet-triplet ratio measurements. According to Bickerton and von Engel,[38] electron temperatures measured by probes in the presence of magnetic field is almost at good as in absence of the field when the negative probe characteristics are taken for T_e estimation. They point out that any error in evaluation of probe T_e is essentially due to assumptions inherent in the probe theory applicable to plasmas in absence of magnetic field. The presence of magnetic field does not alter the situation substantially.

Electron temperature measurements from line intensity ratio method[41] has considerably more limitations. The ordinarily used expression of singlet-triplet intensity ratio

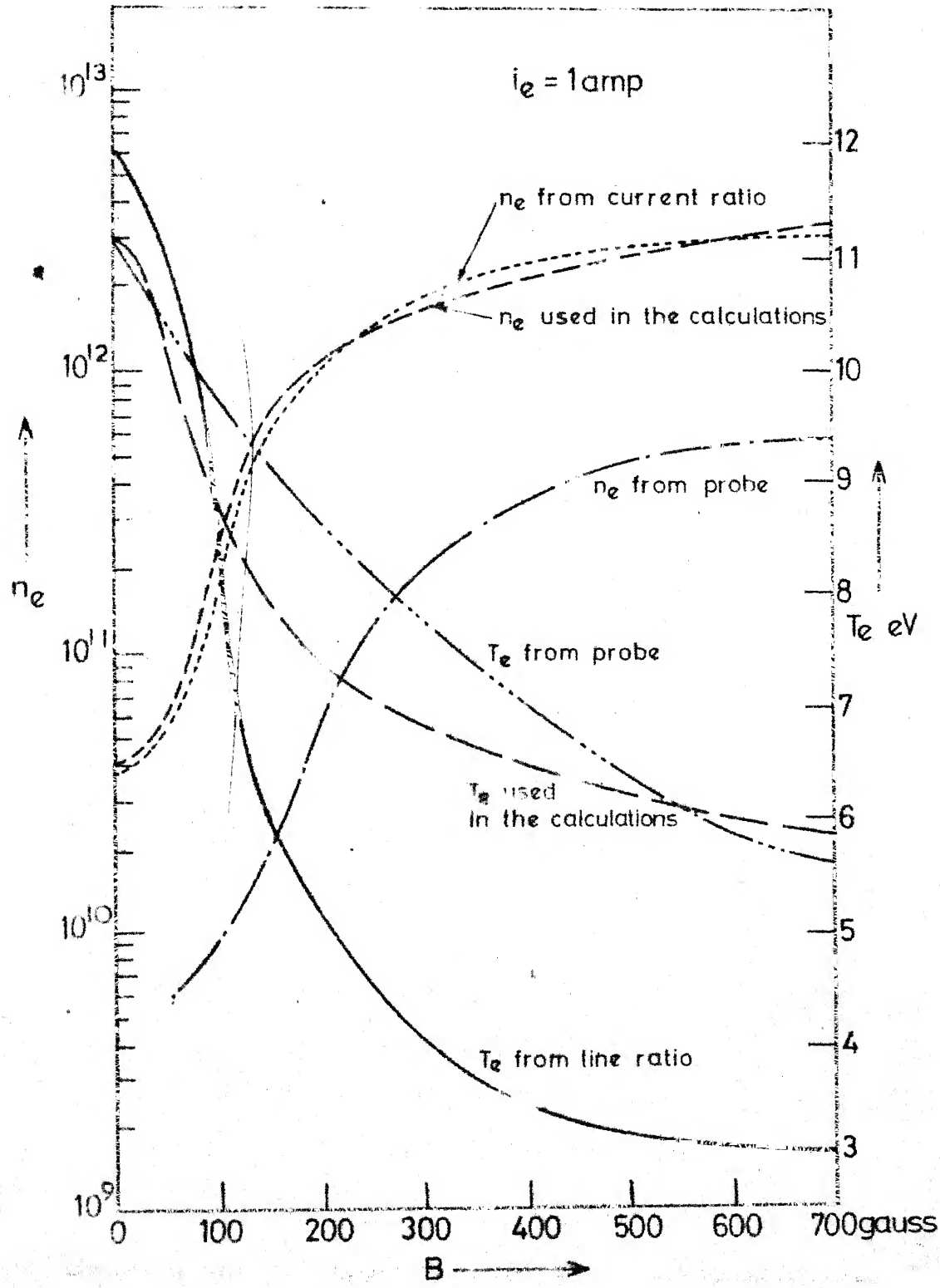

Fig. 4.15 Electron density (n_e), electron temperature (T_e) profiles as a function of the magnetic field(B)

(eq. 3.2) is considered to be independent of electron density. However, if one computes the ratio of I_{5047}/I_{4713} at various T_e and n_e values using a detailed collisional-radiative model, one observes considerable dependence on n_e at least in the range 10^{11} to10^{13}, the n_e range of the present experiments, though at higher and lower densities the ratio is essentially independent of n_e. This is shown in Fig. 4.16. Hence at intermediate densities T_e obtained from this ratio method is likely to be less reliable.

It may be mentioned here that in the present work an attempt was made to obtain T_e estimates from Boltzmann plot for higher lines of $n^3D \rightarrow 2^3P$ series but the intensities of the lines being very weak, measurements could not be made. It has been indicated however that this method gives too low T_e values.[41]

It may be added here that Johnson and Hinnov[58] have pointed out that no acceptable line ratio method for electron temperature determination has been found in the density range of 10^{10} to 10^{14} cm^{-3}. They further comment that absolute intensity measurement of a line should be reasonably good for T_e measurement. But T_e obtained by them using a comparison of the absolute intensities observed with those calculated from a CR model for He plasma is reliable within only ~30%.

Considering all the above facts, it may be taken that the electron temperature obtained by using probes is probably

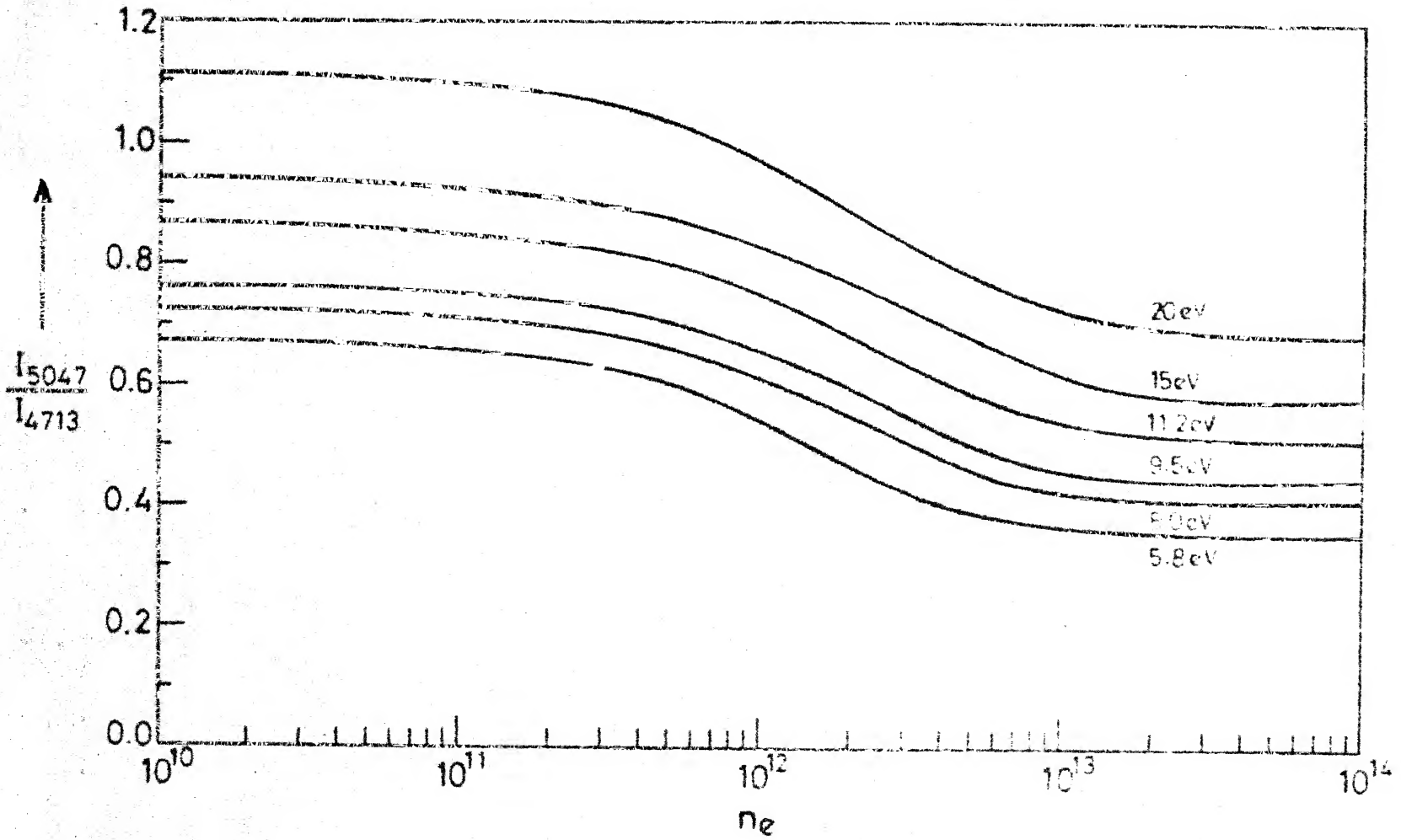

Fig. 4.16 Calculated emission intensity ratios I_{5047}/I_{4713} Vs n_e

closer to the actual situation. With respect to the T_e profile obtained from probe, the profile that gives best match with the experimental enhancement factors has a maximum deviation of 20% at intermediate points and 5% at the end points.

Effect of inclusion of more levels in the model on population densities:

Calculated population densities taking energy levels of HeI up to principal quantum number n=10 and HeII levels up to n=13 were compared with those obtained by taking n up to 12 keeping HeII levels n=13. In the n_e, T_e range of the present investigation, maximum variation found in the calculated population densities for any excited state was less than 1%. It may be recalled that in Johnson's[13] model n=25 was used. But the present model with n=12 matches with Johnson's experimental results when appropriate n_e, T_e, n(1) are used, as does Johnson's n=25 model. From this, it seems that additional levels are quite unnecessary. More detailed comments on Johnson's experimental results will be presented later in this chapter.

Effect of neutral-neutral collisions on the population densities:

Variation in the population densities by including neutral-neutral collisions when compared with those in absence of such process was less than 2%. From an inspection of the values of KN(p,q), KN(p,i) from Table 4.8 and some of the electron impact rate coefficients from Tables 4.2 and 4.3,

such small variation seems to be reasonable because the electron impact collisions are dominant at T_e range of 12-5 eV.

Neutral He temperature T_g :

Neutral temperature estimate was made from Doppler widths of some of the HeI lines. The temperature obtained was about 800°K. Variation of this temperature in the magnetic field was not more than 20%. Hence an upper limit of T_g equal to 1000°K is used in the calculations for enhancement. However, calculations in the T_g range 500-2000°K does not make any noticeable difference in the results.

Effect of variation of n_e, T_e ranges on I_B/I_o(calc) :

In order to find out whether any other range of n_e and T_e values would give better correlation with the experiments, calculations of I_B/I_o were made chosing different sets of n_e and T_e values. Keeping the variation in T_e same (11.2 to 5.9 eV) and also $(n_e^B/n_e^o)_{700} = 80$ as is taken in all calculations, I_B/I_o at 70C is calculated with $n_e^o = 10^{10}$. The results show that calculated I_B/I_o values are 40% higher than the observed values for first and second line of any series, and for higher lines error exceeds 80%. With $n_e^o = 10^{11}$, calculated values are found to be about 20% lower than the experimental values and here again the error is more than 100% for higher levels. Keeping $n_e^o = 4 \times 10^{10}$ and T_e ranging from 12 to 3 V

(as observed in line ratio method), it is found that a 10^3 fold increase in the electron density is required to make the calculated I_B/I_o agree with the experimental results. Such large increase in n_e is not supported by the present experiments.

Absolute population densities of $He^+(4)$:

Although in this work absolute population densities of any level has not been measured, dependability of the calculated population densities can be checked by comparing the calculated values with those experimentally observed by other workers. It will be shown, later in this chapter, that the present model predicts absolute population densities accurately within a factor of 2 of some helium plasma experiments of other workers where absolute densities were experimentally measured. If this is also assumed to be valid in the present work, then from the experimental relative intensities of HeII 4→3 and HeI $4^3S \rightarrow 2^3P$ lines (0.09 at B=0 and 0.059 B=700 gauss), $n(4^3S)$ calculated from the model, and known transition probabilities of the lines, one obtains for $n^+(4) = 1.8 \times 10^4$ (at B=0) and $n^+(4) = 1.04 \times 10^5$ (at B=700 gauss). If only helium ion model is considered such high population densities cannot be explained regardless of the degree (0-100%) of second ionization one assumes. This seems to strongly indicate that HeI states must be responsible in a major way for populating the HeII excited levels.

Effect of $n^+(1)/n^{++}$ variation on HeI and HeII populations :

In the n_e, T_e range of the present study, HeI(p) states are populated mainly from HeI ground state and as a consequence, variation of n^+/n^{++} ratio has little effect on n(p) values; since the n^+/n^{++} ratio would influence n(p) only when contributions from $r_o(p)$ to n(p) become significant. In the calculation of HeII coefficients $r_o^+(i)$, $r_1^+(i)$, and $r_2^+(i)$, from eqs. (4.16) and (4.17), n^+/n^{++} appears as a parameter in the term $\rho(p).n_e.K(p,i).n_E(p)/n_E^+(i)$ and explicit values of the n^+/n^{++} ratios are used in solution of the simultaneous equations. Rewriting eq. (4.19), population densities of HeII(i) are given by

$$n^+(i) = r_o^+(i)\, n_e.n^{++} \cdot \frac{4.14^{-16}}{T_e^{3/2}}\, i^2 \exp(E_i^+/kT_e) + r_1^+(i)\, n(1) \frac{n^{++}}{n^+(1)} \exp(E_i^+ - E_1)/kT_e$$

$$+ r_2^+(i) \cdot i^2\, n^+(1).\exp(E_i^+ - E_1^+)/kT_e \qquad (4.41)$$

where E_i^+ is the ionization potential of the HeII state i and E_1 is the ionization potential of the ground state of HeI to the first continuum.

For a given n_e, T_e, n(1) and n^+/n^{++} values, $n^+(i)$ can be calculated from eq. (4.41). Whereas $r_o^+(i)$ and $r_2^+(i)$ are functions of only n_e and T_e, $r_1^+(i)$ is a function of n_e, T_e and n^+/n^{++}. At $T_e > 8.6$ eV, $n_e < 10^{12}$ and $n(1) \sim 10^{14}$, major contribution to $n^+(i)$ arises from the second term in eq. (4.41), while

at $T_e < 8.5$ eV and $n_e > 10^{12}$ major contribution to $n^+(i)$ is from the third term. At very low electron temperatures and high densities ($T_e < 2$ eV, $n_e > 10^{14}$), the first term in eq. (4.41) becomes important.

Taking $n_e = n^+ + 2n^{++}$, it follows from eq. (4.41), that if the contribution to $n^+(i)$ is from the first or the third term, variation of n^+/n^{++} changes the $n^+(i)$ values to an extent determined by the variation in n^{++} or $n^+(1)$. For $T_e > 8.5$ eV, it is found by calculation of $n^+(i)$ that its (viz., $n^+(4)$ etc.) variation is not significant when the parameter n^+/n^{++} is varied. Not only does this show that HeI states are primarly responsible for populating the HeII(i) states, but also the dominant contribution originates from HeI ground state. This is because, a comparison between the metastable and the ground state ionization coefficient $K(p,i)$'s show that the value for the metastables is about 1-2 orders of magnitude higher (Table 4.7) but the population densities are at least 3 orders of magnitude lower leading to relatively insignificant contribution to HeII(i) from the metastables. From higher states of HeI, the contributions are even less.

Effect of optical thickness on the population densities :

The extent of optical thickness for HeI radiation does not significantly affect He^+ levels and conversely the optical thickness for He^+ radiation does not alter HeI populations much.

In general, if the plasma is optically thick, population densities of all the excited levels increase, compared to the optical thin case. As a result of photoabsorption the increase in population densities of the states directly populated due to absorption (2^1P, 3^1P etc.) is largest. For other levels which are collisionally connected to these states the increase is less. In the HeI system, at lower electron densities, absorption of resonance radiation increases the population of n^1P levels to an extent there is decrease in $\Lambda^{(P,1)x}A(p,1)$ values. If the plasma is partially optically thick then, increase in population densities of the singlet states is higher than the corresponding states in the triplet series.

The difficulties in ascertaining correct values of optical escape factors applicable to a particular plasma is well recognized. This arises mainly due to the uncertainties in L in eq. (4.38). In addition, even small variations in neutral density significantly alter the escape factors. However, the fact that for optically thin conditions triplet level enhancements are explained quite well and n^1P level enhancements are not, is a strong qualitative indication that the population of ^1P levels involve some special processes. Reabsorption of resonance radiation, i.e., partially optically thick condition, seems to be the most reasonable process one can conceive of even though the exact values of optical escape factors may have uncertainties.

Collisional-radiative Models of other Workers Applied to the Present Experimental Results:

Having presented a comparison of the experimentally observed HeI and HeII emission enhancements with the theoretical predictions of the model used in the present work, it should be be of interest to consider calculations of other workers on the helium system and check to what extent the present experimental observations can be explained with their theoretical results. First, calculations of Drawin and Emard[43] are considered. Using Table 2 in Ref. 43, enhancement factors were calculated and are presented here in Table 4.14. The major difference between Drawin and Emard's calculations and the present one is that, in the present case, the sublevels of n = 3,4,5 HeI states are completely separated. In Table 4.14 the experimental values of emission enhancements and those calculated in the present work are also given. One observes that the present calculations provide much better correlations with the experimental enhancement factors of the sublevels than the calculations of Drawin and Emard using coalesced levels. It may be noted that population densities of sublevels obtained from those of the coalesced levels using appropriate Boltzmann factors would not give any better enhancement values than shown in Table 4.14. This is due to the fact that the difference in energy levels between the sublevels is very small even in the case of n=3 state. n=4 and n=5 states have still smaller energy differences between the sublevels and the situation would not improve.

TABLE 4.14

Comparison of emission enhancement factors $(I_B/I_0)_{700}$ calculated from Drawin and Emard's tables (Ref. 43) with the present calculations and experimentally observed values

Emitting Triplet levels	Calc. (Ref. 43)	Experimental observation present work		Calculated values present work
n=3 ($3^3S+3^3P+3^3D$)	14.0	3^3S	16	13.8
		3^3P	9	10.0
		3^3D	12.7	13.2
n=4 ($4^3S+4^3P+4^3D+4^3F$)	5.6	4^3S	8.0	9.2
		4^3P	5.0	4.5
		4^3D	9.5	9.8
n=5 (all triplet levels)	2.25	5^3S	2.0	1.85
		5^3D	3.5	3.0
Emitting Singlet levels				
n=3 ($3^1S+3^1P+3^1D$)	7.5	3^1D	14.5	12.2
		3^1P	4.0	9.0
n=4 ($4^1S+4^1P+4^1D+4^1F$)	5.85	4^1D	9.0	9.4
		4^1S	2.0	5.0
		4^1P	3.0	6.0
n=5 (all singlet levels)	2.9	5^1D	3.0	2.9
		5^1S	2.0	2.0

Turning to Park's[59] work on collisional excitation-deexcitation rate coefficient calculations, one notes that in his scheme of HeI energy levels, he has used separated levels up to n=3 but uses combined singlet-triplet groups of 3^3D and 3^1D, 4^3S and 4^1S, 4^3P and 4^1P, 4^3D and 4^1D, 4^3F and 4^1F, 5^3S and 5^1S, 5^3P and 5^1P, 5^3D and 5^1D, a grouping of the levels 5^3F, 5^1F, 5^3G and 5^1G, and fully coalesced sublevels for n=6 to n=20. Taking this scheme of levels and the rate coefficients provided by him, and using other atomic parameters as described earlier in this chapter, a computer programme was developed to calculate HeI level populations from which enhancement factors could be obtained. HeI enhancement factors calculated from Park's model as well as experimental values from the present work are shown in Table 4.15. It can be seen that the deviations are large. Part of this reason seems to be in his using coalesed triplet and singlet states; discrepancy arises because the triplet and singlet level populations change in markedly different manner with electron density and electron temperature. Also, in his model, $1 \rightarrow n$ excitation for $n > 6$ are neglected.

Applications of the Present Model to Experimental Results of Other Workers :

Though the absolute values of population densities obtained in present calculations seem reasonable, one of the

TABLE 4.15

Comparison of $(I_B/I_O)_{700}$ values obtained by using Park's (Ref.59) energy level scheme and his rate coefficients with those obtained in present calculations

Emitting State	$(I_B/I_O)_{700}$ calculated using Park's scheme	$(I_B/I_O)_{700}^{*}$ calculated using present scheme	$(I_B/I_O)_{700}^{**}$ experimentally observed
3^3S	11.73	13.8	16.
4^3S	1.87	9.2	8
5^3S	1.0	1.95	2.0
4^1S	1.87	5.0	2.0
5^1S	1.0	2.0	2.0
3^3P	8.0	10.0	9.0
4^3P	13.39	4.5	5.0
3^1D	3.7	12.2	14.5
4^1D	10.2	9.4	9.0
5^1D	7.2	2.9	3.0
3^1P	6.41	9.0	4.0
4^1P	13.39	6.0	3.0
3^3D	3.7	13.2	12.0
4^3D	10.2	9.8	9.5
5^3D	7.2	3.0	3.5

* Values corresponding to Table 4.11, column 3.

** Values corresponding to Table 3.2, for $i_e = 1$ amp.

limitations of the present work is that absolute population densities could not be obtained from the experiments, due to lack of a standard lamp in the laboratory and its not being available in the country. While such deficiencies can be made up later with the development of the laboratory facility, it is of interest to try out the model, which seems to explain reasonably satisfactorily emission enhancement factors, to predict absolute population densities in experiments of other workers on helium plasmas. For such a comparison Johnson's[13] experiments in Princeton stellarator C is chosen. His experimental condition involve n_e range 4.2×10^{12}-3.3×10^{13}, T_e range 14.4 eV - 4 eV, and neutral density 4×10^{11}-8.2×10^{13}. For some of these conditions optically thin model can be used in a straightforward manner, but with increasing neutral density, application of partially optically thick condition is required. While calculations were carried out for the entire range of his experimental conditions, and matching is satisfactory, the results for some of the conditions are presented in Table 4.16 and Table 4.17. Table 4.16 presents cases where optically thin conditions can be used. In Table 4.17, at the highest neutral density of 8.2×10^{13}, partially optically thick condition is used. Calculation of the optical thickness was made by taking 3.5 cm as the radius of the plasma cross-section (the maximum distance the light travels from the centre of the plasma) at 50 kilogauss and eq. (4.35) applied to calculate the optical escape factors. Examination of

TABLE 4.16

Comparison of Johnson's experimentally observed values of HeI population densities (Ref. 13) with present calculations using optically thin condition

	Hinnov expt.	Present calc.	Hinnov expt.	Present calc.	Hinnov expt.	Present calc.
T_e eV	10.8		8.5		7.2	
n_e	4.2^{12}		1.9^{13}		1.49^{13}	
States n(1)	8.8^{11}		6.3^{12}		8.5^{12}	
4^1S	6.6^5	4.79^5	2.2^6	2.6^6	1.48^6	2.0^6
5^1S	2.4^5	1.24^5	6.4^5	6.06^5	3.3^5	4.3^5
3^1P	6.9^5	3.0^5	7.4^6	4.5^6	4.5^6	3.1^6
4^1P	3.3^5	2.02^5	1.96^6	2.4^6	1.17^7	1.6^6
5^1P	1.24^5	1.06^5	5.0^5	7.65^5	4.8^5	5.1^5
3^1D	5.1^5	3.28^5	4.0^6	3.57^6	2.4^6	2.7^6
4^1D	3.0^5	1.64^5	1.45^6	1.23^6	9.1^5	9.2^5
5^1D	9.5^4	6.0^4	4.3^5	2.78^5	2.9^5	2.2^5
3^3S	2.7^6	1.85^6	1.2^7	1.6^7	1.06^7	1.4^7
4^3S	7.3^5	5.6^5	2.6^6	4.0^6	1.87^6	3.4^6
5^3S	1.86^5	9.55^4	5.8^5	6.0^5	4.2^5	5.1^5
3^3P	2.1^6	2.42^6	9.7^6	2.0^7	7.9^6	1.6^7
4^3P	4.9^5	4.99^5	1.82^6	2.6^6	1.40^6	2.2^6
5^3P	1.49^5	9.0^4	4.7^5	4.4^5	3.6^5	3.6^5
3^3D	1.26^6	7.7^5	7.8^6	9.4^6	5.0^6	7.7^6
4^3D	3.3^5	3.11^5	1.53^6	2.4^6	1.13^6	2.0^6
5^3D	1.0^5	1.30^5	4.0^5	6.9^5	2.8^5	5.8^5

TABLE 4.17

Comparison of experimentally observed population densities of HeI states by Johnson[13] with present calculations using optically thick conditions

	Hinnov's expt. values	Present cal. optically thin	Present cal. partially optically thick
T_e		4.0	
n_e		1.36^{13}	
n(1)		8.2^{13}	
States			
4^1S	3.6^6	1.8^6	2.0^6
5^1S	1.07^6	3.6^5	4.7^5
3^1P	1.74^7	2.57^6	1.1^7
4^1P	2.6^6	1.2^6	2.1^6
5^1P	6.6^5	2.4^5	2.71^6
3^1D	1.1^7	2.5^6	3.4^6
4^1D	2.6^6	7.5^5	1.37^6
5^1D	5.9^5	1.5^5	2.0^5
3^3S	1.96^7	1.38^7	1.57^7
4^3S	4.0^6	3.17^6	3.4^6
5^3S	7.7^5	3.6^5	4.4^5
3^3P	1.49^7	1.6^7	2.0^7
4^3P	2.4^6	1.8^6	1.87^6
5^3P	7.5^5	2.8^5	2.9^5
3^3D	1.4^7	8.42^6	8.98^6
4^3D	2.6^6	2.0^6	2.5^5
5^3D	6.2^5	5.0^5	5.5^5

Tables 4.16 and 4.17 reveal that the matching of the experimental absolute population densities with those from the model used in the present work is quite satisfactory.

The present model using simultaneous solution for HeI and HeII levels can also be applied to the recent experiments in 'TPD' (Test Plasma by Direct-current Discharge) machine at Nagoya University, reported by Otsuka, Ikee and Ishii.[26] For HeI, absolute populations of 3^3D and 4^1D were measured at several points along the plasma column where observation windows are located. At these windows measurements were carried out also on plasma parameters n_e, T_e and neutral density n_o. They did not make any attempt to explain the observed population densities of HeI states from any theoretical model. Application of the collisional-radiative model used in the present work to TPD machine conditions leads to absolute populations of all the HeI and HeII states out of which only the populations of 3^3D and 4^1D are presented in Table 4.18, the states for which detailed experimental data is available in Ref. 26. It may be noted that the present model provides satisfactory order of magnitude explanation of the experimentally observed populations. Here also, the partially optically thick condition with reduced rate coefficients for the transitions 2^1P-3^1D are used, but at high electron densities, as is the case in TPD experiments, such changes in the rate coefficients have insignificant effect.

TABLE 4.18

Comparison of experimental values of HeI 3^3D and 4^1D and HeII (i=4) population densities (Otsuka, Ikee, Ishii (Ref. 26)) with present calculations

HeI 3^3D, 4^1D Populations

State	T_e	n_e	n_1	n^+	n(p) expt. Ref.26	n(p) present calculations Opt. thin	Opt. thick**
3^3D	window 3 3.17 eV	2.68^{14}	3.0^{14}	2.68^{14}	2.0^7	1.5^7	2.26^7
4^1D					2.1^6	1.6^6	1.8^6

p. 129 In Table 4.18, in place of n_1 values 3.0^{14}, 1.0^{14}, 7.0^{13}, read 2.3^{14}, 2.1^{14}, 2.0^{14}.

p. 130, line 5. In place of heretofore, read henceforth.

HeII(4) Populations

Window No.	T_e	$n^+(4)$ observed	$n^+(4)$ optically thin	$n^+(4)$ optically thick for HeII Lyman radiation*
Window 3	3.17	2.2^5	9.62^4	2.0^5
Window 4	0.88	2.5^6	2.33^7	-
Window 5	0.34	2.6^4	1.37^7	-

* $\Lambda_{12} = 0.0007$, $\Lambda_{13} = 0.06$, $\Lambda_{14} = 0.1$, $\Lambda_{15} = 0.5$ and $\Lambda_{ij} = 1$.

** $\Lambda_{1,5} = 0.0013$, $\Lambda_{1,11} = 0.010$, $\Lambda_{1,18} = 0.07$, $\Lambda_{1,25} = 0.2$, $\Lambda_{1,26} = 0.5$

Absolute values of HeII populations were also obtained in the TPD machine experiments for i=4, from experimental line intensity measurements. The population density of this level, in terms of a collisional-radiative model of only HeII states, can be written as (eq. 10' in Ref. 26; heretofore terminology of Ref.26 is used, different from those used in the present work),

$$n_4 = r_o(4)\, n_e\, n^{++} A(4) + r_1(4)\, n_1 \exp\left[\frac{E_1}{kT_e}\left(\frac{1}{4^2} - 1\right)\right] \quad (4.42)$$

In the terminology of Ref. 26 which considers HeII states separately from HeI levels but along with He^{++} ions, r_o in eq. (4.42) is the contribution from the He^{++} continuum, r_1 is the contribution from the HeII ground state, n_1 the population of HeII ground state, E_1 is the ionization potential of the ground state of HeII, and A is given by

$$A(i) = \frac{i^2 h^3}{(2\pi m k T_e)^{3/2}} \exp\left(\frac{E_1}{i^2 k T_e}\right) = i^2 \frac{4.14 \times 10^{-16}}{T_e(^oK)^{3/2}} \exp\frac{E_1}{i^2 k T_e} \quad (4.43)$$

In their paper, the authors miss the factor i^2 (which has a value of $4^2=16$) in the second equality of eq. (4.43) and calculate a value of $n_4=1.6\times10^6$ cm^{-3}. Further, comparing with the experimental value of 2.5×10^6 at window 4, they erroneously conclude that there is agreement between the experimentally observed and theoretical values.

Necessary correction, however, gives a theoretical value of 2.33×10^7 which is off from the experimental value of

2.5×10^6 by an order of magnitude. Using appropriate r_o values calculated for the model used by Otsuka and others and n^{++} from their Table as they have used, the values for the helium ion HeII (i=4) population density for the TPD plasma conditions are shown in Table 4.18. Use of Drawin's[44] or McWhirter and Hearn's[6] Table for the HeII r_o coefficients yield essentially the same values. Clearly, the calculated n_4 values using HeII model chosen by Otsuka and others show large deviations from the experimentally observed populations.

The conditions of their experiment however merit analysis in terms of applicability of optically thick conditions for HeII radiation. Using the same considerations as presented earlier, a partially optically thick model is justifiable with HeII Lyman radiation optical escape factors as $\Lambda_{12} = 0.0007$, $\Lambda_{13}=0.06$, $\Lambda_{14}=0.1$, $\Lambda_{15}=0.5$ and the remaining $\Lambda_{1j=1}$. Application of r_o, r_1 values thus obtained to eq. (4.42) shows that for the plasma conditions of window 3, the major contribution comes from the ground state of HeII (i=1), hence from the r_1 factors, whereas for the conditions at windows 4 and 5, i.e., at lower T_e values, the dominant contribution is from the He^{++} continuum, i.e. from the r_o values. For the windows 4 and 5 cases, n^{++} concentration is required for calculation of the He^+ (i=4) population, whereas for the case of window 3, n^{++} is not necessary. Assuming the helium ion ground state population as approximately equal to the electron density,

the population density of HeII (i=4) turns out to be 2.0×10^5, within ~20% of the experimentally observed value, which is at least as good as the value obtainable from calculations using only continuum contributions as shown in Table 4.18. This shows that use of a partially optically thick model at T_e=3.17 eV n_4 populations can be explained satisfactorily.

Chapter V

A REVIEW

In the present work emission intensities of HeI and HeII line radiation have been measured in a helium plasma column subjected to a longitudinal magnetic field 0-700 gauss. The measurements involve 16 lines of HeI and the 4685 A line of HeII. The emission intensities were found to increase with increasing magnetic field and in many cases were found to go through a maximum and then decrease in the magnetic field range of the investigation. It was observed that, less the electron density, more pronounced is the effect of emission intensity enhancement.

Plasma parameters n_e, T_e were measured using Langmuir probes, n_e also from emission intensities using a emission current ratio method, and T_e also from a singlet-triplet intensity ratio method. Electron densities were found to

increase by a factor of about 80 with increasing field, associated with a concurrent fall of electron temperature from about 11 eV to about 6 eV.

As an attempt to explain the observed plasma line emission, a general collisional-radiative model is formulated which features completely separated sublevels up to n=5 and coalesced level for n=6 to n=12. 13 levels of HeII (n=1-13) are included in the model, making a total of 45 levels. In addition to the usual radiative and electron impact processes, direct ionization-excitation processes to populate the excited states of HeII from HeI states, as well as atom-atom collisions are also incorporated. Neglecting diffusive losses for the excited states, 43 equations of HeI and HeII are simultaneously solved with respect to the ground state populations of HeI and HeII. This gives the population coefficients from which population densities of various levels are obtained for a wide range of n_e, T_e values and emission intensity enhancement factors are calculated therefrom. The model explains reasonably well the observed enhancement factors.

The model is then compared with collisional-radiative models used by other workers. It was found that the models which use combined singlet-triplet levels make poor predictions of enhancement factors. This is probably due to the marked difference in behaviour of the singlet and triplet levels as a function of n_e, T_e, and combination of the levels

However, that the population densities which arise out of calculations of the collisional-radiative model (and which explain the emission enhancements well) is reasonable is shown by the extent to which it predicts the absolute population densities of Stellarator experiments of Johnson and TPD experiments of Otsuka, Ikee and Ishii. Experimentally measured population density ratios of HeI and HeII states is an important additional point in this regard.

As regards diagnostic methods, it is well recognized that no single method can be depended on for all conditions in plasmas, and it is for this reason more than one method was used. The $n_e(B)$ profile from the probe shows that it is lower by approximately a constant factor from the corresponding n_e values obtained from the emission current ratio method. It is quite possible that a constant factor in probe density calculation is missing - may be an estimate of the effective probe area, which if incorporated will make the probe densities close to the actual situations. Whereas T_e measurements from higher level intensities would have been desirable, the measurements could not be made due to weak intensities. That weak intensities may be expected follows from a comparison of the population densities in the present work and some cases where such T_e measurements have been made. In the present work, $n(8)=9.93^5$, $n(9)=5.9^5$, $n(10)=4.4^5$, whereas in Drawin, Klan and Ringler's work $n(8)=1.63^7$, $n(9)=1.8^7$, $n(10)=1.9^7$ and in Ikee and Takeyama's

work $n(8)=8.19^{8}$, $n(9)=6.5^{8}$ and $n(10)=6.21^{8}$. It must be admitted however that a detailed spatial n_e, T_e profile would be valuable. However, with present experimental arrangement very precise measurements of such profiles are difficult. A 9 cm diameter new plasma tube with such facilities is under construction, where such measurements will be possible and additional side-on measurements of radiation, followed by appropriate Abel transformation, ought to give spectroscopic values of local plasma parameters as well.

Whereas there are undoubted uncertainties about the optical escape factors, chiefly arising from the uncertainties of absorption lengths L, it has been clearly shown that even with considerable changes in the value of L, there would not be much difference in the matching of most of the emission enhancement factors.

The direct ionization-excitation processes included in the model comprise a significant addition, not known to have been used in any other collisional-radiative model. Though the values of rate coefficients used are higher than the estimates of Dalgarno and McDowell, they are compatible with the ionization-excitation cross-section given by Drawin. It should be emphasized here that if such ionization-excitation processes are not incorporated, i.e., there is no direct contribution of the neutral states to the ionic excited states, the observed

population densities of HeII cannot be explained. This is regardless of whether one assumes near complete ionization of He^+ (so that HeII states are populated mainly from the second continuum and cascading) or all ions are in He^+ states so that the HeII states are populated mainly from excitation from HeII (i=1). If one considers that hydrogenic HeII rate coefficients are among the most accepted of the rate coefficients, this point becomes more meaningful. As for the ^1P-^1D rate coefficient, it may be mentioned that the change is not too unreasonable compared to the degree of certainty to which most other rate coefficients are known. Such changes are sometimes made to see what makes the theoretical results correspond the experimental data. Furthermore, even if these coefficients were not changed, the basic pattern and quality of matching would not have been significantly worse.

On the positive side, one might mention the following points about the present work. It provides a collisional-radiative model in which HeI and HeII levels[62] are considered together, and useful applications made thereof. In higher temperature plasmas such model would be increasingly necessary where one needs to deal with more of HeII population densities. That it explains several experimental results of other workers is an important point in support. Lastly, whereas there have been stray reports on emission enhancements, this is perhaps

the first effort, to the knowledge of the present author, which makes a systematic study of emission enhancements of helium plasmas in magnetic field, and also explains the observed phenomena in terms of fundamental collisional and radiative processes.

REFERENCES

1. H. W. Drawin in 'Reactions under Plasma Conditions', ed. M. Venugopalan, Wiley-Interscience, New York (1971) pp 55-123.

2. R. W. P. McWhirter in 'Plasma Diagnostic Techniques', ed. R.H. Huddlestone and S.L. Leonard, Academic Press (1968), p. 202.

3. T. Holstein, Phys. Rev., 83, 1159 (1951).

4. D.R. Bates, A.E. Kingston and R.W.P. McWhirter, Proc. Roy. Soc. (Lond), A267, 297 (1962).

5. H.W. Drawin, F. Emard and K. Katsonis, Z. Naturforschung, 28a, 1422 (1973).

6. R.W.P. McWhirter and A.G. Hearn, Proc. Phys. Soc. (Lond), 82, 641 (1963).

7. L.C. Johnson and E. Hinnov, J. Quant. Spectrosc. Radiat. Transfer, 13, 333 (1973).

8. C. Park, J. Quant. Spectrosc. Radiat. Transfer, 8, 1633 (1968).

9. R.J. Giannaris and F.P. Incropera, J. Quant. Spectrosc. Radiat. Transfer, 13, 167 (1973).

10. R. W. Motley and A.F. Kuckes, 5th International Conference on Phenomena in Ionized Gases, Munich (1961), p. 651.

11. E. Hinnov and J.G. Hirschberg, 5th International Conference on Phenomena in Ionized Gases, Munich (1961), p. 638.

12. E. Hinnov and J.G. Hirschberg, Phys. Rev., 125, 795 (1962).

13. L.C. Johnson, Phys. Rev. 155, 64 (1967).

14. L.C. Johnson and E. Hinnov, Phys. Rev., 187, 143 (1969).

15. H. Myers, Phys. Rev. 130, 1639 (1963).

16. C.B. Collins and W.W. Robertson, J. Chem. Phys., 40, 2202 (1964).

17. M.A. Gusinow, J.B. Gerardo and J.T. Verdeyen, Phys. Rev., 149, 91 (1966).

18. G.K. Born and R.G. Buser, Phys. Rev., 181, 423 (1969).

19. F. Robben, W.B. Kunkel and L. Talbot, Phys. Rev., 132, 2363 (1963).

20. M. Gryzinski, Phys. Rev., 115, 374 (1959).

21. I. Ya Fugol, P. L. Pakhomov and G.P. Reznikov, Optics and Spectroscopy, 16, 510 (1964).

22. A. A. Newton and M.C. Sexton, J. Phys. B, 1, 669 (1968).

23. R. Ikee and H. Takeyama, J. Quant. Spectrosc. Radiat. Transfer, 15, 543 (1975).

24. R. Ikee and H. Takeyama, J. Quant. Spectrosc. Radiat. Transfer, 15, 701 (1975).

25. H.W. Drawin and F. Emard, Z. Physik, 243, 326 (1971).

26. M. Otsuka, R. Ikee and K. Ishii, J. Quant. Spectrosc. Radiat. Transfer, 15, 995 (1975).

27. H. Takeyama and Y. Takezaki, J. Quant. Spectrosc. Radiat. Transfer, 8, 1023 (1968).

28. H. Takeyama and Y. Takezaki, J. Quant. Spectrosc. Radiat. Transfer, 8, 1863 (1968).

29. N. D'Angelo, Phys. Rev., 121, 505 (1961).

30. D.R. Bates and A.E. Kingston, Proc. Roy. Soc., A279, 32 (1964).

31. D.R. Bates, K. L. Bell and A.E. Kingston, Proc. Phy. Soc., 91, 288 (1967).

32. H. W. Drawin, Z. Naturforschung, 19a, 1451 (1964).

33. H. Boersch, J. Geiger and M. Topschowsky, Z. Naturforschung, 26a, 198 (1971).

34. R. L. Monroe, Can. J. Phys., 51, 564 (1973).

35. A. Simon, Phys. Rev., 98, 317 (1955).

36. W.P. Allis, in 'Handbuch der Physik', Vol. 21, Springer-Verlag, Berlin, 1956.

37. D. Bohm. E.H.S. Burhop, H.S.W. Massey and R.W. Williams in 'The Characteristics of Electrical Discharges in Magnetic Field', Vol. 5, Ed. A. Guthrie and R.K. Wakerling, McGraw-Hill, New York, 1949.

38. R.J. Bickerton and A. von-Engel, Proc, Phys. Soc., 69B, 468 (1956).

39. J. L. Delcroix in 'Plasma Physics', Vol. 2, John Wiley and Sons, (1968) pp. 136-141.

40. A. K. Hui, U.K. Roy Chowdhury and P.K. Ghosh, Ind. J. Tech. 12, 512 (1974).

41. R. J. Sovie, J. Quant. Spectrosc. Radiat. Transfer, 8, 833 (1968).

42. H. W. Drawin, Z. Physik, 228, 99 (1969).

43. H.W. Drawin and F. Emard, Report EUR-CEA-FC 697, Fontenay-aux-Roses, France (1973).

44. H.W. Drawin & F. Emard, Report EUR-CEA-FC-534, Fontenay-aux-Roses, France (1970).

45. J.B. Hasted, 'Physics of Atomic Collisions' Butterworths (1964) pp. 457-451.

46. H.W. Drawin, F. Klan and H. Ringler, Z. Naturforschung, 26a, 186 (1971).

47. W.L. Wiese, M.W. Smith and B.M. Glennon, NSRDS-NBS 4, 1, pp 9-15 (1966).

48. L.C. Green, P.P. Rush and C.D. Chandler, Astrophys. J., Suppl. Series, 3, 37 (1957).

49. M. Gryzinski, Phys. Rev. 138, 336 (1965).

50. H.W. Drawin, Report EUR-CEA-FC 383, Fontenay-aux-Roses (1967).

51. B.L. Moiseiwitsch and S.J. Smith, Rev. Mod. Physics, 40, 238 (1968).

52. H.A. Kramers, Phil. Mag., 46, 836 (1923).

53. M.J. Seaton, Monthly Notes of Royal Astronomical Soc. 119, 81 (1959).

54. A. Dalgarno and M.R.C. McDowell, in 'The Airglow and the Auroae', ed. A. Dalgarno and E.B. Armstrong, Pergamon, N.Y. (1955) p. 340.

55. H.W. Drawin and F. Emard, Plasma Physik, 13, 144 (1973)

56. A. K. Hui and P. K. Ghosh, 12th International Conference on Phenomena in Ionized Gases, Eindhoven, 1975, p. 54.

57. E. K. Shaw and G. S. Kino, Phys. Fluids, 12, 1513 (1969).

58. L. C. Johnson and E. Hinnov, Phys. Fluids, 12, 1947 (1969).

59. C. Park, J. Quant. Spectrosc. Radiat. Transfer, 11, 7 (1971).

60. R. F. Giovanelli, Austral J. Sci. Res. 1, 295 and 289 (1948)

61. R. Mawe, Brit. J. Appl. Phys. 18, 107 (1967)

The author is greateful to the examiner to point out these two (61,60) useful references in connection with CR model and HeI and HeII levels used in a single model by diff ouert method.

APPENDIX

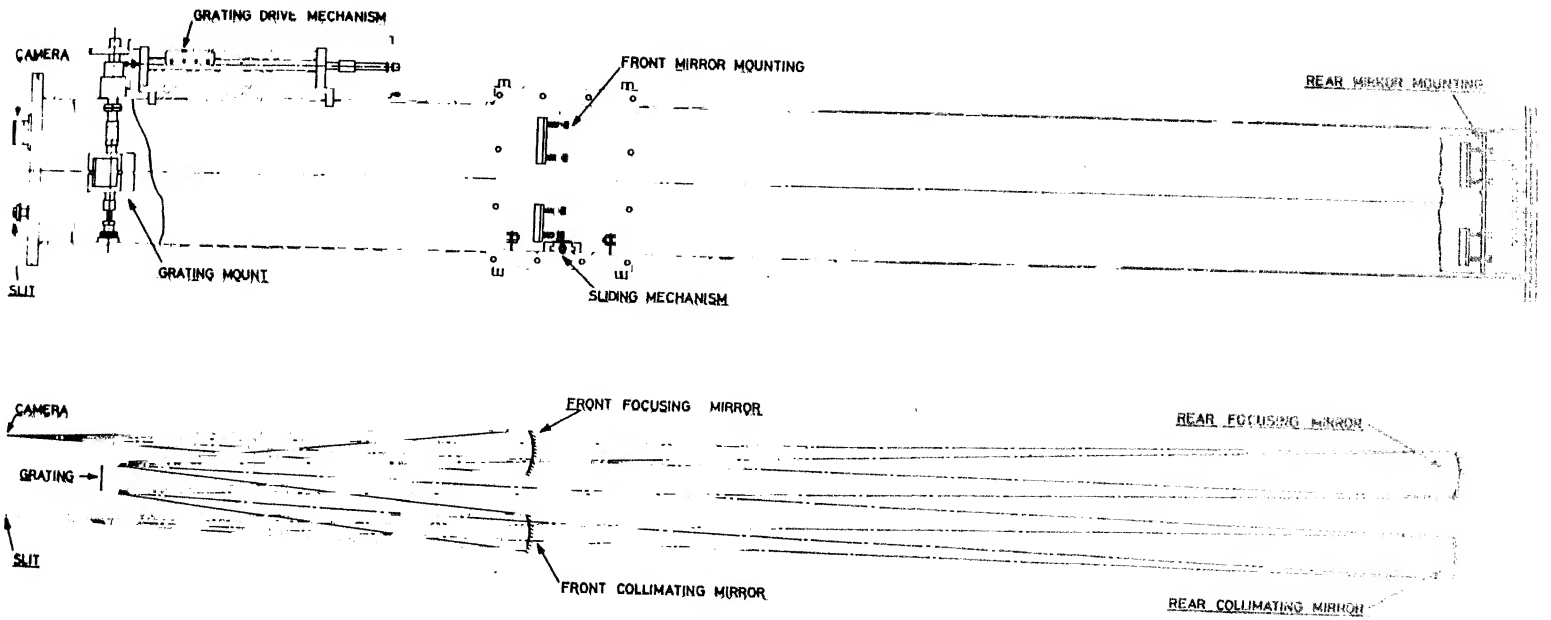

1 Schematic Diagram of the 2.1 m/6.4 m Dual Dispersion Spectrograph used in the Present Work

Fig. A.1

VITAE

The author hails from Kumta, situated in West Coast of Karnataka. After successful completion of school final from Gibb High School, Kumta, he joined Dr. A.V.B. College, Kumta for B.Sc. degree. He completed B.Sc. in 1966 and then joined for M.Sc. in Karnatak University, Dharwar. After completing M.Sc. in 1968, he worked as a lecturer in Sri J.C.B.M. College, Sringeri between 1968 and 1970. In July 1970, he joined the Department of Chemistry, IIT Kanpur for Ph.D. programme. Presently he is working as a Senior Research Assistant in the Department of Chemistry, IIT Kanpur.